

Experimental and Computational Study of Isomerically Pure Soluble Aza-phthalocyanines and Azasubphthalocyanines of Varying Number of Aza Units

Martin Liebold^a, Eugen Sharikow^a, Elisabeth Seikel^a, Lukas Trombach^b, Klaus Harms^b, Petr Zimčík^c, Veronika Nováková^c, Ralf Tonner^{b,*}, and Jörg Sundermeyer^{a,*}

^a Fachbereich Chemie und Wissenschaftliches Zentrum für Materialwissenschaften (WZMW), Philipps-Universität Marburg, Hans-Meerwein-Straße 4, 35032 Marburg, Germany. e-mail: jsu@chemie.uni-marburg.de

^b Fachbereich Chemie, Philipps-Universität Marburg, Hans-Meerwein-Straße 4, 35032 Marburg, Germany. e-mail: tonner@chemie.uni-marburg.de

^c Department of Pharmaceutical Chemistry and Drug Control, Faculty of Pharmacy in Hradec Králové, Charles University in Prague, Heyrovského 1203, Hradec Králové, 500 05 Czech Republic e-mail: petr.zimcik@faf.cuni.cz

Abstract: Herein, we present a series of isomerically pure, peripherally alkyl substituted, soluble and low aggregating azaphthalocyanines as well as their new, smaller hybrid homologues, the azasubphthalocyanines. The focus lies on the effect of the systematically increasing number of aza building blocks [-N=] replacing the non peripheral [-CH=] units and its influence on physical and photophysical properties of these chromophores. The absolute and relative HOMO-LUMO energies of azaphthalocyanines was analyzed using UV-Vis, CV and compared to density functional theory calculations (B3LYP, TD-DFT). Crystals of substituted subphthalocyanine, N₂-Pc*H₂ and N₄-[Pc*Zn·H₂O] were obtained out of DCM. For the synthesis of the valuable tetramethyltetraline phthalocyanine building block a new highly efficient synthesis involving a nearly quantitative Co^{II} catalyzed aerobic autoxidation step is introduced replacing inefficient KMnO₄/pyridine as oxidant. The lowering of the HOMO level is revealed as the determining factor for the trend in the adsorption energies by electronic structure analysis.

Introduction

Phthalocyanines (Pc) and structurally related isosteric octaazaphthalocyanines, in particular pyrazinoporphyrazines (Ppz), probably became one of the technologically most prominent classes of organic dyes. There are numerous applications, including absorbers in dye sensitized solar cells (DSCs),^{1,2,3,4} semiconductors in organic field effects transistors (OFETs),⁵ or photoconductors in laser printers.⁶ Traditionally, they serve as dye ingredient in lacquers, paints,⁷ and plastics.⁸ More recently, they are used as colour filters in liquid crystal display,⁸ as fluorescent markers,⁹ as sensors or as sensitizers in photodynamic therapy (PDT).¹⁰ On one side, the characteristic aggregation and π -stacking of these 42 π electron extended HÜCKEL aromatic systems causes their optoelectronic materials properties. On the other side, aggregation typically leads to molecules completely insoluble in organic solvents.⁸ By introducing bulky axial metal ligands,^{11,12} and/or peripheral or non peripheral ring substituents,^{13,14} the solubility in common organic solvents is increased and aggregation decreased. In current research, the investigation of [-CH=], [-N=] units is a hot topic. Recently, symmetrical A₄-type phthalocyanines and naphthalocyanines as well as their aza-analogues were investigated with respect to their singlet oxygen generation and

photostability.¹⁵ A selective access to a class of *meso* substituted Pc derivatives, namely tetrabenzotriazaporphyrins (TBTAP), has been reported as well.¹⁶ Unfortunately, one *tert*-butyl group at the peripheral position commonly used to gain solubility of a Pc always leads to mixtures of up to four stereoisomers as a consequence of the cyclotetramerisation.¹⁴ Commonly used two peripheral long n-alkyl or -OR, -SR substituents per isoindoline unit lead to one stereoisomer, however, it becomes difficult to get highly ordered crystalline Pc phases. Linking two peripheral *tert*-butyl groups via a joint C-C bond together leads to chromophores soluble enough for chromatography and ¹H NMR spectroscopy, at the same time sterically demanding enough to avoid intermolecular deactivation paths of their excited state.¹⁷ Such a best compromise phthalocyanine building block PDN* **1** was first reported by MIKHALENKO *et al.* (Fig. 1).¹⁸ Related symmetrical A₄-type Pc*MX complexes have a higher tendency to form well-ordered and even single-crystalline phases.¹¹ However, the 8-step synthesis of Pc*H₂ might not have looked appealing to followers, probably because a side chain oxidation of the 1,1,4,4,5,6-hexamethyltetraline intermediate to the corresponding *o*-dicarboxylic acid (Scheme 1) by KMnO₄ in pyridine was drastically limiting the overall yield of the ligand.¹⁸ Here, we report a much more attractive method and selective

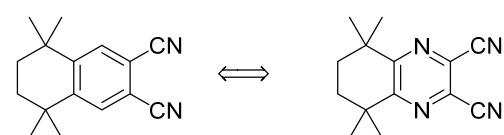
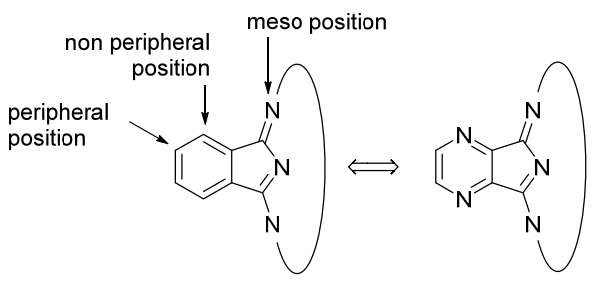


Figure 1. Discussed isoindoline and pyrrolopyrazine units derived from phthalodinitile **1** and pyrazinedinitril **2**.

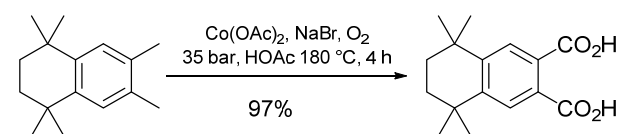
catalytic aerobic oxidation as replacement of this synthesis step. It is suggested to call this sterically demanding soluble and compact phthalocyanine derivative with 16 methyl groups Pc^*H_2 , following the common terminology of prominent organometallic ligands Cp (C_5H_5) and Cp^* (C_5Me_5). The corresponding soluble pyrazinoporphyrazine Ppz^*H_2 has been introduced by us only recently.¹² The aim of this study is to apply the precursors PDN^* (**1**) and PyzDN^* (**2**) to synthesize and fully characterize a complete series of diaza-, tetraaza-, and hexaaza- $\text{N}_x\text{-Pc}^*\text{M}$ hybrid compounds as well as their subphthalocyanine homologues Spc^*BCl , diaza-, tetraaza-, and hexaaza- $\text{N}_x\text{-[Spc}^*\text{BCl]}$ (or $\text{[Sppz}^*\text{BCl]}$ for $n=6$), respectively (Fig. 2 and 3). Despite of the fact, that a large number of lower-symmetry phthalocyanines of A_{4-n}B_n -type and subphthalocyanines of an A_{3-n}B_n -type is described in literature, only few of such aza derivatives are systematically studied.^{19,20} We were interested in a systematic study of photophysical properties and optoelectronic response upon stepwise substitution of $[-\text{CH}=]$ units by $[-\text{N}=]$ units in these hybrid chromophores. In the following we correlate UV-Vis data with electro-analytically gained oxidation and reduction potentials measured by CV, and compare these results with results of DFT calculations. Density functional theory has been found to perform well for the discussion of trends in excitation energies along a series,²¹ although the derivation of accurate absolute excitation energies needs more sophisticated methods.²² It was found before, that the investigation of the HOMO-LUMO energy gap can be a good indicator for the excitation energy observed.²¹ The reduced symmetry in protonated H_2Pc^* or A_{4-n}B_n -type aza-analogues $\text{N}_x\text{-Pc}^*\text{M}$ should lead to splitting of the Q-band.¹⁹

Knowing and predicting the trend in the HOMO-LUMO gap, designing the absolute HOMO-LUMO energies, as well as adding a permanent dipole moment to these chromophores and control their aggregation are fundamentals needed to control level alignment at internal interface to wide band gap semiconductors such as TiO_2 or ZnO .^{1,3,4} Understanding exciton dynamics and exciton dissociation into mobile charges at ideal model heterojunctions is of fundamental importance, e.g. for optimizing DSSCs.

Results and Discussion

Synthesis. The respective dinitrils PDN^* **1**^{18,23,24} and PyzDN^* **2**¹² have been described in literature. The overall yield limiting key step in the 8-step synthesis of PDN^* **1** is the oxidation of

1,1,4,4,5,6-hexamethyltetraline to the 1,1,4,4-tetramethyltetraline-6,7-dicarboxylic acid building block. So far this stoichiometric oxidation was accomplished by treatment with large excess of potassium permanganate in hot pyridine. This procedure is hampered with unreliable yields of 15–60% and large amount of poisonous waste. Here we report a green catalytic access to this key intermediate, which will promote drastically its future use in the synthesis of soluble, non-aggregating, isomerically pure phthalocyanines (Scheme 1).



Scheme 1. New catalytic oxidation of 1,1,4,4,5,6-hexamethyltetraline to phthalic acid key building block.

Our protocol is similar to conditions used in the industrial autoxidation of *para*-xylene to terephthalic acid with dioxygen in the presence of cobalt acetate catalyst and a bromide promotor.²³ The yield increases to 97%, the waste is negligible, water is formed as by-product. The product precipitated in crystalline state, solvent glacial acid and even catalyst can be fully recycled. With large excess of glacial acid or in the presence of acetic anhydride the isolated product is corresponding phthalic anhydride, which saves even one reaction step in the synthesis of PDN^* **1**. The radical chain mechanism induced by intermediate $\text{Co}(\text{OAc})_3$ is discussed in the electronic supplement. H atom abstraction occurs exclusively at the benzylic sp^3 CH bond. This type of side-chain oxidation can also be carried out in lower yield without bromide promotor, but higher amounts of $[\text{Co}(\text{OAc})_2]\cdot 4\text{H}_2\text{O}$ and MEK are necessary.²⁴

The azaphthalocyanines $\text{N}_x\text{-Pc}^*\text{H}_2$, shown in Fig. 2, were synthesized in a cyclotetramerization reaction following the reliable protocol of reacting PDN^* **1** and PyzDN^* **2** in a suspension of lithium in *n*-octanol at 180 °C.¹⁹ After workup with phosphoric acid and washing with methanol the mixture of the resulting four $\text{N}_x\text{-Pc}^*\text{H}_2$ **4a**, **5a**, **6a**, and **7a**, Pc^*H_2 **3a**, and Ppz^*H_2 **8a** was separated via gradient column chromatography PE/EE 10:1 → 1:1. Ppz^*H_2 **8a** could be finally eluted using DCM. Using a 1:1 ratio of PDN^* **1** and PyzDN^* **2** in this random co-cyclisation an overall yield of 39% of mixed (aza)phthalocyanines was obtained and separated by MPLC into six fractions: Main product is the A_2B_2 isomer **5a** (17%)

tetraazaphthalocyanine $N_4\text{-Pc}^*\text{H}_2$, followed by $AB_3\text{ N}_6\text{-Pc}^*\text{H}_2$ **7a** (9%) and Ppz^*H_2 **8a** (9%). Minor product was the ABAB isomer of $N_4\text{-Pc}^*\text{H}_2$ **6a** (<1%) as well as $A_3B\text{ N}_2\text{-Pc}^*\text{H}_2$ **4a** (3%) and Pc^*H_2 **3a** (1%). Even by increasing the amount of PDN^* **1**, or by increasing the temperature of the reaction, **5a** was obtained as main product. KOBAYASHI *et al.* reported about this phenomenon, when different electron deficient phthalonitriles with different sterical demand were used.¹⁹ Due to the similar steric bulk of both dinitriles, we assume a strong electronic influence in the reaction leading to a precyclisation of electron poor PyzDNs. $A_2B_2\text{ N}_4\text{-Pc}^*\text{H}_2$ isomer **5a** was differentiated from ABAB isomer **6a** by means of ^1H NMR and UV/Vis spectroscopy. After chromatographic isolation of the pure $N_x\text{-Pc}^*\text{H}_2$, all zinc complexes Pcs, $N_x\text{-[Pc}^*\text{Zn]}$ **3b-8b** were obtained using $[\text{Zn(hmds)}_2]$ or $[\text{Zn(OAc)}_2]\text{-}2\text{H}_2\text{O}$ as metallating agents. Attempts to purify mixtures of zinc complexes by chromatography were of limited success.

In addition, we attempted to synthesize compounds **5a** and **6a** via KOBAYASHI ring expansion.²⁵ Following this synthetic strategy, we synthesized a series of azasubphthalocyanines $N_x\text{-[Spc}^*\text{BCl]}$ **9-12** shown in Fig. 3. $[\text{Spc}^*\text{BCl}]$ **9** and $[\text{Sppz}^*\text{BCl}]$ **12** was synthesized according to literature known procedures, using boron trichloride in a solvent such as toluene or *o*-xylene.²⁰ Compared to $[\text{Spc}^*\text{BCl}]$ **9** with 13% yield, $[\text{Sppz}^*\text{BCl}]$

12 could be obtained in surprisingly high yields of 35%. $N_2\text{-[Spc}^*\text{BCl]}$ **10** and $N_4\text{-[Spc}^*\text{BCl]}$ **11** were obtained by using both dinitriles PN^* **1** and PyzDN^* **2** in a ratio 1:1. The ring expansion was attempted with $[\text{Spc}^*\text{BCl}]$ **9**, $[\text{Sppz}^*\text{BCl}]$ **12**, and $N_4\text{-[Spc}^*\text{BCl]}$ **11**. Therefore, the isoindoline compound of PN^* **1**, or PyzDN^* **2** in case of $[\text{Spc}^*\text{BCl}]$ **9**, was generated *in situ* by introducing ammonia in a NaOMe/MeOH solution.

To $[\text{Sppz}^*\text{BCl}]$ **12**, the isoindoline of **1** was added in DMSO and the solution stirred at 120°C for 8 h, yielding $AB_3\text{ N}_6\text{-[Pc}^*\text{M}]$ **7**. In the case of $[\text{Spc}^*\text{BCl}]$ **9**, reacting with the isoindoline of PyzDN^* **2**, no ring expansion can be observed. A ring expansion is favoured, the more electron deficient the Spc is, the more electron rich the isoindoline compound is, respectively. In the case of the insertion of isoindoline of **1** in $N_4\text{-[Spc}^*\text{BCl}]$ **9**, $A_2B_2\text{ N}_4\text{-Pc}^*\text{H}_2$ **5a** was obtained. This verifies the electronic influence of the pyrazine units upon cyclotetramerisation.

UV/Vis spectroscopy and CV. The synthesized $N_x\text{-Pc}^*\text{H}_2$ have been characterized by using UV/Vis spectroscopy and cyclic voltammetry (CV). By increasing the number of pyrazine units, a gradual hypsochromic shift of the Q-band can be observed, the higher the number of inserted [-N=] units is: from 707 nm for Pc^*H_2 **3a** to 652 nm for Ppz^*H_2 **8a** in THF, and from 575 nm for

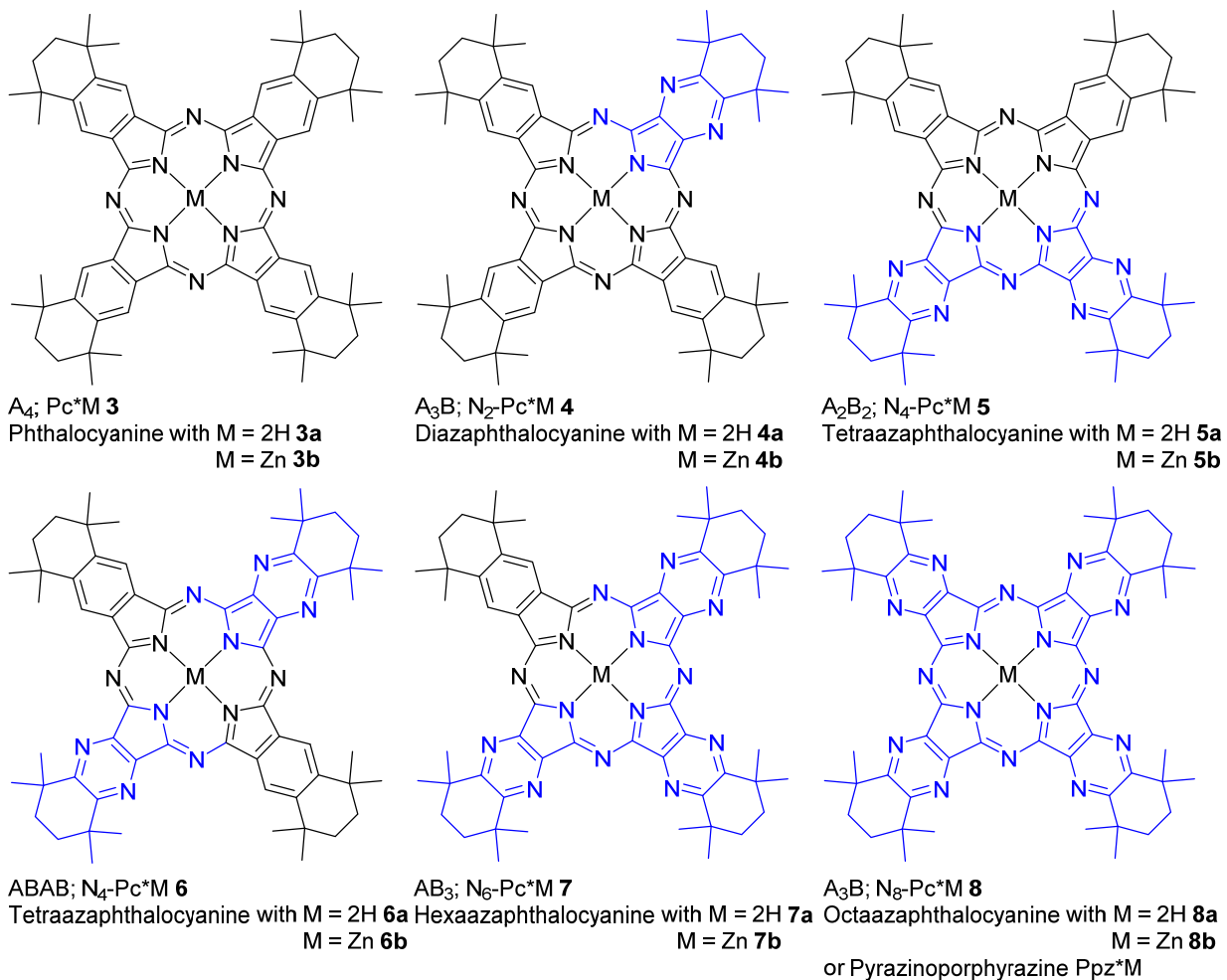


Figure 2. Discussed azaphthalocyanines $N_x\text{-[Pc}^*\text{M]}$ ($M = 2\text{H}, \text{Zn}, n = 0, 2, 4, 6, 8$).

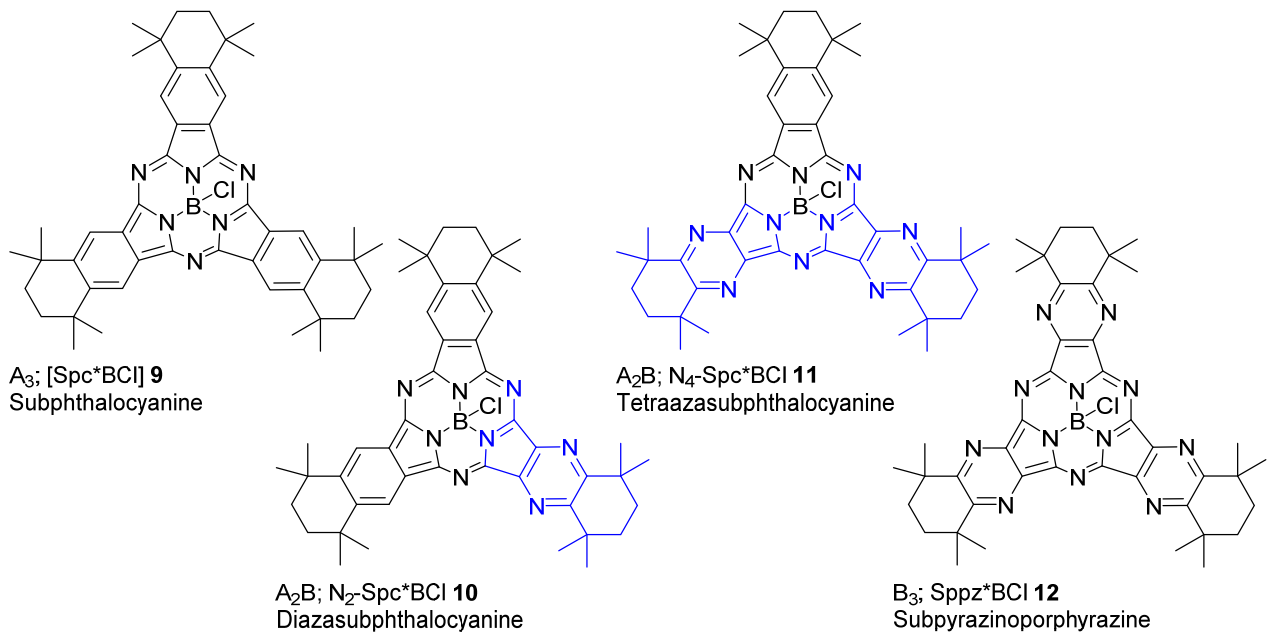


Figure 3. Discussed azasubphthalocyanines $N_x[\text{Spc}^*\text{BCI}]$ ($n=0, 2, 4, 6$).

[Spc^*BCI] 9 to 533 nm for [Sppz^*BCI] 12 in MeOH. The studied Pcs were of lower symmetry either due to the presence of the different number of pyrazine units or due to presence of central hydrogens in $N_x\text{-Pc}^*\text{H}_2$ that was reflected in the splitting of the Q-bands. In the metal-free series $N_x\text{-Pc}^*\text{H}_2$, the splitting occurred for all the macrocycles although, e.g. in case of **4a** and **7a** was only barely detectable and in particular for the former one manifested only by asymmetric broadening of the Q-band (Fig. 4). The strongest splitting was expected to be visible for ABAB type macrocycle **6a**. In this case, however, seemingly one main Q-band was detected. Closer inspection, however, revealed a shoulder at 701 nm as an indication of the split band. This small-intensity band at 701 nm was also detected in fluorescence excitation spectra (see electronic supplement, Fig. SA).

Considering this small band, the splitting of the Q-band is then the strongest in the series of all studied Pcs in accordance with literature data for lower symmetrical Pcs.²⁶ After insertion of a zinc atom, the lower symmetrical $A_3\text{B}$ and AB_3 $N_x[\text{Pc}^*\text{Zn}]$ **4b** and **7b** showed a weak splitting of their Q-bands. This is caused by the $1e_g$ orbitals, which are not degenerate anymore. Single unperturbed Q-band was expectedly observed for both symmetrical **3b** and **8b** but also for $A_2\text{B}_2$ isomer **5b** although being of lower C_{2v} symmetry. This observation is, however,

typical for adjacent isomers of $A_2\text{B}_2$ type and has been reported several times in literature.^{26,27}

The UV/Vis spectra correlate with the measured CVs. In Table 1, the measured and computed excitation energies are listed. The optical values, calculated by using UV/Vis spectroscopy, are in agreement with the determined redox excitation energies observed in CV measurements.

Table 1. Obtained oxidation and reduction potentials of $N_x\text{-Pc}^*\text{H}_2$ in DCM.^a potentials E_{red}^1 , E_{red}^2 , and E_{ox} are expressed as $E_{1/2}$ (in V vs. SCE) with Fc/Fc^+ as the internal standard. ^b potential difference as the difference between the first oxidation and reduction potential. ^c UV/Vis data. ^d calculated HOMO-LUMO gap, from determined optical UV/Vis values.

	Ppz'H ₂ (8a)	N ₆ -Pc'H ₂ (7a)	N ₄ -Pc'H ₂ (6a)	N ₄ -Pc'H ₂ (5a)	N ₂ -Pc'H ₂ (4a)	Pc'H ₂ (3a)
E_{ox} / V	0.87	0.35	0.28	0.36	0.43	0.67
$E_{\text{red}}^1 / \text{V}$	-1.05	-1.47	-1.47	-1.37	-1.23	-0.97
$E_{\text{red}}^2 / \text{V}$	-1.37	-1.82	-1.79	-1.77	-1.65	-1.36
$E_g^{\text{CV}} / \text{V}$ ^b	1.92	1.82	1.75	1.73	1.67	1.58
$\lambda_{\text{max}} / \text{nm}$ ^c	655	660	674	680	687	711
HOMO-LUMO ^{optical} / eV ^d	1.89	1.87	1.85	1.82	1.80	1.74
HOMO-LUMO ^{calc.} / eV	1.52	1.44	1.36	1.41	1.35	1.35
HOMO-(LUMO+1) ^{calc.} / eV	1.59	1.56	1.52	1.46	1.45	1.37

The computed Q-band positions give the right trend in comparison to experiments, although the absolute numbers are around 100-130 nm smaller. The same conclusion holds for the HOMO-LUMO gap. It is found that the correlation is much better with the LUMO+1 orbital (D_{HL+1}) which is depicted in Figure SI-1 in the supporting information. A detailed discussion is given in the computational section. CV measurements were carried out with an rhd-instruments setup, using a 2000 μ L microcell in a glovebox. As working electrode a Pt electrode was used, a gold or Pt counter electrode as well as an Pt pseudo reference electrode. The compounds were measured in a 0.5 N [TBA]PF₆ in DCM solution using a 5 mmol solution of the N_x-Pc*H₂. All measurements have been carried out using a 0.1 mmol Fc in DCM as reference. All measured N_x-Pc*H₂ show one reversible oxidation process and two reversible reduction potentials, with exception for the Ppz*H₂ **8a**, as shown in Figure 4. In this case, no reversible redox process was observed. In agreement with the Q-band position, as measured by UV/Vis spectroscopy, the energy gap was increasing with the number of pyrazine units in the N_x-Pc*H₂. The increasing electron deficiency of the aromatic system correlating with the increasing number of [-N=] is also seen in ¹H NMR spectroscopy. An expected low field shift of the aromatic protons, the methylene protons, as well as the methyl protons by increasing the number of [-N=] can be observed. In summary, an almost linear trend could be observed in UV/Vis, CV and computational calculations. The origin of this trend is analysed in the computational discussion part below.

Photophysical properties. Electronic absorption spectra of the compounds are displayed in Fig. SI-1-3 of the supporting information. The Q-band can be shifted from 450 nm to 710 nm. The following trend is observed: the higher the number of inserted [-N=] atoms in the subphthalocyanine series (**9-12**), the more blue-shifted the Q-band within one type of π -system. At the high energy end we find the hexaaza-subphthalocyanines (533 nm) followed by tetraaza- (555 nm) and diaza-subphthalocyanines (566 nm) and finally the parent subphthalocyanine (575 nm). Same trend is observed for the phthalocyanine series in the region [Ppz*Zn] (640 nm) – Pc*H₂ (710 nm): The most blue-shifted Q-band is observed for octaaza-phthalocyanine, followed by hexaaza-, followed by the A₂B₂ and ABAB isomers of tetraaza-, of diaza- and finally by the parent phthalocyanine. Fluorescence emission spectra of all derivatives were measured in THF or MeOH (Fig. 4). They follow the same trends as the absorption spectra. The higher the number of [-N=] units replacing [-CH=], the more blue-shifted the maxima of the FL bands. Their shape and order mirrored the absorption Q-band with only small Stokes shifts (6 – 26 nm) between absorption and emission maximum. Position of the emission maximum can be finely tuned using the proper composition of the macrocycle (Fig. 4) that can be advantageously used in design of new fluorophores or photosensitizers with selected excitation and emission wavelength. Excitation spectra perfectly matched the absorption ones confirming that the compounds were in monomeric form in the solution during measurements and that

the photophysical data were not affected by aggregation (Figs. 4, and SI-1-3). Exception from this observation was detected for the weakest fluorescent of **8a**. In this case, the excitation spectrum was substantially different from the absorption one indicating that a different species (e.g. partially deprotonated on the central NH)²⁸ is responsible for the fluorescence emission. It might be connected with very weak fluorescent properties of **8a** as suggested below that do not allow detection of its signal. Consequently, the emission from the new species prevails even when present as very minor component. In the zinc series N_x-[Pc*Zn], the sum of the fluorescence quantum yield ($\Phi_F = 0.18\text{-}0.35$) and singlet oxygen quantum yield ($\Phi_\Delta = 0.56\text{-}0.73$) for a particular compound, were relatively constant (Table 2, Fig. 5) reaching values typically close to 0.9. The only difference between the compounds in the series was in relative contribution of the two processes. Different situation was observed in the metal-free series N_x-Pc*H₂. The sum of the quantum yields was significantly decreasing with the increasing number of aza-substitution with compounds **7a** and **8a** being almost photophysically inactive (from the point of view of Φ_F and Φ_Δ).

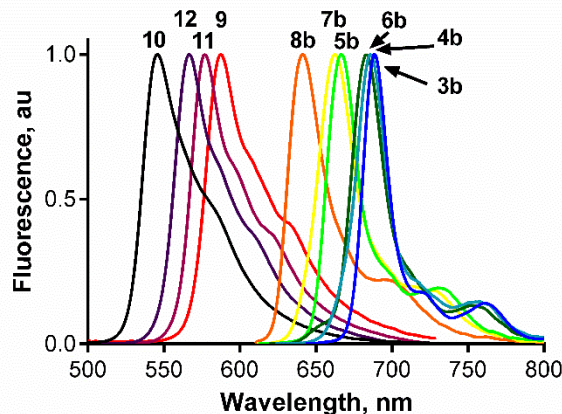


Figure 4. Normalized emission spectra of N_x-Pc*Zn in THF ($\lambda_{\text{exc}} = 598$ nm) and N_x-Spc*BCl in MeOH ($\lambda_{\text{exc}} = 490$ nm).

This interesting phenomenon does not have a clear explanation at this moment but is fully consistent with recently reported photophysical data for some metal-free Ppz.^{28,29} The presented series **3a-8a** is, however, unique as the photophysical data for metal-free derivatives are reported only from the members lying on the edges of the N_x-Pc*H₂ series (i.e. only for x = 0 and x = 8).

The trend observed on the Fig. 5 clearly indicated that the introduction of the nitrogens into the Pc ring increases the feasibility of this unknown non-radiative relaxation pathway in a stepwise manner. In the N_x-[Spc*BCl] series, the photophysical data resembled those obtained for zinc derivatives ($\Phi_F \sim 0.20$,

Table 2. Electronic and photophysical data of $N_x\text{-Pc}^*\text{M}$ in THF and $N_x\text{-Spc}^*\text{BCl}$ in MeOH. ^aabsorption maximum (λ_{\max}), fluorescence emission maximum (λ_F), fluorescence lifetime (τ_F), fluorescence quantum yield (Φ_F), singlet oxygen quantum yield (Φ_Δ). ^b $\lambda_{\text{exc}} = 371$ nm or 634 nm. ^cwith [PcZn] ($\Phi_{F(\text{THF})} = 0.32$, $\lambda_{\text{exc}} = 598$ nm) and rhodamin G6 ($\Phi_{F(\text{EtOH})} = 0.94$, $\lambda_{\text{exc}} = 490$ nm) as reference for $N_x\text{-[Pc}^*\text{M]}$ and $N_x\text{-[Spc}^*\text{BCl]}$, respectively. ^dwith ZnPc ($\Phi_{\Delta(\text{THF})} = 0.53$) and bengal rose ($\Phi_{\Delta(\text{MeOH})} = 0.76$) as reference for $N_x\text{-[Pc}^*\text{M]}$ and $N_x\text{-[Spc}^*\text{BCl]}$, respectively.

	λ_{\max} (B-band) / nm	λ_{\max} (Q-band) / nm	λ_F / nm	τ_F / ns ^b	Φ_F^{c}	Φ_Δ^{d}	$\Phi_F + \Phi_\Delta$
Pc*H ₂ 3a	343	707, 673	711	5.52	0.42	0.16	0.58
N ₂ -Pc*H ₂ 4a	343	686	692	3.45	0.33	0.14	0.47
N ₄ -Pc*H ₂ 5a	358	678, 653	684	1.62	0.14	0.07	0.21
N ₄ -Pc*H ₂ 6a	353	668, (701)	674	1.79	0.16	0.10	0.26
N ₆ -Pc*H ₂ 7a	349	658, 643	664	3.92 (26%), 0.63 (74%)	0.06	0.04	0.10
N ₈ -H ₂ 8a	345	652, 623	658	2.15 (29 %), 0.36 (71%)	0.03	0.05	0.08
[Pc*Zn] 3b	350	683	689	3.31	0.31	0.59	0.90
N ₂ -[Pc*Zn] 4b	353	679, 668	686	2.69	0.25	0.63	0.88
N ₄ -[Pc*Zn] 5b	356	658	667	3.08	0.35	0.56	0.91
N ₄ -[Pc*Zn] 6b	355	679, 651	687	1.98	0.18	0.73	0.91
N ₆ -[Pc*Zn] 7b	353	648	663	2.69	0.27	0.62	0.89
N ₈ -[Pc*Zn] 8b	347	633	642	2.98	0.30	0.57	0.87
[Spc*BCl] 9	266	575	587	2.04	0.18	0.65	0.82
N ₂ -[Spc*BCl] 11	272	566	577	2.19	0.21	0.62	0.82
N ₄ -[Spc*BCl] 12	288	555	567	2.85	0.23	0.64	0.87
[Sppz*BCl] 10	301	533	546	2.98	0.19	0.69	0.87

$\Phi_\Delta \sim 0.65$) with sum of Φ_F and Φ_Δ over 0.80 indicating that both these processes are predominant in the relaxation of the excited states also in Spc derivatives.

validating the fluorescence data. Only in case of metal-free **7a** and **8a**, the decay curves were biexponential with increased contribution of the fast component. It supports the fact that another relaxation pathway occurs by the metal-free compounds as proposed above.

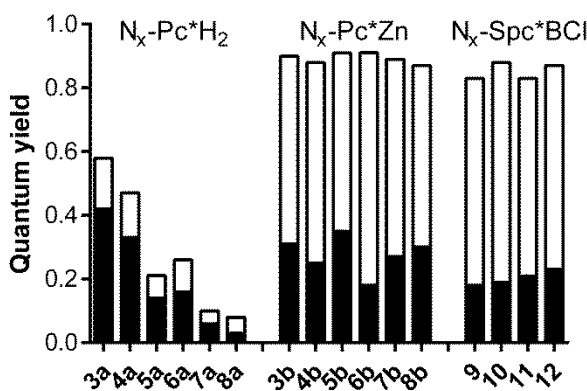


Figure 5. Fluorescence quantum yields (Φ_F , full columns) and singlet oxygen quantum yields (Φ_Δ , blank columns) for $N_x\text{-[Pc}^*\text{M}]$ in THF and $N_x\text{-[Spc}^*\text{BCl}]$ in MeOH.

The data are well comparable with the reported values of Spcs with different peripheral substitution.³⁰ No significant differences between fluorescence and singlet oxygen production were observed in dependence on the number of nitrogen atoms. The fluorescence emission properties were complemented by the fluorescence lifetimes (Table 2).

The fluorescence decays were characterized by mono-exponential curves for most of the studied compounds and τ_F values correlated well with the Φ_F values (Fig. SI-4) further

Crystal structure of [Spc*BCl], $N_2\text{-Pc}^*\text{H}_2$, and $A_2\text{B}_2\text{N}_4\text{-[Pc}^*\text{Zn}\cdot\text{H}_2\text{O}]$. Suitable crystals for X-Ray diffraction of [Spc*BCl] **9**, $N_2\text{-Pc}^*\text{H}_2$ **4a** and $A_2\text{B}_2\text{N}_4\text{-[Pc}^*\text{Zn}\cdot\text{H}_2\text{O}]$ **5b** were obtained from a saturated DCM-*d*₂ solution. Of all compounds, selected crystallographic datas are collected in the supporting information. [Spc*BCl] **9** crystallizes in the orthorombic crystal system Cmc₂1. The molecular structure of [Spc*BCl] **9** is shown in Fig. 6. Similar, to other literature known subphthalocyanines the boron(III)-atom in the [Spc*BCl] **9** is almost perfect tetrahedrally surrounded by one chlorine atom and three nitrogen atom. The boron is out of plane to the π -system. These are the reasons why only three isoindoline units are around the smaller boron atom, and causes the π -system to contract. In the crystal structure, the annulated methyl substituted cyclohexene ring shows the typical twisted chair conformation, which explains the multiplett of the methylene group observed in ¹H NMR spectroscopy (Fig. SI-6). The characteristic bond lengths of the B-Cl and B-N^{isoindoline} are listed in Table 3, compared to the first literature known [SpcBCl] by KIETAIBL.³¹

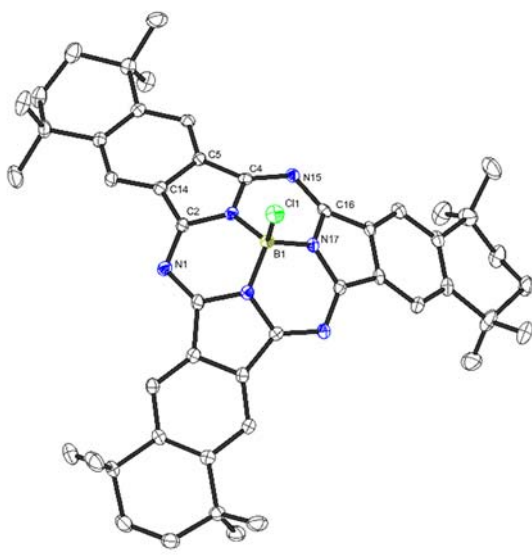


Figure 6. Molecular structure of $[Spc^*BCl]$ **9** in crystal. Bond distances and angles and the lattice structure are presented in the SI.

With a bond length of B-Cl of 1.85 \AA , it is within the expected range, as well as all values found for C-C bonds in the aromatic system and C-N bonds of pyrrole units. The bowl depth of 0.56 \AA , as a value for the position boron atom above the inclined [-BN₃-] plane is also comparable to $[SpcBCl]$.³¹ In addition to the $[Spc^*BCl]$ **9**, $[Sppz^*BCl]$ was crystallised, but because the low quality of the crystal an appropriate discussion of the bond length is not possible, but in comparison to $[Spc^*BCl]$ information of the molecular arrangement in solid state can be obtained. The structure of $[Sppz^*BCl]$ is attached to the SI.

Table 3: Selected bond length (\AA) and angles ($^\circ$) of $[Spc^*BCl]$ **3** and $[SpcBCl]$.^a

	$[Spc^*BCl]$ (3)	$[SpcBCl]$
B1-Cl1	1.852(4)	1.863(7)
B1-N1	1.480(3)	1.466(8)
B1-N3	1.479(4)	1.468(5)
B1-N5	1.480(3)	1.466(8)
N1-B1-Cl1, N3-B1-Cl1, N5-	112.2(2), 115.7(2),	113.8(19, 112.8(1),
B1-Cl1	112.2(2)	113.8(1)
N1-B1-N3, N3-B1-N5,	105.4(2), 105.0(3),	105.1(1), 105.3(0),
N1-B1-N5	105.4(2)	105.3(0)
¶Isoindoline	44.2	43.1-44.3

The free ligand of $N_2-[Pc^*H_2]$ **4a** was crystallized and a monoclinic system with a $P2_1/c$ space group was determined. Here, also the twisted-chair conformation of the methylene ring is visible. The crystal structure is disordered, so in every molecule the non-peripheral position is partly occupied by a quarter [-N=]

units and three quarters [-CH=], for the same reason, each NH position is occupied with a factor of 0.5 as shown in Fig. 7 in light blue. The molecular arrangement differs from unsubstituted Pc , where a *heringbone* pattern is typical.

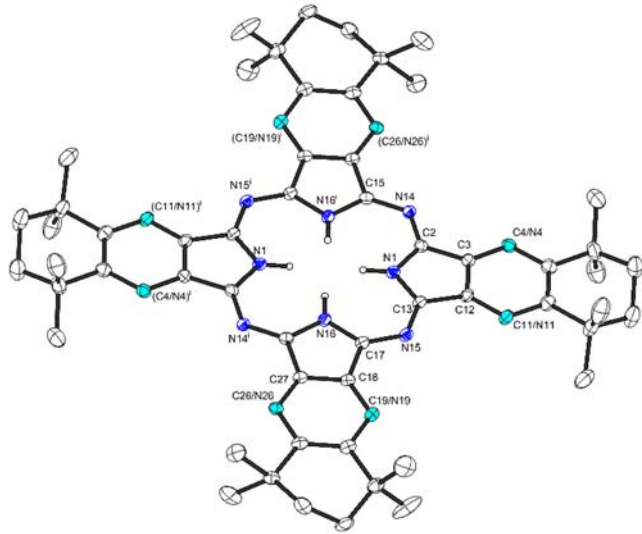


Figure 7. Molecular structure of $N_2\text{-}Pc^*\text{H}_2$ **4a** in the crystal. Corresponding C and N positions of pyrazine and benzene rings are statistically 75:25 occupied. Bond distances and angles and the lattice structure are presented in the SI. Similar to the previously reported strucuture of $Pc^*\text{H}_2$, in one unit cell the molecules are orientated perpendicular to each other.

For the first time, a lower symmetrical, alkyl substituted $N_4\text{-}[Pc^*\text{Zn}\cdot\text{H}_2\text{O}]$ was structurally characterized. In comparison to known zinc phthalocyanines bearing water as axial ligand, such as $[Pc\text{Zn}\cdot\text{H}_2\text{O}]\cdot2\text{dmf}$,³² in the molecular packing the described perpendicular orientation of the molecules is visible. Furthermore, the axial water pulls the zinc out of the ligand cavity [-MN₄-].

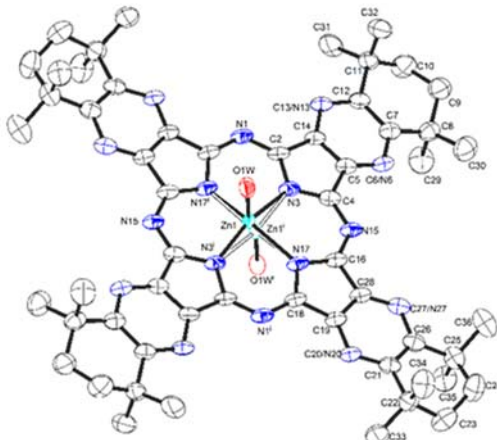


Figure 8. Molecular structure of $A_2B_2 N_4\text{-}[Pc^*\text{Zn}] 5b$ in crystal. Corresponding C and N positions of pyrazine and benzene rings are statistically 75:25 occupied. Bond distances and angles and the lattice structure are presented in the SI.

Computational Studies

The electronic structure of the compounds presented here are further analysed with density-functional theory using the PBE and B3LYP exchange-correlation functionals and including dispersion corrections (DFT-D3) for the structural optimization. With the aim to derive trends with increasing nitrogen substitution, the series from $[Pc^*\text{M}]$ to $[Ppz^*\text{M}]$ with $\text{M} = \text{H}_2, \text{Zn}$ was investigated. All structures including regioisomers and tautomers are shown in Fig. SI-5 in the supporting information. For **6a**, two regioisomers A_2B_2 and ABAB, were found which are separated by only 5.6 kJ mol^{-1} . Furthermore, for compounds **4a**, **5a** and **7a**, two tautomers are observed. Only for the more favored regioisomer of **6a** (A_2B_2), a significantly lower stability of one tautomer is found ($\Delta E = 56.4 \text{ kJ mol}^{-1}$). For all other compounds, an equilibrium of tautomers under experimental conditions can be concluded ($\Delta E = 4.0 \text{ kJ mol}^{-1}$). For the Zn-substituted phthalocyanines, the two regioisomers **5b** and **6b** show an energy difference of 1.6 kJ mol^{-1} . Due to the small energy differences, the analysis of the electronic structure was therefore carried out for all isomers described.

The absorption characteristics for all compounds as derived from time-dependent density functional theory (TD-DFT) computations are summarized in Table SI-1 in the supporting information. The density functional used (B3LYP) has previously been found to provide good agreement with experiment.²¹ The values for $Pc^*\text{H}_2$ **3a** are comparable although a smaller basis set was used before.²¹

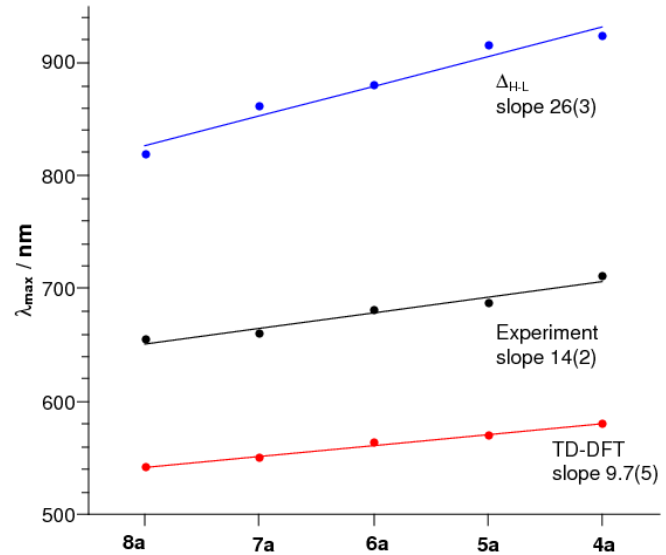


Figure 9: Orbital energies for HOMO (black), LUMO (red), and LUMO+1 (blue) for varying N-content of $Pc^*\text{H}_2$. Orbitals for $Pc^*\text{H}_2$ are depicted.

We find – with few exceptions – two absorption energies for the Q-bands as was found earlier for unsymmetric Pc derivatives.¹⁹ The splitting is nevertheless very small and is not relevant for the interpretation of experimental UV/Vis spectra since the peaks observed are broader than the energy differences computed here (Fig. 4). The absorption maxima upon increase of the nitrogen content in going from $Pc^*\text{H}_2$ **3a** to $Ppz^*\text{H}_2$ **8a** are shifting to higher absorption energies, independent of hydrogen or Zn being in the center. An exception is tautomer **5a_T** which has a higher excitation energy than **4a**.

Since this tautomer is much less stable than **5a**, it will not be observed in the experimental spectrum. The shift to higher excitation energies here is stronger than was found for the substitution of the bridging carbon atom by nitrogen.¹⁹ Oscillator strengths are rather large and very similar for both Q-bands. They do not change along the series of compounds investigated.

The character of the Q-bands is in all cases dominated by the $\text{HOMO}\rightarrow\text{LUMO}$ or the $\text{HOMO}\rightarrow\text{LUMO+1}$ transition. The small energy differences in the absorption maxima of the Q-bands can therefore be understood by the close energetic proximity of the LUMO and LUMO+1 orbital (Fig. 9). But even for the most symmetric molecules carrying hydrogen, the orbitals do not have the same energy and therefore lead to different Q-band energies. This is a consequence of the necessity to choose one tautomer in the computations. The resulting structure exhibits inequivalent nitrogen atoms in the ring, leading to the different

orbital energies of LUMO and LUMO+1 which are located either on the hydrogen-carrying or the hydrogen-free nitrogen atoms (orbital insets in Fig. 9).

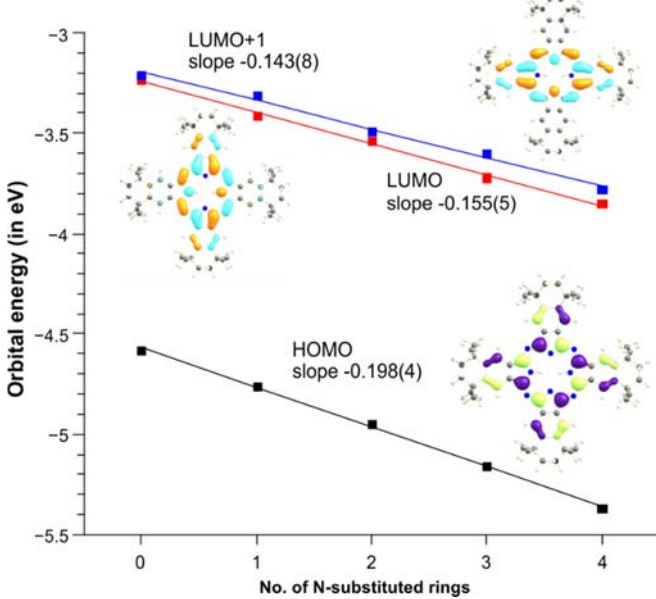


Figure 10: Trend of experimental (black), TD-DFT (red), and D_{H-L} (blue) absorption maxima with linear regression curves for Pc^*H_2 .

In experiment, the tautomeric equilibrium will result in an averaging of this difference and thus lead to only one, broader excitation in addition to the usual broadening effects in UV/Vis spectra.

The difference between frontier orbital energies ($\Delta HOMO/LUMO$ and $\Delta HOMO/LUMO+1$ in Table SI-1) gives much higher values than the computed excitation energies due to the missing orbital relaxation in this estimate. Nevertheless, the trend is the same compared to the TD-DFT results: increase of the gap with increased nitrogen content. The comparison of experimental excitation energies and computed ones from TD-DFT and the $\Delta H-L$ approach is shown in Fig. 10. The experimental trend of increasing excitation energies with increasing nitrogen content is reproduced by both computational approaches. But both approaches fail to quantitatively reproduce the experimental slope and the absolute excitation energies, while the more accurate TD-DFT approach gives results in better agreement with experiment. This indicates that both computational approaches are appropriate for deriving trends in excitation energies for substituted phthalocyanines but further improvement is needed to achieve a quantitative agreement.

Since the frontier orbital gap is a suitable description for the excitation energies, the question arises if the excitation energy trend observed in the aza-substituted phthalocyanines is due to a change in the energy levels of occupied or unoccupied orbitals. The orbital energies for the lowest-energy structures of the series of compounds investigated is shown in Fig. 10. While LUMO and LUMO+1 show a similar slope, the occupied

HOMO shows a quicker decrease in energy upon nitrogen substitution (larger slope). Thus, lowering the HOMO energy is the determining factor for the experimentally observed trend in the excitation energies.

The dipole moment μ and polarizability α are crucial quantities for the application of phthalocyanines. Both values are listed in Table SI-1 for the series of compounds investigated. The observed dipole moment of up to 1.25 a.u. can easily be rationalized by looking at the structure of the compounds investigated. The N-substituted rings show higher electron density and are thus always at the negative end of the dipole moment vector. In case of more than one ring being N-substituted, the direction of the dipole moment can be derived from vector addition. The polarizability of the compounds is also included and shows a slight increase upon substitution of C-H groups by the more polarizable N atom. Every aza-substituted ring adds approx. 23 a.u. to the isotropic polarizability and the trend is irrespective of hydrogen or Zn being in the center of the molecule.

Conclusions

We presented the first systematic study on the synthesis, the spectroscopic, electroanalytical, photophysical, structural, and computational analysis of three complete series of azaphthalocyanines and azasubphthalocyanines: $N_x-Pc^*H_2$ or $N_x-[Pc^*Zn]$ ($n = 0, 2, 4, 6, 8$), and $N_x-[Spc^*BCl]$ ($n = 0, 2, 4, 6$), respectively.

Whereas non-aggregating soluble A_4 -type phthalocyanines and B_4 -type pyrazinoporphyrazines (octaazaphthalocyanines) are easily isolated in pure form and well studied in literature, this paper is dedicated to the unsymmetrical hybrid chromophores of $A_{4-n}B_n$ and $A_{3-n}B_n$ -type. The effect of increasing number of $[-CH=]$ units being stepwise substituted by $[-N=]$ units on photophysical (UV-Vis, fluorescence) and electrochemical (CV) properties were correlated with the results of computational calculations (TD-DFT). This study offers insight to predict trends of the absolute HOMO and LUMO levels and of the HOMO-LUMO gap, of the absolute chromophore dipole moment and polarizability, and maybe even of their singlet-oxygen versus fluorescence quantum yield by chemical design. These are fundamental properties relevant to applications of such chromophores as sensitizers in dye sensitized solar cells (DSSCs)³³, their injection of electrons into a wide band gap inorganic semiconductor CB³⁴ on the one hand, or as singlet oxygen generators in PDT³⁵ by energy transfer on the other hand. All chromophores described herein are suitable for organic molecular beam epitaxy, they can be sublimed in HV without decomposition while parent azaphthalocyanines, e.g. $PpzH_2$ or $PpzZn$, do not sublime without decomposition.

The synthesis of this class of weakly aggregating, soluble azaphthalocyanines, N_x-Pc^*M and $N_x-[Spc^*BCl]$, has been greatly improved by introducing a highly selective catalytic aerobic oxidation of the 1,1,4,4,5,6-hexamethyltetraline to corresponding phthalic acid key building block. For the first time, insight into the molecular and lattice structures of

symmetrical 2,2,5,5-tetramethylcyclohexane substituted [Spc^{*}BCl] and Sppz [Sppz^{*}BCl], as well as of lower symmetry N₂-Pc^{*}H₂ and A₂B₂-type N₄-[Pc^{*}Zn] was gained via single crystal XRD.

Upon increasing number of [-N=] units replacing [-CH=] a linear increase of the HOMO-LUMO gap and the excitation energies was observed. The optical HOMO-LUMO levels were correlating with the potentials determined by CV. Computational analysis gave the correct trend regarding the increase of excitation energies upon aza-substitution with ground state (DFT) and excited state (TD-DFT) methods although quantitative agreement needs refined methods. The trend can be traced back to the HOMO energy rising quicker than the LUMO and LUMO+1 energies. Transitions from the HOMO into these two orbitals determines the Q-bands. The trends in computed dipole moments and polarizabilities are in line with the substitution patterns. Strong dipole moments are observed for asymmetrically substituted N_x-[Pc^{*}M] molecules while polarizability increases with the increasing nitrogen content. Both methods – frontier orbital gap and time-dependent density functional theory – provide the right trends but fails to reproduce the absolute values observed in experiment.

The photophysical determination of fluorescence versus singlet oxygen quantum yield evidenced that a fast non-radiative relaxation pathway occurs for the metal-free derivatives N_x-Pc^{*}H₂ and that the feasibility of this process clearly increases with number of nitrogen atoms in the macrocycle core. For the N_x-[Spc^{*}BCl] and N_x-[Pc^{*}Zn] series, the photophysical data revealed essentially 100% quantum yield as sum of fluorescence quantum yields (Φ_F) and singlet oxygen quantum yields (Φ_A), non-radiative decay paths are suppressed. Thus fine tuning of absorption and emission maxima was demonstrated in these two series of dyes.

Experimental Section

6,7-Dicyano-1,1,4,4-tetramethyltetraline (PN* **1**,¹⁸ 5,5,8,8-tetramethyl-5,6,7,8-tetrahydro-chinoxaline-2,3-carbodinitrile (PyzDN* **2**),^{12,36} and precursors were prepared according to literature known procedures. The final dinitrils **1** and **2** were purified by using column chromatography or, if necessary, sublimed before use. nOctanol was obtained from Merck, dried according to standard methods and all reactions were handled using standard SCHLENK techniques.

The electronic UV/Vis spectra were recorded on an Avantes AvaSpec-2048 spectrometer in a glovebox. IR spectra were recorded on a BrukerAlpha FT-IR spectrometer with an ATR measurement setup (diamondcell) in a glovebox using neat samples. APCI-HR mass spectra were measured with a Finnigan LTQ-FT spectrometer using dichloromethane/acetonitrile as solvent. ¹H and ¹³C NMR spectra were recorded on a Bruker AVII 300 MHz. X-ray diffraction (XRD) analyses was performed on a QUEST area detector system using Mo K α radiation ($\lambda = 71.073$ pm) at 100 K. Stoe Quest software was used for integration and data reduction; structure solution and

refinement was done with the WinGX program suite using BRUKER SAINT, xt v2014/1 and SHELX-2014/7. Molecular graphics were produced with Diamond 4.0. The SQUEEZE routine of the PLATON program package was used in these cases to remove the corresponding delocalized electron density from the data sets.

Cyclovoltametric measurements were carried out with an rhd-instruments setup, using a closed microcell in glovebox. As working electrode a Pt electrode was used, a gold or Pt counter electrode as well as an Ag reference electrode. The compounds have been measured in a 0.5 M TBAF in DCM solution using 5 mmol N_x-Pc^{*}H₂. All measurements have been carried out using a 0.1 mmol Fc in DCM as reference.

Synthesis of 1,1,4,4-tetramethyltetraline-6,7-dicarboxylic acid
0.05 g NaBr (486 μ mol), 125 mg [Co(OAc)₂]-4H₂O (502 μ mol), 3.00 g 1,1,4,4,6,7-hexamethyltetraline (13.9 mmol, 1 eq) were added in an autoclave. The autoclave was charged with 20 bar O₂ heated to 180 °C, 90 min. The pressure increased to 30 bar, dropped down to 20 bar. Autoclave was charged as often as necessary, until the pressure stayed the same. Carboxylic acid was precipitated out of the solution and washed with water. A second/third portion was yielded overnight, filtered, washed with water and finally dried in vacuum.

Yield: 97%. - ¹H NMR (300 MHz, [D₆]DMSO, 25 °C): $\delta = 13.07$ (s, 2 H, COOH), 7.57 (s, 2 H, Ar-H), 1.66 (s, 4 H, CH₂), 1.25 (s, 12 H, CH₂) ppm. - MS (ESI(+), MeOH): *m/z* = 277.1436, cal. for C₁₆H₂₀O₄+H₁: 277.1434. **Additional information:** Depending on the amount of glacial acid, the formation of the anhydride can be observed, which is the product of the following step in the synthesis of PN*. An up-scaling of the reaction is possible.

General procedure for N_x-[Spc^{*}BCl]: 1 eq PN* **1** (or PyzDN* **2**, or as a mixture) were dissolved in 2 mL toluene per 5 mmol dinitril. Fresh boron trichloride solution (1 N in heptane or in *o*-xylene, 1 eq) was added at once and then heated to 150 °C in a closed Schlenk tube. The yellowish solution turned into a deep pink. After heating for 2-5 h the solution was added on a short pluck of silica to remove insoluble byproducts. Spcs were purified by a column chromatography with silica gel 60 Merck and eluted with PE/EE 10:1.

[Spc^{*}BCl]: Yield: 13%. - R_f (Tol/THF 30:1) = 0.27. - ¹H NMR (300 MHz, C₆D₆, 25 °C): $\delta = 8.91$ (s, 6 H, Ar-CH), 1.65-1.52 (m, 12 H, CH₂), 1.42 (s, 18 H, CH₃), 1.10 (s, 18 H, CH₃) ppm. - ¹H NMR (300 MHz, [D₂]DCM, 25 °C): $\delta = 8.84$ (s, 6 H, Ar-CH), 1.94-1.80 (m, 12 H, CH₂), 1.66 (s, 18 H, CH₃), 1.44 (s, 18 H, CH₃) ppm. - ¹³C NMR (75 MHz, CDCl₃, 25 °C): $\delta = 150.0$, 148.3, 130.0, 120.6, 35.5, 35.3, 32.6, 32.1, 30.1 ppm. - IR: $\tilde{\nu} = 2959$ (m), 2925 (m), 2861 (m), 1729 (w), 1623 (w), 1466 (m), 1259 (m), 1088 (s), 796 (s), 662 (m) cm⁻¹. - UV/Vis (DCM): $\lambda = 582$ (s), 528 (sh), 318 (s), 267 (s) nm. - Fluorescence (DCM, $\lambda_{ex} = 350$ nm): $\lambda = 592$ nm. - MS (APCI-HRMS(+)): *m/z* = 761.4247 [M+H]⁺, cal. for C₄₈H₅₄B₁Cl₁N₆+H: 761.4272.

[Sppz^{*}BCl]: Yield: 35%. - R_f (Tol/THF 30:1) = 0.35. - ¹H NMR (300 MHz, CDCl₃, 25 °C): $\delta = 1.94$ -2.07 (m, 12 H, CH₂), 1.75 (s, 18 H, CH₃), 1.52 (s, 18 H, CH₃) ppm. - ¹³C NMR (75 MHz, CDCl₃, 25 °C): $\delta = 162.9$, 146.2, 140.7, 39.3, 34.0, 30.2, 30.8 ppm. - IR: $\tilde{\nu} = 2956$ (m), 2922 (m), 2859 (m), 1708 (w), 1557 (m), 1454 (s), 1371 (s), 1356 (m), 1243 (vs), 1107 (s), 1045 (s), 798 (s), 733 (m) cm⁻¹. - UV/Vis (DCM): $\lambda = 534$ (s), 489 (sh), 334 (m), 303 (s) nm. -

Fluorescence (DCM, $\lambda_{\text{ex}} = 350$ nm): $\lambda = 546$ nm. - **MS** (APCI-HRMS(+)): $m/z = 767.3964$ [M+H]⁺, cal. for C₄₂H₄₉B₁Cl₁N₁₂+H: 767.3980.

N₄-[Spc^{*}BCl]: Yield: 2%. - **¹H NMR** (300 MHz, CDCl₃, 25 °C): $\delta = 8.76$ (s, 2 H, ArCH), 1.76-1.48 (m, 12 H, CH₂), 1.67 (s, 6 H, CH₃), 1.65 (s, 6 H, CH₃), 1.64 (s, 6 H, CH₃), 1.36 (s, 6 H, CH₃), 1.36 (s, 6 H, CH₃), 1.34 (s, 6 H, CH₃) ppm. - **IR** (ATR, 400-4000 cm⁻¹): $\tilde{\nu} = 2957$ (m), 2869 (w), 1455 (m), 1253 (m), 1088 (s), 1020 (s), 797 (s), 701 (m), 516 (m) cm⁻¹. - **UV/Vis** (DCM): $\lambda = 557$ (s), 506 (sh), 330 (m), 296 (s) nm. - **MS** (APCI-HRMS(+)): $m/z = 765.4075$ [M+H]⁺, cal. for C₄₄H₅₁B₁Cl₁N₁₀+H: 765.4082.

N₂-[Spc^{*}BCl]: Yield: 3%. - **¹H NMR** (300 MHz, CDCl₃, 25 °C): $\delta = 8.87$ (s, 2 H, ArCH), 8.78 (s, 2 H, ArCH), 1.73-1.50 (m, 12 H, CH₂), 1.67 (s, 6 H, CH₃), 1.42 (s, 6 H, CH₃), 1.38 (s, 6 H, CH₃), 1.36 (s, 6 H, CH₃), 1.05 (s, 6 H, CH₃), 1.03 (s, 6 H, CH₃) ppm. - **IR** (ATR, 400-4000 cm⁻¹): $\tilde{\nu} = 2960$ (m), 2925 (w), 2861 (w), 1459 (w), 1259 (s), 1090 (s), 1016 (s), 791 (s), 695 (m) cm⁻¹. - **UV/Vis** (DCM): $\lambda = 572$ (s), 519 (sh), 327 (m), 303 (s) nm. - **MS** (APCI-HRMS(+)): $m/z = 763.4173$ [M+H]⁺, cal. for C₄₆H₅₃B₁Cl₁N₈+H: 763.4177.

The N_x-[Spc^{*}BCl] are unstable towards light in solution and should be kept in the dark under inert gas. In the ¹H NMR N_x-[Spc^{*}BCl] free dinitrile of degenerated N_x-[Spc^{*}BCl] was observed which could not be separated.

Synthesis of N_x-Pc^{*}H₂ 240 mg lithium was dissolved in 10 mL noctanol at 120 °C within 20 min. After cooling down to rt, 1.0 g PN* **1** (4.19 mmol, 2 eq) and 1.0 g PyzDN* **2** (4.16 mmol, 2 eq) were added and stirred for 10 h at 180 °C. The solutions had a change in color to deep green. After cooling down to rt, 100 mL MeOH and 3 mL H₃PO₄ were added. The solution was further washed 3 x 100 mL with MeOH. The product mixture was separated using gradient column chromatography with PE/EE 10:1 → 1:1. First, P^c*H₂ **3a** and N₂-Pc^{*}H₂ **4a** was eluted, then the ABAB and A₂B₂ N₄-Pc^{*}H₂ **5a**, **6a** was eluted. After changing the solvent to PE/EE 1:1 N₆-Pc^{*}H₂ **7a** was eluted. Finally Ppz^{*}H₂ **8a** was eluted with DCM.

(¹Pc^{*}H₂: Yield: 20 mg, 20.9 mmol, 1%. - **¹H NMR** (300 MHz, CDCl₃, 25 °C): $\delta = 9.91$ (s, 8 H, Ar-H), 1.79 (s, 16 H, CH₂), 1.54 (s, 48 H, CH₃), -0.01 (s, 2 H, NH) ppm. - **UV/Vis** (DCM): $\lambda = 710$ (s), 677 (s), 647 (sh), 615 (sh), 343 (s), 295 (sh), 231 (sh) nm. - **MS** (APCI-HRMS(+)): $m/z = 955.6096$ [M+H]⁺, cal. for C₆₄H₇₅N₈+H: 955.6109.

N₂-Pc^{*}H₂: Yield: 48 mg, 50.1 mmol, 3%. - **¹H NMR** (300 MHz, CDCl₃, 25 °C): $\delta = 9.69$ (s, 2 H, Ar-H), 9.65 (s, 2 H, Ar-H), 9.42 (s, 2 H, Ar-H), 2.19 (s, 4 H, CH₂), 2.07 (s, 8 H, CH₂), 2.04 (s, 4 H, CH₂), 1.90 (s, 12 H, CH₃), 1.83 (s, 12 H, CH₃), 1.81 (s, 12 H, CH₃), 1.81 (s, 12 H, CH₃), -0.07 (s, 2 H, NH) ppm. - **¹³C NMR** (75 MHz, C₆D₆, 25 °C): $\delta = 160.6, 149.8, 149.2, 148.6, 137.0, 133.0, 132.2, 122.2, 121.6, 39.1, 36.1, 36.1, 35.9, 35.4, 35.3, 34.7, 32.9, 32.8, 32.7, 30.9$ ppm. - not all quartary atoms could be detected. - **IR** (ATR, 400-4000 cm⁻¹): $\tilde{\nu} = 2956$ (m), 2921 (s), 2855 (m), 1711 (w), 1688 (w), 1498 (m), 1301 (s), 1071 (s), 1022 (m), 755 (s), 722 (m) cm⁻¹. - **UV/Vis** (DCM): $\lambda = 687$ (s), 619 (sh), 340 (s), 306 (s), 232 (s) nm. - **MS** (APCI-HRMS(+)): $m/z = 957.5992$ [M+H]⁺, cal. for C₆₂H₇₂N₁₀+H: 957.6014.

ABAB N₄-Pc^{*}H₂: Yield: <1%. - **R_f** (PE/EA 4:1) = 0.53. - **¹H NMR** (CDCl₃, 300 MHz): $\delta = 9.79$ (s, 4 H, Ar-H), 2.22 (s, 8 H, CH₂), 2.11 (s, 8 H, CH₂), 1.90 (s, 24 H, CH₃), 1.85 (s, 24 H, CH₃), -0.68 (s, 2 H,

NH) ppm. **¹³C NMR** (C₆D₆, 75 MHz): $\delta = 29.8, 33.0, 36.5$ ppm. - **UV/Vis** (DCM): $\lambda = 672$ (s), 642 (sh), 607 (s), 347 (s), 309 (s) nm. - **MS** (APCI-HRMS(+)): $m/z = 959.5922$ [M+H]⁺, cal. for C₆₀H₇₀N₁₂+H: 959.5919.

A₂B₂ N₄-Pc^{*}H₂: **Yield:** 342 mg, 357 mmol, 17%. - **¹H NMR** (300 MHz, CDCl₃, 25 °C): $\delta = 9.56$ (s, 2 H, Ar-H), 9.50 (s, 2 H, Ar-H), 2.20 (s, 8 H, CH₂), 2.05 (s, 8 H, CH₂), 1.91 (s, 24 H, CH₃), 1.81 (s, 12 H, CH₃), 1.80 (s, 12 H, CH₃), -0.04 (s, 2 H, NH) ppm. - **¹³C NMR** (75 MHz, C₆D₆, 25 °C): $\delta = 162.4, 150.0, 149.6, 145.1, 144.4, 135.2, 134.8, 122.7, 122.0, 39.4, 39.3, 36.1, 36.0, 35.2, 34.6, 34.5, 32.7, 32.7, 21.1, 30.8$ ppm. - **IR** (ATR, 400-4000 cm⁻¹): $\tilde{\nu} = 2915$ (m), 2857 (m), 1358 (s), 1328 (s), 1148 (s), 1128 (s), 761 (m), 752 (m), 679 (s), 543 (w) cm⁻¹. - **UV/Vis** (DCM): $\lambda = 680$ (s), 656 (s), 625 (sh), 348 (s), 232 (s) nm. - **MS** (APCI-HRMS(+)): $m/z = 959.5921$ [M+H]⁺, cal. for C₆₀H₇₀N₁₂+H: 959.5919.

N₆-Pc^{*}H₂: **Yield:** 178 mg, 185 mmol, 9%. - **¹H NMR** (300 MHz, CDCl₃, 25 °C): $\delta = 9.75$ (s, 2 H, Ar-H), 2.22 (s, 4 H, CH₂), 2.19 (s, 12 H, CH₂), 1.93 (s, 12 H, CH₃), 1.91 (s, 12 H, CH₃), 1.90 (s, 12 H, CH₃), 1.83 (s, 12 H, CH₃), -0.53 (s, 2 H, NH) ppm. - **¹³C NMR** (75 MHz, C₆D₆, 25 °C): $\delta = 162.0, 139.1, 131.3, 134.1$ (w), 132.9 (w), 132.9 (w), 131.3 (w), 127.1 (w), 123.1, 46.0, 41.3 (w), 39.7, 39.3, 36.3, 34.5, 32.8, 31.8, 31.7, 31.1, 30.9, 30.8, 29.8, 29.5, 29.3, 29.2, 28.6, 28.1, 27.5, 27.5 ppm. - not all quartary atoms could be detected. - **IR** (ATR, 400-4000 cm⁻¹): $\tilde{\nu} = 2957$ (s), 2924 (s), 1727 (s), 1693 (w), 1511 (s), 1457 (m), 1411 (m), 1072 (m), 1021 (s), 756 (w), 744 (m), 677 (s) cm⁻¹. - **UV/Vis** (DCM): $\lambda = 660$ (s), 597 (sh), 343 (s), 234 (s) nm. - **MS** (APCI-HRMS(+)): $m/z = 961.5825$ [M+H]⁺, cal. for C₅₈H₆₈N₁₄+H: 961.5824.

(¹Ppz^{*}H₂: **Yield:** 174 mg, 181 mmol, 9%. - **¹H NMR** (300 MHz, CDCl₃, 25 °C): $\delta = 2.22$ (s, 16 H, CH₂), 1.93 (s, 48 H, CH₂), -1.02 (s, 2 H, NH) ppm. - **UV/Vis** (DCM): $\lambda = 655$ (s), 621 (s), 576 (s), 343 (s), 231 (s) nm. - **MS** (APCI-HRMS(+)): $m/z = 963.5732$ [M+H]⁺, cal. for C₅₆H₆₆N₁₆+H: 963.5729.

Additional Information (1): The characterization of the P^c*H₂ and Ppz^{*}H₂ results of a separate synthesis; here the compounds only have been identified by APCI-HRMS and UV-Vis spectroscopy.

Ring Expansion of a Spc N₆-Pc^{*}H₂ and N₄-Pc^{*}H₂: could be obtained by inserting 1.1 eq isoindoline of PN* **1** in the corresponding Spc [Sppz^{*}BCl] or N₄-[Spc^{*}BCl]. Therefore, the solution was stirred in DMSO at 120 °C, 8 h. After removing the solvent under reduced pressure the product was purified by column chromatography PE/EE 1:1.

The N₆-/N₄-Pc^{*}H₂ could be identified by using ¹H NMR, UV-Vis spectroscopy and APCI-HRMS. All data correlated with the ones described above.

Synthesis of [N_x-Pc^{*}Zn] 1 eq N_x-Pc^{*}H₂ was dissolved in 2 mL toluene/5 mmol P^c. 1.1 eq [Zn(hmdu)₂] was added at once. The solution was stirred for 30 min at 75 °C until the conversion to N_x-[Pc^{*}Zn] was completed (NMR control). The solvent was evaporated as well as the rest of the HHMDS and [Zn(hmdu)₂] and finally washed out with Et₂O. The compounds were dried in vacuum.

N₂-[Pc^{*}Zn]: **Yield:** 80%. - **¹H NMR** (300 MHz, C₆D₆, 25 °C): $\delta = 9.97$ (s, 4 H, Ar-H), 9.94 (s, 2 H, Ar-H), 1.92 (s, 4 H, CH₂), 1.86 (s, 12 H, CH₃), 1.80 (s, 12 H, CH₂), 1.56 (s, 24 H, CH₃), 1.46 (s, 12 H, CH₃) ppm. - **UV/Vis** (DCM): $\lambda = 675$ (s), 613 (sh), 360 (s),

228 (s) nm. - **Fluorescence** (DCM, $\lambda_{\text{ex}} = 350$ nm) $\lambda = 697$ nm. - **MS** (APCI-HRMS(+)): $m/z = 1019.5139$ [M+H]⁺, cal. for C₆₂H₇₀N₁₀+H: 1019.5149.

ABAB N₄-[Pc^{*}Zn]: R_f (Tol/THF 20:1) = 0.63. - **¹H NMR** (C₆D₆, 300 MHz): $\delta = 9.96$ (s, 4 H, Ar-H), 1.91 (s, 8 H, CH₂), 1.85 (s, 24 H, CH₃), 1.78 (s, 8 H, CH₂), 1.45 (s, 25 H, CH₃) ppm. - **UV/Vis** (DCM): $\lambda = 687$ (s), 657 (s), 631 (sh), 596 (sh), 357 (s) nm. - **MS** (APCI-HRMS(+)): $m/z = 1021.5073$ [M+H]⁺, cal. for C₆₀H₆₈N₁₂Zn₁+H₁: 1021.5054.

A₂B₂ N₄-[Pc^{*}Zn]: Yield: 71%. - **¹H NMR** (300 MHz, C₆D₆, 25 °C): $\delta = 9.93$ (s, 2 H, Ar-H), 9.91 (s, 2 H, Ar-H), 1.91 (s, 8 H, CH₂), 1.83 (s, 8 H, CH₂), 1.78 (s, 24 H, CH₃), 1.53 (s, 12 H, CH₃), 1.43 (s, 12 H, CH₃) ppm. - **¹H NMR** (300 MHz, [D₂]DCM, 25 °C): $\delta = 9.59$ (s, 2 H, Ar-H), 9.56 (s, 2 H, Ar-H), 2.24 (s, 8 H, CH₂), 2.08 (s, 8 H, CH₂), 1.93 (s, 12 H, CH₃), 1.92 (s, 12 H, CH₃), 1.83 (s, 12 H, CH₃), 1.82 (s, 12 H, CH₃) ppm. - **UV/Vis** (DCM): $\lambda = 666$ (s), 601 (sh), 361 (s) nm. - **Fluorescence** (DCM, $\lambda_{\text{ex}} = 350$ nm) $\lambda = 680$ nm. - **MS** (APCI-HRMS(+)): $m/z = 1021.5043$ [M+H]⁺, cal. for C₆₀H₆₈N₁₂+H: 1021.5054.

N₆-[Pc^{*}Zn]: Yield: 78%. - **¹H NMR** (300 MHz, C₆D₆, 25 °C): $\delta = 9.96$ (s, 2 H, Ar-H), 1.89 (s, 12 H, CH₂), 1.83 (s, 12 H, CH₃), 1.79 (s, 24 H, CH₃), 1.76 (s, 4 H, CH₂), 1.43 (s, 12 H, CH₃) ppm. - **UV/Vis** (DCM): $\lambda = 662$ (s), 649 (s), 357 (s), 227 (s) nm. - **Fluorescence** (DCM, $\lambda_{\text{ex}} = 350$ nm) $\lambda = 673$ nm. - **MS** (APCI-HRMS(+)): $m/z = 1023.4959$ [M+H]⁺, cal. for C₅₈H₆₆N₁₄+H: 1023.4959.

Photophysical measurements. The steady-state fluorescence spectra were measured using an AMINCO-Bowman Series 2 luminescence spectrometer. For singlet oxygen and fluorescence determination as well as the titration experiments, the dye samples were purified by preparative TLC on Merck aluminum sheets coated with silica gel 60 F254 to ensure high purity. Both the Φ_{Δ} and Φ_F values were determined by comparative methods using unsubstituted zinc phthalocyanine (ZnPc) as a reference ($\Phi_{\Delta(\text{THF})} = 0.53$, $\Phi_{F(\text{THF})} = 0.32$) for N_x-[Pc^{*}M]. The photophysical data for N_x-[Spc^{*}BCl] series were determined with rhodamin G6 ($\Phi_{F(\text{EtOH})} = 0.94$) and bengal rose ($\Phi_{\Delta(\text{MeOH})} = 0.76$) as reference compounds and long-pass filter FGL455 instead of OG530 for Φ_{Δ} determination. All of the experiments were performed in triplicate, and the data represent the means of the measurements (estimated error ±10%). For Φ_F determination, the sample and reference were excited at 598 nm and 490 nm for N_x-[Pc^{*}M] and N_x-[Spc^{*}BCl], respectively, and the absorbance at the Q-band maximum was maintained at less than 0.05 to avoid the inner filter effect. The emission spectra were corrected for the instrument response. The Φ_F values were corrected for the refractive indices of the solvents. The time-resolved fluorescence measurements were performed on FS5 fluorometer (Edinburgh Instruments) with picosecond pulsed diode lasers excitation at 371 nm (EPL-375, pulse width ~ 68 ps) and 634 nm (EPL-635, pulse width ~ 81 ps). The decay curves were fitted to exponential functions with Fluoracle software (Edinburgh Instruments).

Computational details. Unconstrained structural optimizations of the compounds investigated were carried out with density functional theory (DFT), using the PBE³⁷ exchange-correlation functional together with the def2-TZVPP³⁸ basis set for all elements adding a semiempirical dispersion correction term

(DFT-D3).³⁹ Orbital energies were derived on this level. The Gaussian09⁴⁰ optimizer together with Turbomole 6.5⁴¹ energies and gradients was used. The resolution-of-identity⁴² and the multipole accelerated RI-J⁴³ approximation was applied throughout. The excitation energies were derived from time-dependent DFT computations using B3LYP⁴⁴/def2-TZVPP and the Tamm-Danoff approximation as implemented in the ORCA⁴⁵ package. The RIJCOSX approximation was used. Polarizabilities and dipole moments were derived with PBE/def2-TZVPP with ORCA.

Acknowledgements

This work was funded by DFG within SFB 1083. The singlet oxygen study was supported by LOEWE Priority Program SynChemBio. We also would like to thank J. Wallauer and rhd-instruments for their advice in our CV measurements.

Notes and References

- 1 A. Hagfeldt, G. Boschloo, L. Sun, L. Kloo and H. Pettersson, *Chem. Rev.*, 2010, **110**, 6595.
- 2 a) I. Bruder, A. Ojala, C. Lennartz, S. Sundarraj, J. Schöneboom, R. Sens, J. Hwang, P. Erk and J. Weis, *Solar Energy Materials and Solar Cells*, 2010, **94**, 310; b) I. Bruder, J. Schöneboom, R. Dinnebier, A. Ojala, S. Schäfer, R. Sens, P. Erk and J. Weis, *Organic Electronics*, 2010, **11**, 377; c) M. G. Walter, A. B. Rudine and C. C. Wamser, *J. Porphyrins Phthalocyanines*, 2010, **14**, 759; d) H. Imahori, T. Umeyama and S. Ito, *Acc. Chem. Res.*, 2009, **42**, 1809; e) P. Y. Reddy, L. Giribabu, C. Lyness, H. J. Snaith, C. Vijaykumar, M. Chandrasekharam, M. Lakshmikantam, J.-H. Yum, K. Kalyanasundaram, M. Grätzel and M. K. Nazeeruddin, *Angewandte Chemie (International ed. in English)*, 2007, **46**, 373;
- 3 E. Palomares, M. V. Martinez-Diaz, S. A. Haque, T. Torres and J. R. Durrant, *Chem. Commun.*, 2004, 2112.
- 4 I. López-Duarte, M. Wang, R. Humphry-Baker, M. Ince, M. V. Martínez-Díaz, M. K. Nazeeruddin, T. Torres and M. Grätzel, *Angew. Chem. Int. Ed.*, 2012, **51**, 1895.
- 5 J. Zaumseil and H. Sirringhaus, *Chemical Reviews*, 2007, **107**, 1296.
- 6 a) Y. Wang and D. Liang, *Advanced materials (Deerfield Beach, Fla.)*, 2010, **22**, 1521; b) K.-Y. Law, *Chem. Rev.*, 1993, **93**, 449; c) D. Lee, H. B. Kim, *Korean Journal of Chemical Engineering*, 2009, **26**, 673;
- 7 Peter Erk, Heidi Engelsberg, ed., *Phthalocyanines Dyes and Pigments*, Elsevier Science, San Diego, 2003.
- 8 D. Wöhrle, G. Schnurpfeil, S. Makarov and O. Suvora, *Chemie in unserer Zeit*, 2012, **46**, 12.
- 9 a) V. Novakova, M. Miletin, K. Kopecky and P. Zimcik, *Chem. Eur. J.*, 2011, **17**, 14273; b) V. Novakova, P. Hladík, T. Filandrová, I. Zajícová, V. Krepsová, M. Miletin, J. Lenčo and P. Zimcik, *Physical chemistry chemical physics : PCCP*, 2014, **16**, 5440; c) Y. Bian, J. Jiang, Y. Tao, Choi, Michael T M, R. Li, Ng, Anthony C H, P. Zhu, N. Pan, X. Sun, D. P. Arnold, Z.-Y. Zhou, H.-W. Li, Mak, Thomas C W and Ng, Dennis K P, *J. Am. Chem. Soc.*, 2003, **125**, 12257; d) X.-J. Jiang, S.-L. Yeung, P.-C. Lo, W.-P. Fong and Ng, Dennis K. P., *J. Med. Chem.*, 2011, **54**, 320; e) M. Machacek, A. Cidlina, V. Novakova, J. Svec, E. Rudolf, M. Miletin, R. Kučera, T. Simunek and P. Zimcik, *J. Med. Chem.*, 2015, **58**, 1736;
- 10 a) R. W. Boyle and D. Dolphin, *Photochemistry and Photobiology*, 1996, **64** (3), 469; b) E. A. Luk'yanets, *J. Porphyrins Phthalocyanines*, 1999, **3**, 424; c) A. P. Castano, T. N. Demidova and M. R. Hamblin, *Photodiagnosis and Photodynamic Therapy*, 2004, **1**, 279; d) L. B. Josefson and R. W. Boyle, *British journal of pharmacology*, 2008, **154**, 1; e) Leung, S C H, P.-C. Lo, Ng, D K P, W.-K. Liu, K.-P. Fung and W.-P. Fong, *British journal of pharmacology*, 2008, **154**, 4;
- 11 a) W. Darwish, S. Schlecht, A. Schaper, M. Fröba, K. Harms, W. Massa and J. Sundermeyer, *Z. anorg. allg. Chem.*, 2009, **635**, 1215; b) W. Darwish, E. Seikel, R. Käsmarker, K. Harms and J. Sundermeyer, *Dalton transactions* (Cambridge, England : 2003), 2011, **40**, 1787; c) W. Darwish, E. Seikel, K. Harms, O. Burghaus and J. Sundermeyer, *Dalton Trans.*, 2011, **40**, 1183; d) E. Seikel, B. Oelkers and J. Sundermeyer, *Inorg. Chem.*, 2012, **51**, 2709;
- 12 E. Seikel, B. Oelkers, O. Burghaus and J. Sundermeyer, *Inorg. Chem.*, 2013, **52**, 4451.
- 13 a) M. Hanack, S. Knecht, R. Polley and L. R. Subramanian, *Synthetic Metals*, 1996, **80**, 183; b) D. Dini, M. Hanack, H.-J. Egelhaaf, J. C. Sancho-García and J. Cornil, *The journal of physical chemistry. B*, 2005, **109**, 5425; c) S. Knecht, K. Düür, G. Schmid, L. R. Subramanian and M. Hanack, *J. Porphyrins Phthalocyanines*, 1999, **3**, 292; d) M. Hanack, D. Meng, A. Beck, M. Sommerauer and L. R. Subramanian, *J. Chem. Soc., Chem. Commun.*, 1993, 58;
- 14 S. Rodríguez-Morgade and M. Hanack, *Chem. Eur. J.*, 1997, **3**, 1042.
- 15 V. Novakova, P. Reimerova, J. Svec, D. Suchan, M. Miletin, H. M. Rhoda, V. N. Nemykin and P. Zimcik, *Dalton Trans.*, 2015, **44**, 13220.
- 16 a) A. Díaz-Moscoso, G. J. Tizzard, S. J. Coles and A. N. Cammidge, *Angewandte Chemie (International ed. in English)*, 2013, **52**, 10784; b) A. N. Cammidge, I. Chambrier, M. J. Cook, D. L. Hughes, M. Rahman and L. Sosa-Vargas, *Chem. Eur. J.*, 2011, **17**, 3136;
- 17 a) Wong, Edwin W Y, A. Miura, M. D. Wright, Q. He, C. J. Walsby, S. Shimizu, N. Kobayashi and D. B. Leznoff, *Chemistry (Weinheim an der Bergstrasse, Germany)*, 2012, **18**, 12404; b) E. W. Y. Wong, C. J. Walsby, T. Storr and D. B. Leznoff, *Inorg. Chem.*, 2010, **49**, 3343;
- 18 S. A. Mikhaleko, L. A. Solov'eva and E. A. Luk'yanets, *The Journal of General Chemistry of the USSR*, 1991, **61**, 996.
- 19 J. Mack and N. Kobayashi, *Chem. Rev.*, 2011, **111**, 281.
- 20 Christian G. Claessens, David González-Rodríguez, Charles M. McCallum, Ronald S. Nohr, Heinz-Peter Schuchmann, Tomás Torres, *Journal of Porphyrins Phthalocyanines*, 2007, **11**, 181.
- 21 T. Furuyama, K. Satoh, T. Kushiya and N. Kobayashi, *J. Am. Chem. Soc.*, 2014, **136**, 765.
- 22 L. Goerigk and S. Grimme, *J. Chem. Phys.*, 2010, **132**, 184103.
- 23 H. D. Holtz, *J. Org. Chem.*, 1971, **37**, 2069.
- 24 a) R. C. Palmer, *Industrial and Engineering Chemistry*, 1942, **34**, 1028; b) W. F. Brill, *Industrial and Engineering Chemistry*, 1960, **52**, 837; c) A. Onopchenko, J. G. D. Schulz and R. Seekircher, *J. Chem. Soc. D*, 1971, 939;
- 25 N. Kobayashi, R. Kondo, S. Nakajima and T. Osa, *J. Am. Chem. Soc.*, 1990, **112**, 9640.
- 26 Z. Musil, P. Zimcik, M. Miletin, K. Kopecky and J. Lenco, *Eur. J. Org. Chem.*, 2007, 4535.
- 27 N. Kobayashi, H. Miwa and V. N. Nemykin, *J. Am. Chem. Soc.*, 2002, **124**, 8007.
- 28 V. Novakova, M. Lásková, H. Vavřičková and P. Zimcik, *Chem. Eur. J.*, 2015, **21**, 14382.
- 29 a) J. Svec, P. Zimcik, L. Novakova, O. A. Rakitin, S. A. Amelichev, P. A. Stuzhin and V. Novakova, *Eur. J. Org. Chem.*, 2015, **3**, 596; b) P. Zimcik, V. Novakova, K. Kopecky,

- M. Miletin, R. Z. Uslu Kobak, E. Svandrikova, L. Váchorová and K. Lang, *Inorg. Chem.*, 2012, **51**, 4215;
- 30 B. del Rey, U. Keller, T. Torres, G. Rojo, F. Agulló-López, S. Nonell, C. Martí, S. Brasselet, I. Ledoux and J. Zyss, *J. Am. Chem. Soc.*, 1998, **120**, 12808.
- 31 H. Kietabl, *Monatsh. Chem.*, 1974, **105**, 405.
- 32 L.-Y. Cui, J. Yang, Q. Fu, B.-Z. Zhao, L. Tian and H.-L. Yu, *Journal of Molecular Structure*, 2007, **827**, 149.
- 33 M.-E. Ragoussi, M. Ince and T. Torres, *Eur. J. Org. Chem.*, 2013, **2013**, 6475.
- 34 M. V. Martinez-Diaz, G. de La Torre and T. Torres, *Chemical communications (Cambridge, England)*, 2010, **46**, 7090.
- 35 S. Senthilarasu, S. Velumani, R. Sathyamoorthy, G. Canizal, P. J. Sebastian, J. A. Chavez, R. Perez, A. Subbarayan and J. A. Ascencio, *Applied Physics A: Materials Science & Processing*, 2003, **77**, 383.
- 36 a) P. Jones, Villeneuve, G. B., C. Fei, J. DeMarte, A. J. Haggarty, K. T. Nwe, D. A. Martin, A.-M. Lebuis, J. M. Finkelstein, B. J. Gour-Salin, T. H. Chan and B. R. Leyland-Jones, *J. Med. Chem.*, 1998, 3062; b) D. D. Coffman, E. L. Jenner and R. D. Lipscomb, *J. Am. Chem. Soc.*, 1958, 2864;
- 37 J. P. Perdew, K. Burke and M. Ernzerhof, *Phys. Rev. Lett.*, 1996, **77**, 3865.
- 38 F. Weigend and R. Ahlrichs, *Phys Chem Chem Phys*, 2005, **7**, 3297.
- 39 a) S. Grimme, J. Antony, S. Ehrlich and H. Krieg, *J. Chem. Phys.*, 2010, **132**, 154104; b) S. Grimme, S. Ehrlich and L. Goerigk, *J Comput Chem*, 2011, **32**, 1456;
- 40 M. J. Frisch, G. W. Trucks, H. B. Schlegel, G. E. Scuseria, M. A. Robb, J. R. Cheeseman, G. Scalmani, V. Barone, B. Mennucci, G. A. Petersson, H. Nakatsuji, M. Caricato, X. Li, H. P. Hratchian, A. F. Izmaylov, J. Bloino, G. Zheng, J. L. Sonnenberg, M. Hada, M. Ehara, K. Toyota, R. Fukuda, J. Hasegawa, M. Ishida, T. Nakajima, Y. Honda, O. Kitao, H. Nakai, T. Vreven, J. A. Montgomery Jr., J. E. Peralta, F. Ogliaro, M. Bearpark, J. J. Heyd, E. Brothers, K. N. Kudin, V. N. Staroverov, R. Kobayashi, J. Normand, K. Raghavachari, A. Rendell, J. C. Burant, S. S. Iyengar, J. Tomasi, M. Cossi, N. Rega, J. M. Millam, M. Klene, J. E. Knox, J. B. Cross, V. Bakken, C. Adamo, J. Jaramillo, R. Gomperts, R. E. Stratmann, O. Yazyev, A. J. Austin, R. Cammi, C. Pomelli, J. W. Ochterski, R. L. Martin, K. Morokuma, V. G. Zakrzewski, G. A. Voth, P. Salvador, J. J. Dannenberg, S. Dapprich, A. D. Daniels, Farkas, J. B. Foresman, J. V. Ortiz, J. Cioslowski, D. J. Fox, Gaussian09 Revision C.01, Gaussian Inc. Wallingford CT 2009.
- 41 TURBOMOLE V6.5 2011, a development of University of Karlsruhe and Forschungszentrum Karlsruhe GmbH, 1989-2007, TURBOMOLE GmbH, since 2007; available from <http://www.turbomole.com> (last accessed: 11.06.2015).
- 42 a) M. von Arnim and R. Ahlrichs, *Journal of Computational Chemistry*, 1998, **19**, 1746; b) F. Weigend, *Phys. Chem. Chem. Phys.*, 2002, **4**, 4285;
- 43 M. Sierka, A. Hogekamp and R. Ahlrichs, *The Journal of Chemical Physics*, 2003, **118**, 9136.
- 44 a) A. D. Becke, *J. Chem. Phys.*, 1993, **98**, 5648; b) P. J. Stephens, J. F. Devlin, C. F. Chabalowski and M. J. Frisch, *J. Phys. Chem.*, 1994, **98**, 11623;
- 45 F. Neese, *WIREs Comput Mol Sci*, 2012, **2**, 73.

Supporting Information

to

Experimental and Computational Study of Isomerically Pure Soluble Azaphthalocyanines and Azasubphthalocyanines of Varying Number of Aza Units

Martin Liebold^a, Eugen Sharikow^a, Elisabeth Seikel^a, Lukas Trombach^b, Klaus Harms^b, Petr Zimčík^c, Veronika Nováková^c, Ralf Tonner^{b,*}, and Jörg Sundermeyer^{a,*}

^a Fachbereich Chemie und Wissenschaftliches Zentrum für Materialwissenschaften (WZMW), Philipps-Universität Marburg, Hans-Meerwein-Straße 4, 35032 Marburg, Germany.

e-mail: jsu@chemie.uni-marburg.de

^b Fachbereich Chemie, Philipps-Universität Marburg, Hans-Meerwein-Straße 4, 35032 Marburg, Germany.

e-mail: tonner@chemie.uni-marburg.de

^c Department of Pharmaceutical Chemistry and Drug Control, Faculty of Pharmacy in Hradec Králové, Charles University in Prague, Heyrovského 1203, Hradec Králové, 500 05 Czech Republic

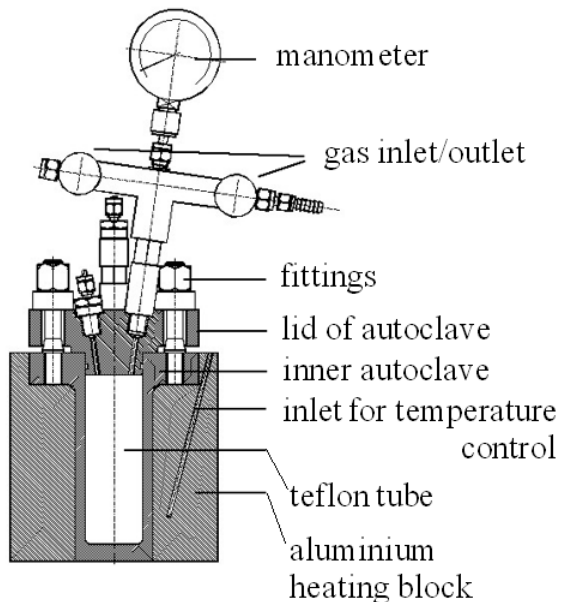
e-mail: petr.zimcik@faf.cuni.cz and veronika.novakova@faf.cuni.cz

Table of Contents

1.1	Experimental Section	S1
1.1.1	Synthesis of PDN [*]	S2
1.1.2	Alternative Synthesis of 1,1,4,4-Tetramethyltetralin-6,7-dicarboxylic acid	S2
1.1.3	Alternative Synthesis of the Anhydride of.....	S3
1.1.4	Synthesis of PyzDN [*]	S4
1.1.5	Synthesis of [Spc [*] BCl]	S5
1.1.6	Synthesis of [Sppz [*] BCl]	S6
1.1.7	Synthesis of Azasubphthalocyanines N _x -[Spc [*] BCl]	S6
1.1.8	Synthesis of Asymmetrical Phthalocyanines: N _x -Pc [*] H ₂	S8
1.1.9	Synthesis of N _x -Pc [*] H ₂	S8
1.1.10	Synthesis of N ₄ -[Pc [*] Zn] using [Zn(OAc) ₂].....	S11
1.2	Suggested radical autoxidation mechanism of tetraline IV.....	S12
1.3	Absorbance and Emission Spectra	S13
1.4	Theoretical Calculations.....	S16
1.5	¹ H NMR Spectra.....	S18
1.5.1	Subphthalocyanines	S18
1.5.2	Azaphthalocyanines	S19
1.6	Cylovoltammetric measurements	S20
1.7	Crystal Structures	S21
1.7.1	Crystal Structure of [Spc [*] BCl].....	S22
1.7.2	Crystal Structure of N ₂ -Pc [*] H ₂	S29
1.7.3	Crystal Structure of A ₂ B ₂ N ₄ -[Pc [*] Zn·H ₂ O].....	S42
1.7.4	Crystal Structure of [Sppz [*] BCl] Crystallographer: Dr. Benjamin Oelkers	S54
1.8	References	S55

1.1 Experimental Section

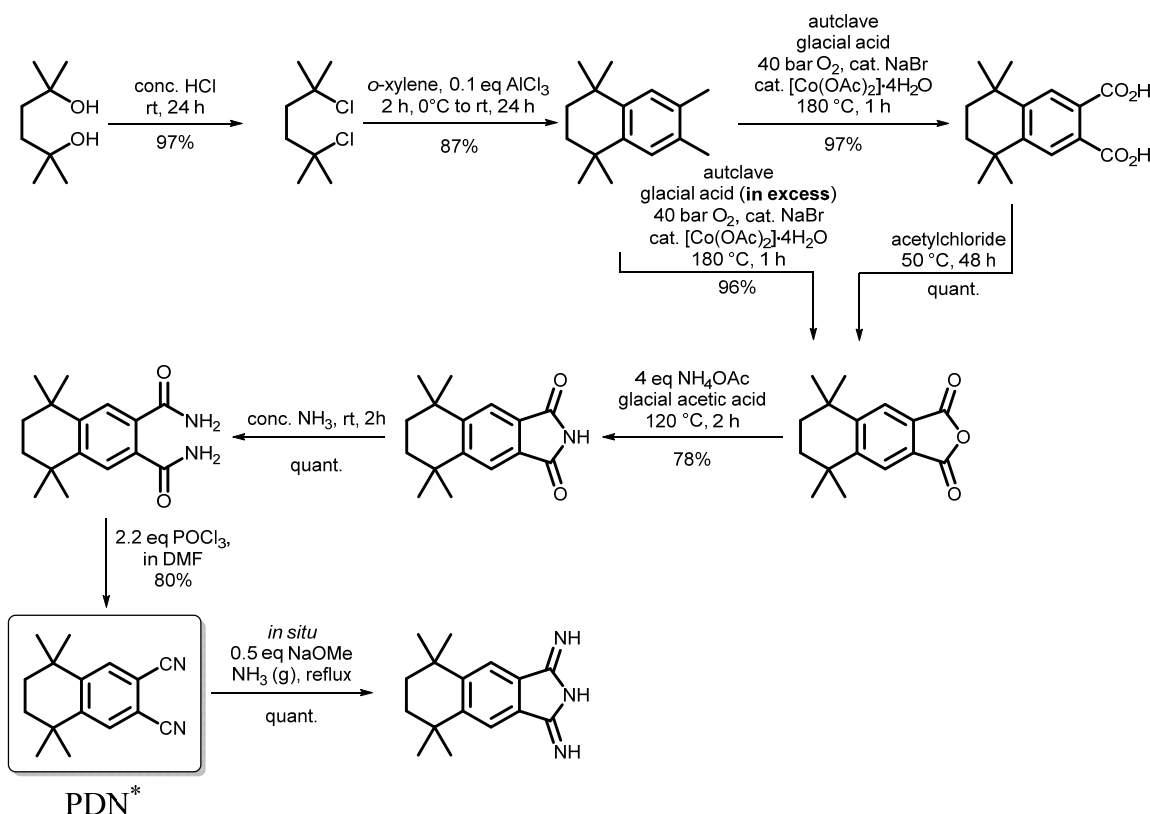
All reactions in which high pressure was needed, were carried out in an autoclave. Therefore, a glass (pressure <10 bar) or a steel autoclave (<100 bar) was used. The 100 mL stainless steel autoclaves *V4A-Edelstahlautoklaven* were constructed by the precision engineering department of the Philipps-Universität Marburg (Department of Chemistry). Solids and liquids were weighed out in a 100 mL teflon flask or in the corresponding glass flask, a magnetic stirrer was added and the autoclave was closed and sealed using EPDM-O-rings of CLEFF DICHTUNG company. The actual pressure was regulated using a manometer. The temperature was adjusted using a corresponding aluminium block in which the thermometer of the magnetic stirrer MR 3003 HEIDOLPH could be added (Pt-100-thermal element). If necessary, the heating block might be preheated (for *Pc* reactions). If necessary, the glass autoclaves were heated in an oil bath. A sketch of the steel autoclave is displayed in **Fehler! Verweisquelle konnte nicht gefunden werden..**



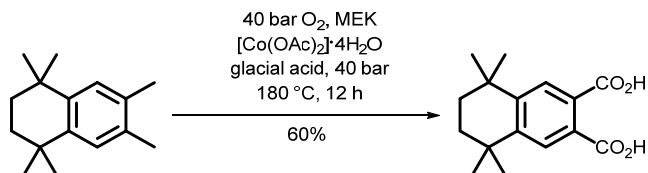
Sketch of the used steel autoclave: *V4A-stainless steel autoclave*.

1.1.1 Synthesis of PDN^{*}

The synthesis of the PDN^{*} **1** was carried out according to MIKHALENKO.^[1] The synthesis of 1,1,4,4-tetramethyltetralin-6,7-dicarboxylic acid (VI) was modified by using an overpressure of O₂ in a [Co(OAc)₂][·]4H₂O catalytic autoclave reaction.

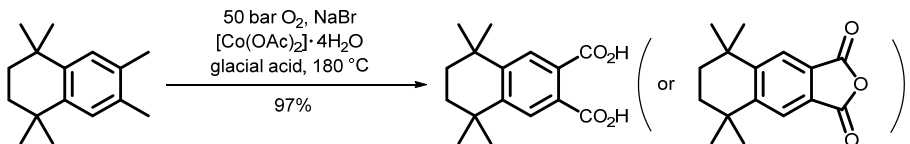


1.1.2 Alternative Synthesis of 1,1,4,4-Tetramethyltetralin-6,7-dicarboxylic acid



Method a) The reaction was carried out in an autoclave reaction as described in method b), using 50 bar O₂ and 0.1 eq [Co(OAc)₂][·]4H₂O as catalyst, 5 eq MEK as cocatalyst instead of NaBr, and 5 mL glacial acetic acid /g tetraline as solvent. The mixture was stirred for 12 h while the autoclave was recharged several times with O₂, until the pressure stayed constant. Workup was carried out according to method b).

Yield: 60% (only carboxylic acid was observed). - **¹H NMR:** according to analysis below.



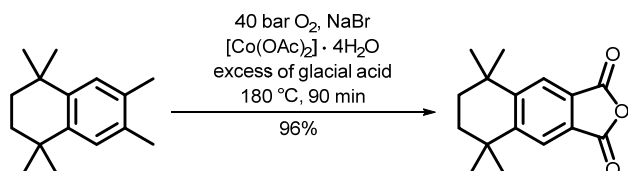
Method b) 15 g tetraline (69.3 mmol, 1 eq) were dissolved in 50 mL glacial acid in a 100 mL teflon tube and added into an autoclave (steel autoclave as visible in “Methods” section **Fehler! Verweisquelle konnte nicht gefunden werden.**). The teflon tube was additionally filled-up with 750 mg [Co(OAc)₂]·4H₂O (3 mmol, 4 mol%) and 300 mg NaBr (3 mmol, 4 mol%). The mixture was briefly stirred until everything was dissolved. The autoclave was charged with O₂ to a pressure of 20 bar. With stirring, the solution was heated to 180 °C. After a short period of initiation (<30 min) the reaction started and the pressure decreased. The autoclave was recharged with O₂ to 50 bar as often as necessary, until the pressure stayed constant at about 50 bar. After 2 h, the reaction was complete. The reaction may also be stirred overnight. The resulting solution was concentrated under reduced pressure and was washed with water to remove Co-salts and NaBr traces. The product can be additionally precipitated in 20% aq. HCl (500 mL/20 g acid), followed by filtration and washing with water.

Yield: 18.5 g, 67 mmol, 97%. - **¹H NMR** (DMSO-*d*₆, 300 MHz): δ = 13.07 (s, 2 H, COOH), 7.57 (s, 2 H, Ar-CH), 1.66 (s, 4 H, -CH₂), 1.25 (s, 12 H, -CH₃) ppm. - **MS** (ESI(+), MeOH): *m/z* = 277.1436, cal. for C₁₆H₂₀O₄+H₁: 277.1434. - **Elemental analysis** (C₁₆H₂₀O₄, M = 276.33): fnd. (cal.): C 69.83% (69.55%), H 7.18% (7.30%), N 7.53% (0.00%).

Additional information: In some cases, the corresponding anhydride was detected by ¹H NMR spectroscopy. The amount of anhydride is dependent on the amount of glacial acid used in the reaction in ratio to the tetraline amount. No other by-products could be observed. A complete turnover was determined. The high nitrogen value in elemental analysis is caused by the measurement in closed setup in the glovebox, neither in the synthesis nor in precursor steps were nitrogen containing chemicals used.

1.1.3 Alternative Synthesis of the Anhydride of

1,1,4,4-Tetramethyltetralin-6,7-dicarboxylic acid

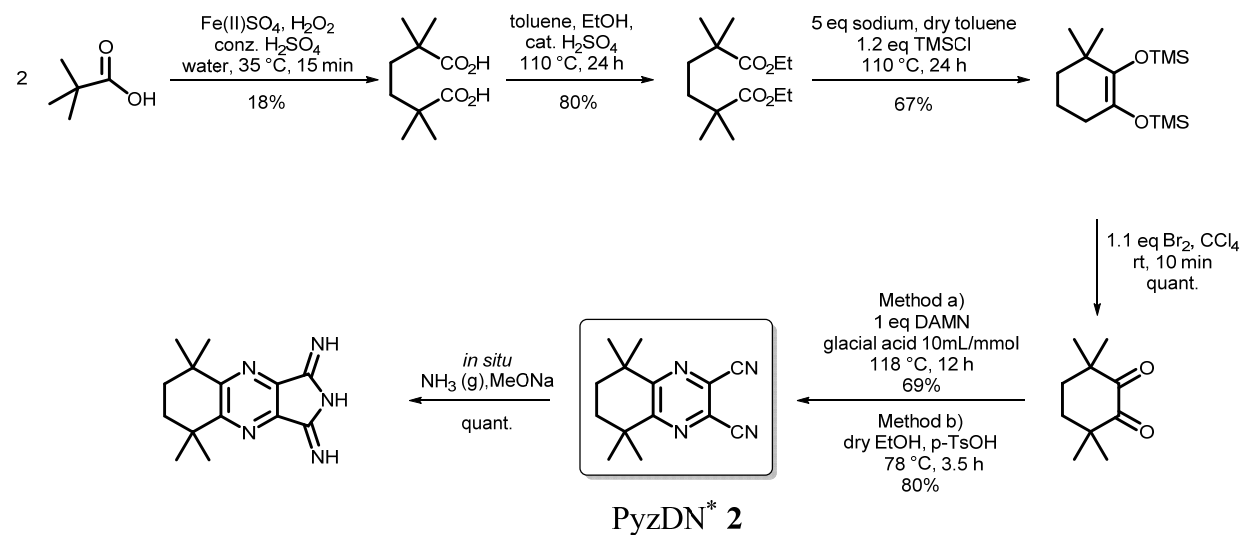


50 mg NaBr (486 µmol, ~3.5 mol%), 125 mg [Co(OAc)₂]·4H₂O (502 µmol, ~3.5 mol%), 3.00 g tetraline (13.9 mmol, 1 eq) were added into an autoclave and dissolved in 10 mL glacial acid. The autoclave was charged with 20 bar O₂ and heated to 180 °C for 90 min. The pressure increased to 30 bar, dropped down to 20 bar and was recharged to 30-40 bar two more times. The autoclave was recharged as often as needed, until the pressure stayed constant. Carboxylic acid anhydride was precipitated out of the solution and washed with water. A second/third portion was yielded overnight, filtered, washed with water and finally dried in vacuum.

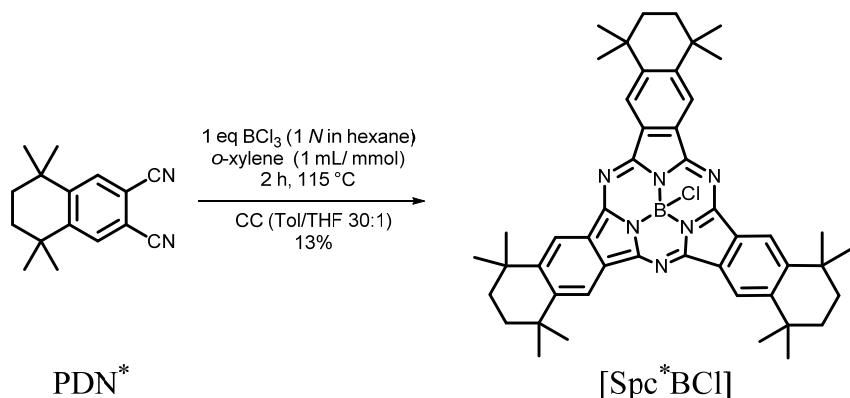
Yield: 3.43 g, 13.3 mmol, 96%. - ¹H NMR (CDCl₃, 300 MHz): δ = 7.95 (s, 2 H, Ar-CH), 1.76 (s, 4 H, -CH₂), 1.36 (s, 12 H, -CH₃) ppm.

1.1.4 Synthesis of PyzDN^{*}

The synthesis of 3,3,6,6-tetramethylcyclohexane-1,2-dione (**XIV**) was carried out following the procedure of JONES.^[2] The synthesis of PyzDN^{*} **2** was carried out according to the procedure of SEIKEL.^[3]



1.1.5 Synthesis of [Spc^{*}BCl] [4,5]



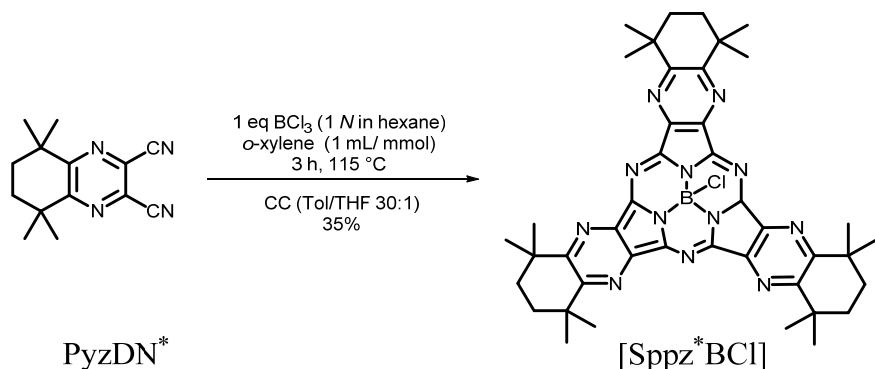
General Procedure 1: Synthesis of $[\text{Spc}^{(*)}\text{BX}]$.

1 eq PDN was dissolved in 2 mL toluene /5 mmol PDN. Fresh BCl_3 solution (1 M in heptane or in *o*-xylene, 3 eq BCl_3 per intended $[\text{SpcBCl}]$) was added at once and then heated to 150 °C. The yellowish solution turned deep pink. After heating for about 5 h, the solution was loaded onto a short silica pluck, purified with DCM/EE to remove the boron compounds and then purified by CC (PE/EA 10:1).

Yield: ~5%. - R_f (PE/EE 10:1) = 0.4. - **$^1\text{H NMR}$** (C_6D_6 , 300 MHz): δ = 8.91 (s, 6 H, Ar-CH), 1.65-1.52 (m, 12 H, - CH_2), 1.42 (s, 18 H, - CH_3), 1.10 (s, 18 H, - CH_3) ppm. - **$^1\text{H NMR}$** (CD_2Cl_2 , 300 MHz): δ = 8.84 (s, 6 H, Ar-CH), 1.94-1.80 (m, 12 H, - CH_2), 1.66 (s, 18 H, - CH_3), 1.44 (s, 18 H, - CH_3) ppm. - **$^{13}\text{C NMR}$** (CD_2Cl_2 , 75 MHz): δ = 149.6, 149.2, 129.4, 120.4, 36.0, 35.3, 32.9, 32.3 ppm. - **UV-Vis** (DCM): λ = 582 (s), 528 (sh), 318 (s), 267 (s) nm. - **Fluorescence** (DCM, λ_{ex} = 350 nm): λ = 592 nm. - Φ_F (λ_{ex} = 490 nm) = 0.18. - Φ_Δ = 0.64. - **MS** (APCI-HRMS(+)): m/z = 761.4247 [$\text{M}+\text{H}]^+$, cal. for $\text{C}_{48}\text{H}_{54}\text{B}_1\text{Cl}_1\text{N}_6+\text{H}_1$: 761.4272. - **X-ray:** Crystals could be obtained out of CD_2Cl_2 in the NMR tube at rt.

Additional information: In some cases, degradation of $[\text{Spc}^*\text{BCl}]$ in the form of a fast decolouration was observed in acidic solvents.

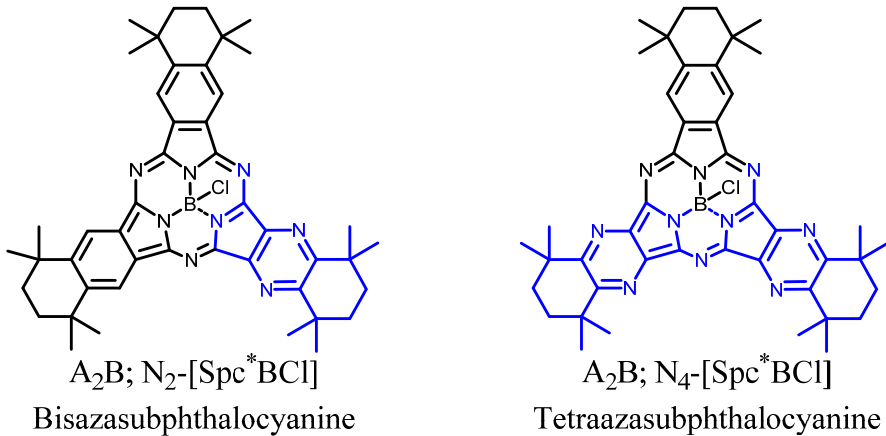
1.1.6 Synthesis of [Sppz^{*}BCl]^[4,5]



According to General Procedure 1 (p. 5). The pink solution was purified by CC (Tol/THF 30:1). The pink solid was dried in vacuum.

Yield: 35%. - R_f (Tol/THF 30:1) = 0.35. - R_f (DCM) = 0.6. - **¹H NMR** (CDCl₃, 300 MHz): δ = 1.94–2.07 (m, 12 H, -CH₂), 1.75 (s, 18 H, -CH₃), 1.52 (s, 18 H, -CH₃) ppm. - **¹H NMR** (CD₂Cl₂, 300 MHz): δ = 1.53 (s, 18 H, -CH₃), 1.78 (s, 18 H, -CH₃), 1.96–2.16 (m, 12 H, -CH₂) ppm. - **UV-Vis** (DCM): λ = 534 (s), 489 (sh), 334 (m), 303 (s) nm. - **Fluorescence** (DCM, λ_{ex} = 350 nm): λ = 546 nm. - Φ_F (λ_{ex} = 490 nm) = 0.19. - Φ_Δ = 0.88. - **MS** (APCI-HRMS(+)): m/z = 767.3964 [M+H]⁺, cal. for C₄₂H₄₈B₁Cl₁N₁₂+H₁: 767.3980.

1.1.7 Synthesis of Azasubphthalocyanines N_x-[Spc^{*}BCl]



According to General Procedure 1 (p. 5), using PDN^{*}/PyzDN^{*} in a 1:1 ratio. After evaporation of the solvent, the solid residue was loaded onto silica and the crude product was purified via gradient CC (Tol → Tol/THF).

[Spc^{*}BCl]: Yield: <1%. - The product was identified by using UV-Vis and MS. The analysis is in accordance to the one described in section 1.1.5.

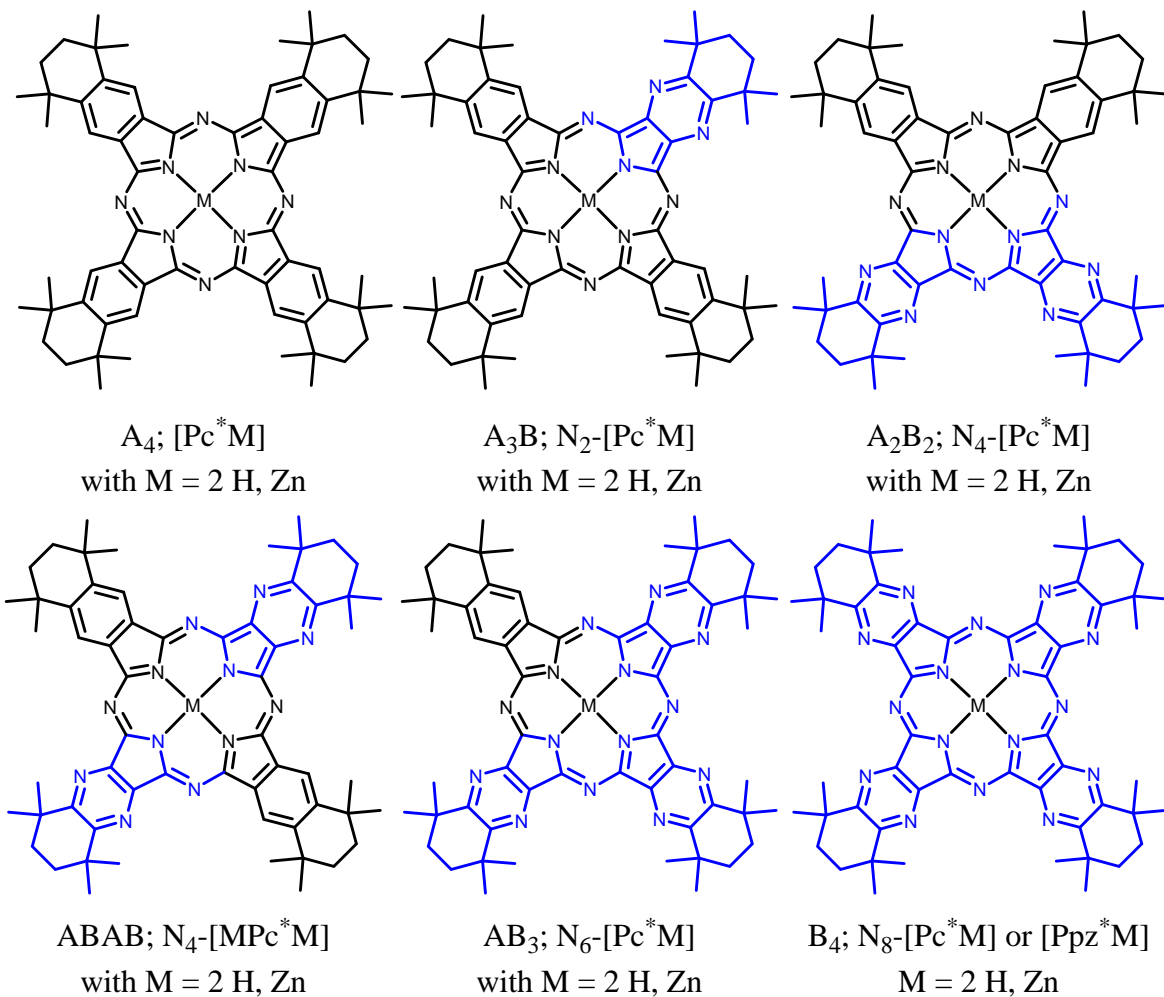
N₂-[Spc^{*}BCl]: Yield: 8 mg, 10.5 μ mol, 1%. - **¹H NMR** (CDCl₃, 300 MHz): δ = 8.87 (s, 2 H, Ar-CH), 8.78 (s, 2 H, Ar-CH), 1.77–1.55 (m, 12 H, -CH₂), 1.38 (s, 9 H, -CH₃), 1.35 (s, 9 H, -

CH_3), 1.05 (s, 9 H, $-CH_3$), 1.03 (s, 9 H, $-CH_3$) ppm. - **UV-Vis** (DCM): $\lambda = 572$ (s), 519 (sh), 327 (m), 303 (s) nm. - **Fluorescence** (DCM, $\lambda_{ex} = 350$ nm): $\lambda = 577$ nm. - Φ_F ($\lambda_{ex} = 490$ nm) = 0.24. - $\Phi_\Delta = 0.67$. - **MS** (APCI-HRMS(+)): $m/z = 763.4162$ [M+H]⁺, cal. for C₄₆H₅₃B₁Cl₁N₈+H₁: 763.4177.

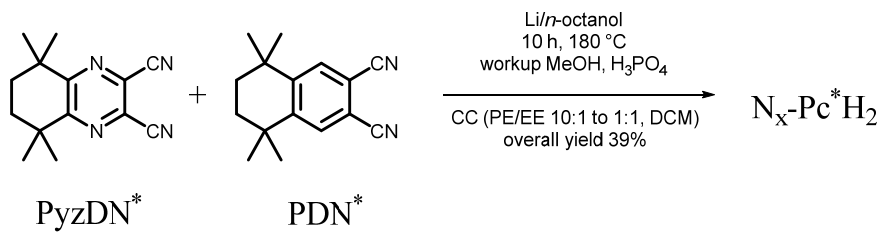
N₄-[Spc^{*}BCl]: Yield: 12 mg, 15.7 μ mol, 2%. - **¹H NMR** (CDCl₃, 300 MHz): $\delta = 8.78$ (s, 2 H, Ar-CH), 1.66-1.51 (m, 12 H, $-CH_2$), 1.38 (s, 9 H, $-CH_3$), 1.38 (s, 9 H, $-CH_3$), 1.35 (s, 9 H, $-CH_3$), 1.35 (s, 9 H, $-CH_3$) ppm. - **UV-Vis** (DCM): $\lambda = 557$ (s), 506 (sh), 330 (s), 296 (s) nm. - **Fluorescence** (DCM, $\lambda_{ex} = 350$ nm): $\lambda = 567$ nm. - Φ_F ($\lambda_{ex} = 490$ nm) = 0.22. - $\Phi_\Delta = 0.65$. - **MS** (APCI-HRMS(+)): $m/z = 765.4069$ [M+H]⁺, cal. for C₄₄H₅₁B₁Cl₁N₁₀+H₁: 765.4082.

[Sppz^{*}BCl]: Yield: <1%. - The analysis is in accordance to the one described in section 1.1.6. **Additional information:** For the synthesis of N_x-[Spc^{*}BCl], depending on the desired product, the corresponding ratios of dinitriles was varied. In the ¹H NMR spectra, dinitriles traces were observed.

1.1.8 Synthesis of Asymmetrical Phthalocyanines: $N_x\text{-Pc}^*\text{H}_2$



1.1.9 Synthesis of $N_x\text{-Pc}^*\text{H}_2$ ^[4]



According to **Fehler!** Verweisquelle konnte nicht gefunden werden. (p. Fehler! Textmarke nicht definiert.), using $\text{PyzDN}^* \text{2}/\text{PDN}^* \text{1}$ in a 1:1 ratio. The solution turned dark green. The isomers were separated by CC (PE(40/60)/EE gradient). At first, Pc^*H_2 and $\text{N}_2\text{-Pc}^*\text{H}_2$ were eluted, then ABAB and the symmetrical $A_2B_2 \text{ N}_4\text{-Pc}^*\text{H}_2$ were eluted. After changing the solvent to PE/EE 1:1 a mixture of $A_2B_2 \text{ N}_4\text{-Pc}^*\text{H}_2$ and $AB_3 \text{ N}_6\text{-Pc}^*\text{H}_2$ was eluted. Finally, Ppz^*H_2 was eluted with pure DCM. In a second CC (DCM), $A_2B_2 \text{ N}_4\text{-Pc}^*\text{H}_2$ and $AB_3 \text{ N}_6\text{-Pc}^*\text{H}_2$ were separated.

Pc^{*}H₂: **Yield:** 2%. - The analysis is in accordance with values in section **Fehler! Verweisquelle konnte nicht gefunden werden.** - $\Phi_F (\lambda_{ex} = 350 \text{ nm}) = 0.44$; - ($\lambda_{ex} = 598 \text{ nm}$) = 0.45. - $\Phi_\Delta = 0.16$.

N₂-Pc^{*}H₂: **Yield:** 4%. - **¹H NMR** (CDCl₃, 300 MHz): $\delta = 9.69$ (s, 2 H, Ar-CH), 9.65 (s, 2 H, Ar-CH), 9.42 (s, 2 H, Ar-CH), 2.19 (s, 4 H, -CH₂), 2.07 (s, 8 H, -CH₂), 2.04 (s, 4 H, -CH₂), 1.90 (s, 12 H, -CH₃), 1.83 (s, 12 H, -CH₃), 1.81 (s, 12 H, -CH₃), 1.81 (s, 12 H, -CH₃), -0.07 (s, 2 H, -NH) ppm. - **¹³C NMR** (C₆D₆, 75 MHz): $\delta = 160.6, 149.8, 149.2, 148.6, 137.0, 133.0, 132.2, 122.2, 121.6, 39.1, 36.1, 36.1, 35.9, 35.4, 35.3, 34.7, 32.9, 32.8, 32.7, 30.9$ ppm. - not all quartary atoms could be detected. - **IR** (ATR, 400-4000 cm⁻¹): $\tilde{\nu} = 3475$ (vw), 3297 (vw), 2956 (m), 2921 (m), 2855 (m), 2555 (vw), 2348 (vw), 1711 (m), 1688 (m), 1621 (m), 1539 (m), 1498 (s), 1460 (m), 1382 (m), 1358 (m), 1328 (m), 1301 (s), 1258 (m), 1242 (m), 1188 (m), 1159 (m), 1140 (m), 1119 (m), 1089 (m), 1071 (m), 1022 (s), 999 (m), 980 (m), 891 (m), 848 (m), 804 (m), 755 (s), 722 (m), 681 (s), 622 (m), 541 (m) cm⁻¹. - **CV** (DCM, [TBA]PF₆, Fc): $E_{ox1} = 0.43$, $E_{red1} = -1.23$, $E_{red2} = -1.65$ V. - **UV-Vis** (DCM): $\lambda = 687$ (s), 619 (sh), 340 (s), 306 (s), 232 (s) nm. - $\Phi_F (\lambda_{ex} = 350 \text{ nm}) = 0.31$; - ($\lambda_{ex} = 598 \text{ nm}$) = 0.33. - $\Phi_\Delta = 0.14$. - **MS** (APCI-HRMS(+)): $m/z = 957.5992$ [M+H]⁺, cal. for C₆₂H₇₂N₁₀+H₁: 957.6014. - **Elemental analysis** (C₆₂H₇₂N₁₀, M = 957.30 g/mol): fnd. (cal.): C: 75.29% (77.79%), H: 8.92% (7.58%), N: 10.14% (14.63%).

A₂B₂ N₄-Pc^{*}H₂: **Yield:** 17%. - **¹H NMR** (CDCl₃, 300 MHz): $\delta = 9.56$ (s, 2 H, Ar-CH), 9.50 (s, 2 H, Ar-CH), 2.20 (s, 8 H, -CH₂), 2.05 (s, 8 H, -CH₂), 1.91 (s, 24 H, -CH₃), 1.81 (s, 12 H, -CH₃), 1.80 (s, 12 H, -CH₃), -0.04 (s, 2 H, -NH) ppm. - **¹H NMR** (Pyridine-*d*₅, 300 MHz): $\delta = 9.87$ (s, 2 H, Ar-CH), 9.68 (s, 2 H, Ar-CH), 1.94 (s, 8 H, -CH₂), 1.76 (s, 8 H, -CH₂), 1.72 (s, 12 H, -CH₃), 1.67 (s, 12 H, -CH₃), 1.46 (s, 12 H, -CH₃), 1.37 (s, 12 H, -CH₃), -0.26 (s, 2 H, -NH) ppm. - **¹H NMR** (C₆D₆, 300 MHz): $\delta = 9.83$ (s, 2 H, Ar-CH), 9.82 (s, 2 H, Ar-CH), 1.86 (s, 8 H, -CH₂), 1.79 (s, 8 H, -CH₂), 1.75 (s, 24 H, -CH₃), 1.48 (s, 12 H, -CH₃), 1.38 (s, 12 H, -CH₃), -0.31 (s, 2 H, -NH) ppm. - **¹³C NMR** (C₆D₆, 75 MHz): $\delta = 162.4, 150.0, 149.6, 145.1, 144.4, 135.2, 134.8, 122.7, 122.0, 39.4, 39.3, 36.1, 36.0, 35.2, 34.6, 34.5, 32.7, 32.7, 21.1, 30.8$ ppm. - **IR** (ATR, 400-4000 cm⁻¹): $\tilde{\nu} = 3526$ (w), 3284 (w), 2915 (s), 2857 (s), 1736 (w), 1638 (w), 1553 (w), 1496 (w), 1455 (s), 1381 (w), 1358 (m), 1328 (m), 1300 (s), 1254 (m), 1242 (m), 1190 (m), 1162 (m), 1148 (m), 1128 (m), 1083 (w), 1048 (w), 1019 (s), 1001 (s), 983 (s), 949 (w), 936 (w), 893 (m), 851 (m), 828 (m), 761 (s), 752 (s), 717 (m), 700 (m), 679 (m), 623 (w), 560 (w), 543 (m), 507 (m), 443 (w), 429 (w) cm⁻¹. - **CV** (DCM, [TBA]PF₆, Fc): $E_{ox1} = 0.28$, $E_{red1} = -1.47$, $E_{red2} = -1.79$ V. - **UV-Vis** (DCM): $\lambda = 680$ (s), 656 (s), 625 (sh),

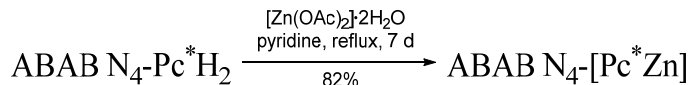
348 (s), 232 (s) nm. - Φ_F ($\lambda_{ex} = 350$ nm) = 0.13; - ($\lambda_{ex} = 598$ nm) = 0.14. - Φ_Δ = 0.07. - **MS** (APCI-HRMS(+)): m/z = 959.5921 [M+H]⁺, cal. for C₆₀H₇₀N₁₂+H₁: 959.5919. - **Elemental analysis** (C₆₀H₇₀N₁₂, M = 959.28 g/mol): fnd. (cal.): C: 72.03% (75.12%), H: 7.36% (7.36%), N: 16.36% (17.52%).

N₆-Pc^{*}H₂: **Yield:** 9%. - **¹H NMR** (CDCl₃, 300 MHz): δ = 9.75 (s, 2 H, Ar-CH), 2.22 (s, 4 H, -CH₂), 2.19 (s, 12 H, -CH₂), 1.93 (s, 12 H, -CH₃), 1.91 (s, 12 H, -CH₃), 1.90 (s, 12 H, -CH₃), 1.83 (s, 12 H, -CH₃), -0.53 (s, 2 H, -NH) ppm. - **¹³C NMR** (C₆D₆, 75 MHz): δ = 162.0, 139.1, 131.3, 134.1 (w), 132.9 (w), 132.9 (w), 131.3 (w), 127.1 (w), 123.1, 46.0, 41.3 (w), 39.7, 39.3, 36.3, 34.5, 32.8, 31.8, 31.7, 31.1, 30.9, 30.8, 29.8, 29.5, 29.3, 29.2, 28.6, 28.1, 27.5, 27.5 ppm. - 6 weak signal, marked with (w); not all quartary atoms could be detected. - **IR** (ATR, 400-4000 cm⁻¹): $\tilde{\nu}$ = 3291 (w), 2957 (s), 2924 (s), 2856 (s), 1727 (s), 1693 (s), 1637 (m), 1540 (m), 1503 (m), 1457 (s), 1411 (m), 1381 (m), 1360 (m), 1330 (m), 1305 (m), 1281 (m), 1257 (s), 1192 (s), 1157 (w), 1139 (m), 1127 (s), 1086 (m), 1072 (m), 1021 (s), 995 (s), 952 (m), 935 (w), 893 (w), 852 (m), 828 (m), 804 (m), 756 (m), 744 (s), 719 (s), 700 (w), 677 (s), 631 (m), 542 (w), 506 (w), 466 (w), 429 (w) cm⁻¹. - **CV** (DCM, [TBA]PF₆, Fc): E_{ox1} = 0.35, E_{red1} = -1.47, E_{red2} = -1.82 V. - **UV-Vis** (DCM): λ = 660 (s), 597 (sh), 343 (s), 234 (s) nm. - Φ_F ($\lambda_{ex} = 350$ nm) = 0.05; - ($\lambda_{ex} = 598$ nm) = 0.03. - Φ_Δ = 0.04. - **MS** (APCI-HRMS(+)): m/z = 961.5825 [M+H]⁺, cal. for C₅₈H₆₈N₁₄+H₁: 961.5824. - **Elemental analysis** (C₅₈H₆₈N₁₄, M = 961.25 g/mol): fnd. (cal.): C: 71.99% (72.47%), H: 9.49% (7.13%), N: 12.38% (20.40%).

Ppz^{*}H₂: **Yield:** 9%. - The analysis is in accordance with values in section **Fehler! Verweisquelle konnte nicht gefunden werden.** - Φ_F ($\lambda_{ex} = 350$ nm) = 0.03; - ($\lambda_{ex} = 598$ nm) = 0.03. - Φ_Δ = 0.05.



1.1.10 Synthesis of N₄-[Pc^{*}Zn] using [Zn(OAc)₂]



General Procedure for the Synthesis of N_x-[Pc^{*}Zn] using [Zn(OAc)₂]:

1 eq ABAB or A₂B₂ N₄-Pc^{*}H₂ was dissolved in pyridine and 1.2 eq [Zn(OAc)₂][.]2H₂O were added. After refluxing for 1 h, the reaction was monitored by TLC (DCM), and was stirred for another 1 h. The resulting blue solutions were concentrated in vacuum, filtered, and washed with an excess of water. After washing the product off the filter paper using CHCl₃/MeOH 3:1, the blue product was dried in vacuum and purified by preparative TLC or CC (Tol/THF 20:1).

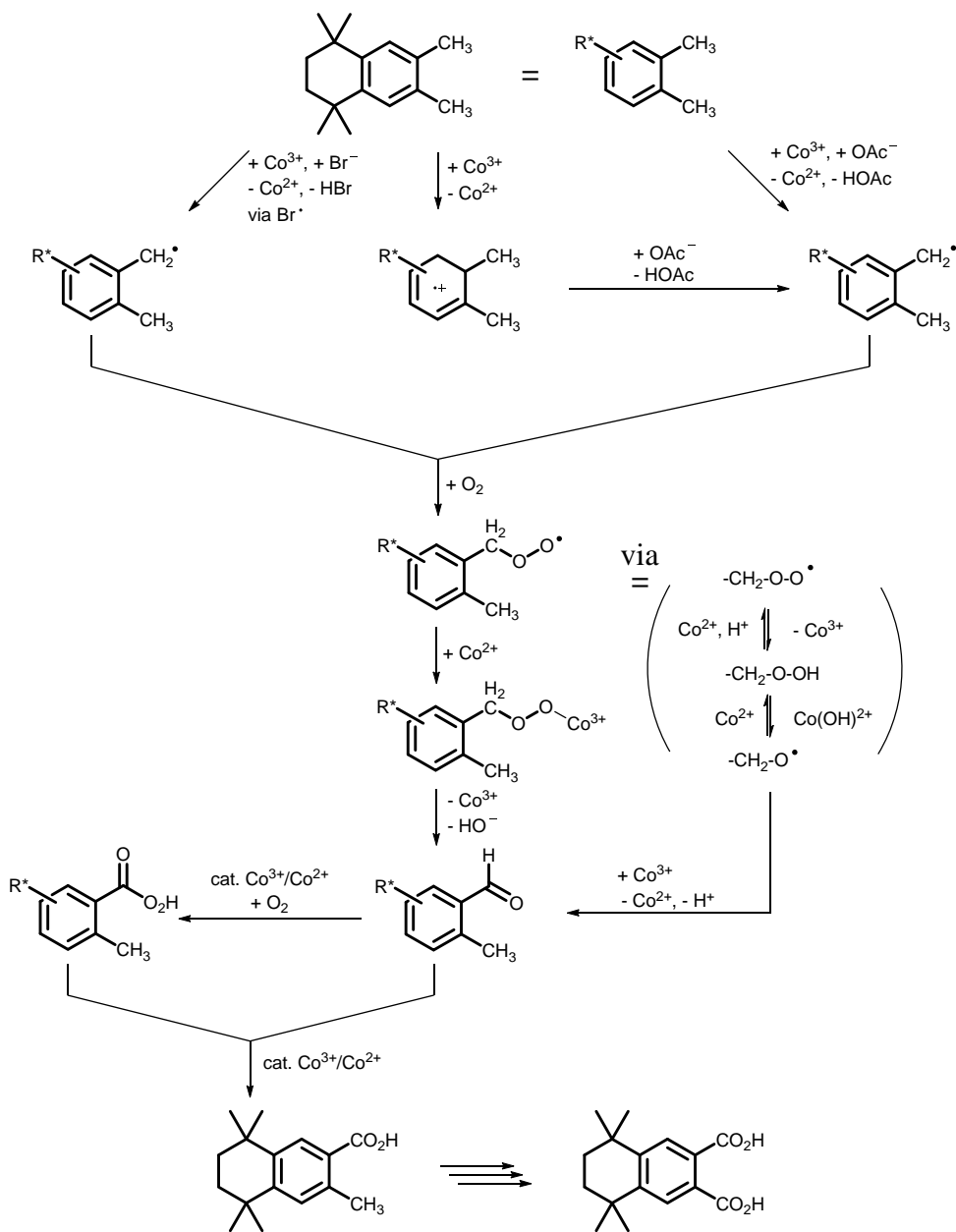
ABAB N₄-[Pc^{*}Zn]: Yield: 82%. - **R_f** (Tol/THF 20:1) = 0.63. - **¹H NMR** (C₆D₆, 300 MHz): δ = 9.96 (s, 4 H, Ar-CH), 1.91 (s, 8 H, -CH₂), 1.85 (s, 24 H, -CH₃), 1.78 (s, 8 H, -CH₂), 1.45 (s, 24 H, -CH₃) ppm. - **UV-Vis** (DCM): λ = 687 (s), 657 (s), 631 (sh), 596 (sh), 357 (s) nm. - **Φ_F** (λ_{ex} = 350 nm) = 0.16; - (λ_{ex} = 598 nm) = 0.18. - **Φ_Δ** = 0.73. - **MS** (APCI-HRMS(+)): *m/z* = 1021.5073 [M+H]⁺, cal. for C₆₀H₆₈N₁₂Zn₁+H₁: 1021.5054.

A₂B₂ N₄-[Pc^{*}Zn]: Yield: 76%. - The analysis is in accordance with the data described above.

All other N_x-[Pc^{*}Zn] are described in the Paper.

1.2 Suggested radical autoxidation mechanism of tetraline IV.

In literature, such Co(III) or Mn(III) assisted aerobic oxidations are discussed as radical chain reactions. Rate determining step is the selective benzylic C-H activation, H abstraction by Co(III)-coordinated acetate (quasi acetyl radical ligands) or by bromine radicals generated in the presence of bromide promotor. Instead of H atom abstraction, a sequence of electron transfer followed by deprotonation of the formed radical cation is discussed. The benzylic radicals Ar-CH₂[·] are trapped by oxygen, the peroxy radical is reduced by Co(II). Hock cleavage leads to a cabaldehyde, which undergoes further metal catalysed autoxidation steps to the carboxylic acid:



1.3 Absorbance and Emission Spectra

Absorption spectra of metal-free (full lines) and zinc complexes (dashed lines) in THF. The spectra were normalized to the same absorption in the B-band. a) 3a, 3b, b) 4a, 4b, c) 5a, 5b, d) 6a, 6b, e) 7a, 7b, f) 8a, 8b.

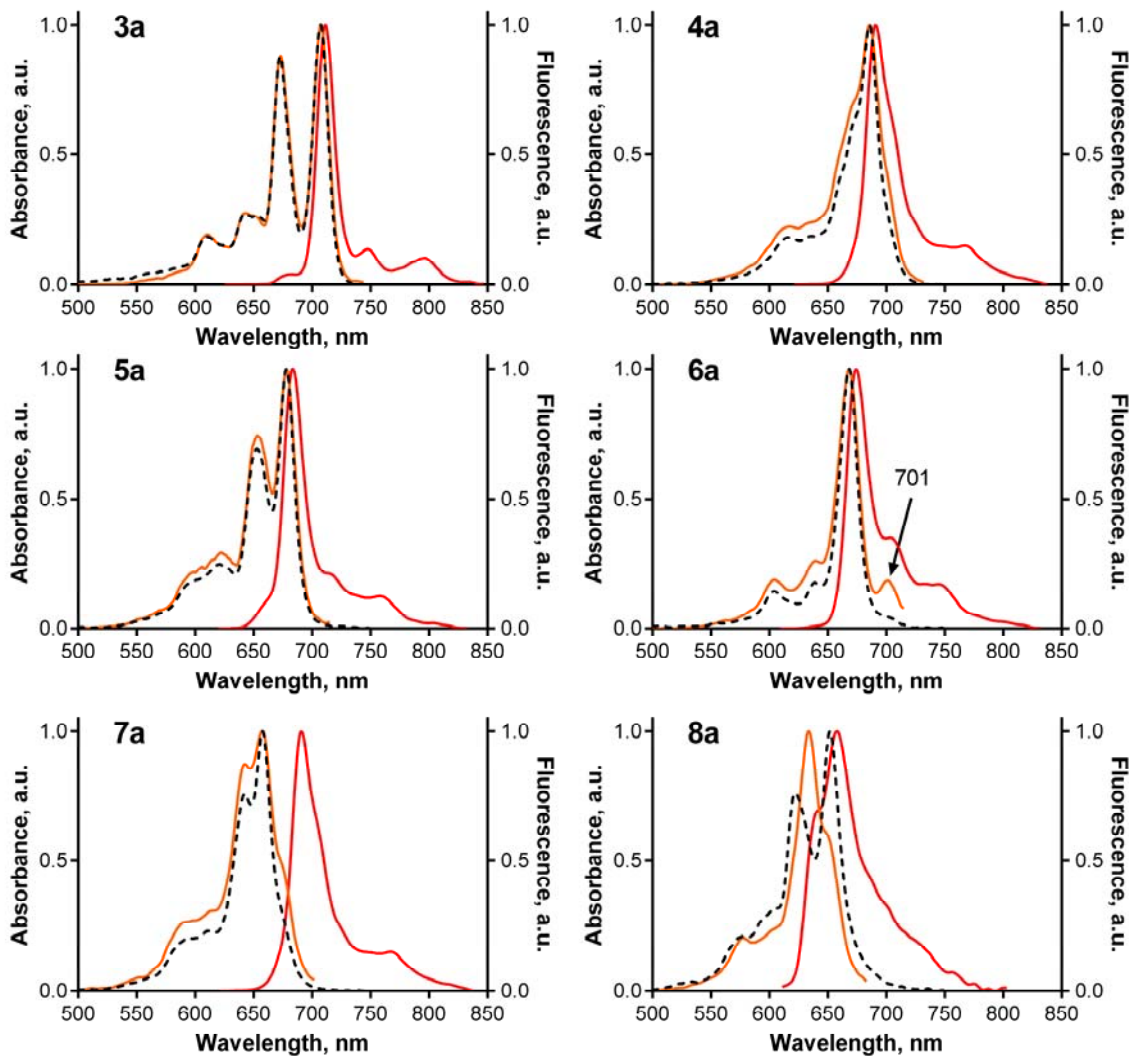


Figure SI-1. Normalized absorption (black, dashed), emission (red) and excitation (orange) spectra of $N_x\text{-Pc}^*\text{H}_2$ in THF.

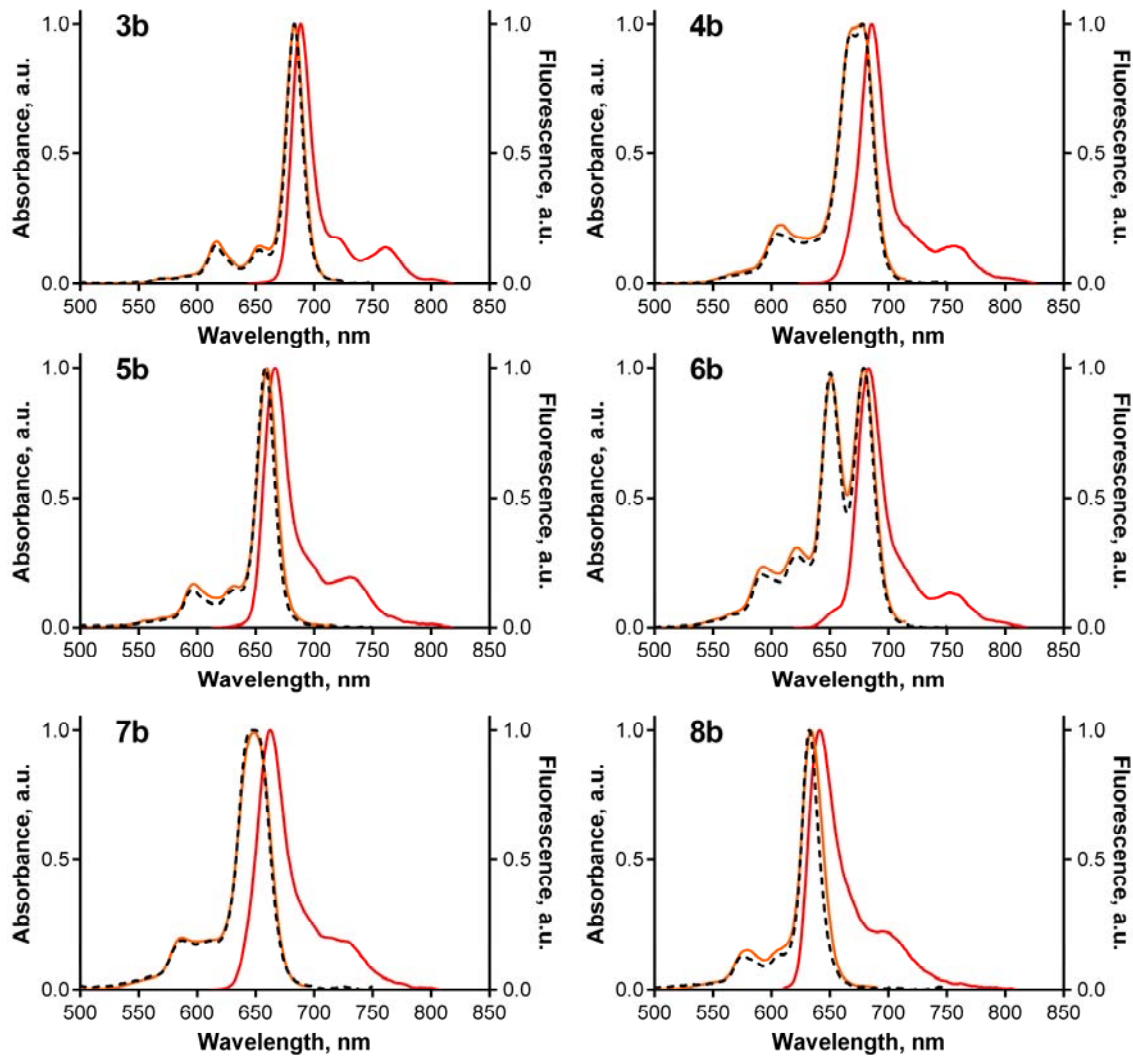


Figure SI-2. Normalized absorption (black, dashed), emission (red) and excitation (orange) spectra of $N_x\text{-Pc}^*\text{Zn}$ in THF.

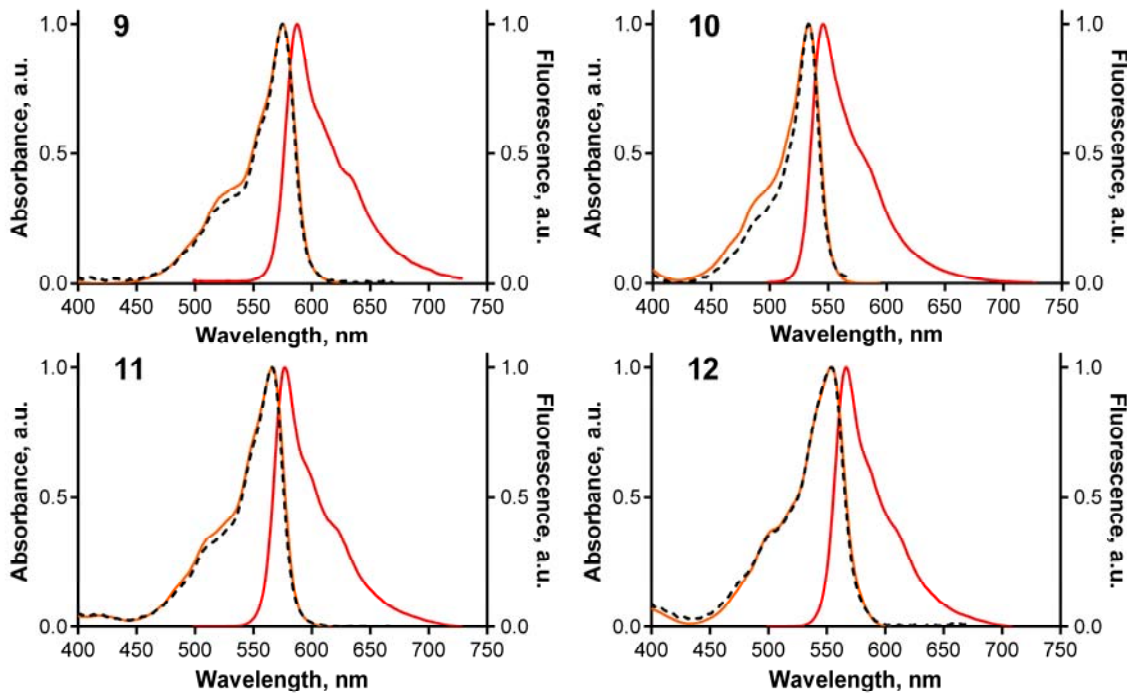


Figure SI-3. Normalized absorption (black, dashed), emission (red) and excitation (orange) spectra of $N_x\text{-Spc}^*\text{BzCl}$ in MeOH.

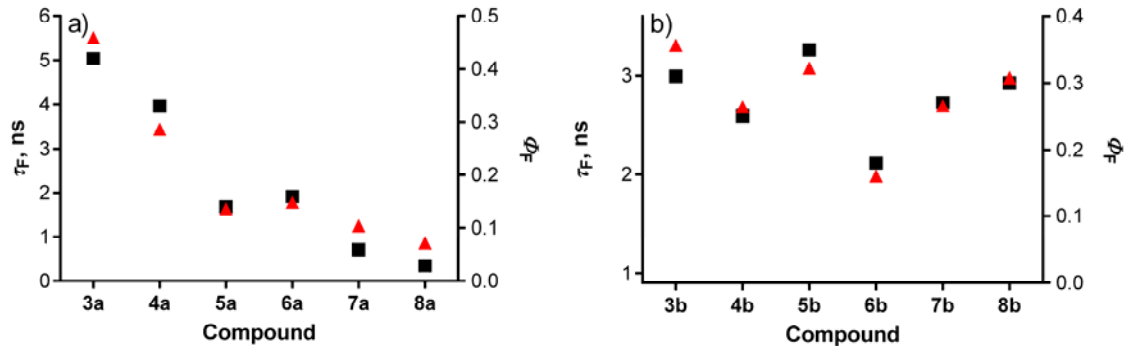


Figure SI-4. Correlation between ϕ_F (black squares) and τ_F (red triangles) values for $N_x\text{-Pc}^*\text{H}_2$ in THF (a) and $N_x\text{-Pc}^*\text{Zn}$ in THF (b). For purposes of this presentation, the relative contribution of each process to the average lifetime for compounds with two lifetime components (**7a** and **8a**) was calculated.

1.4 Computational results

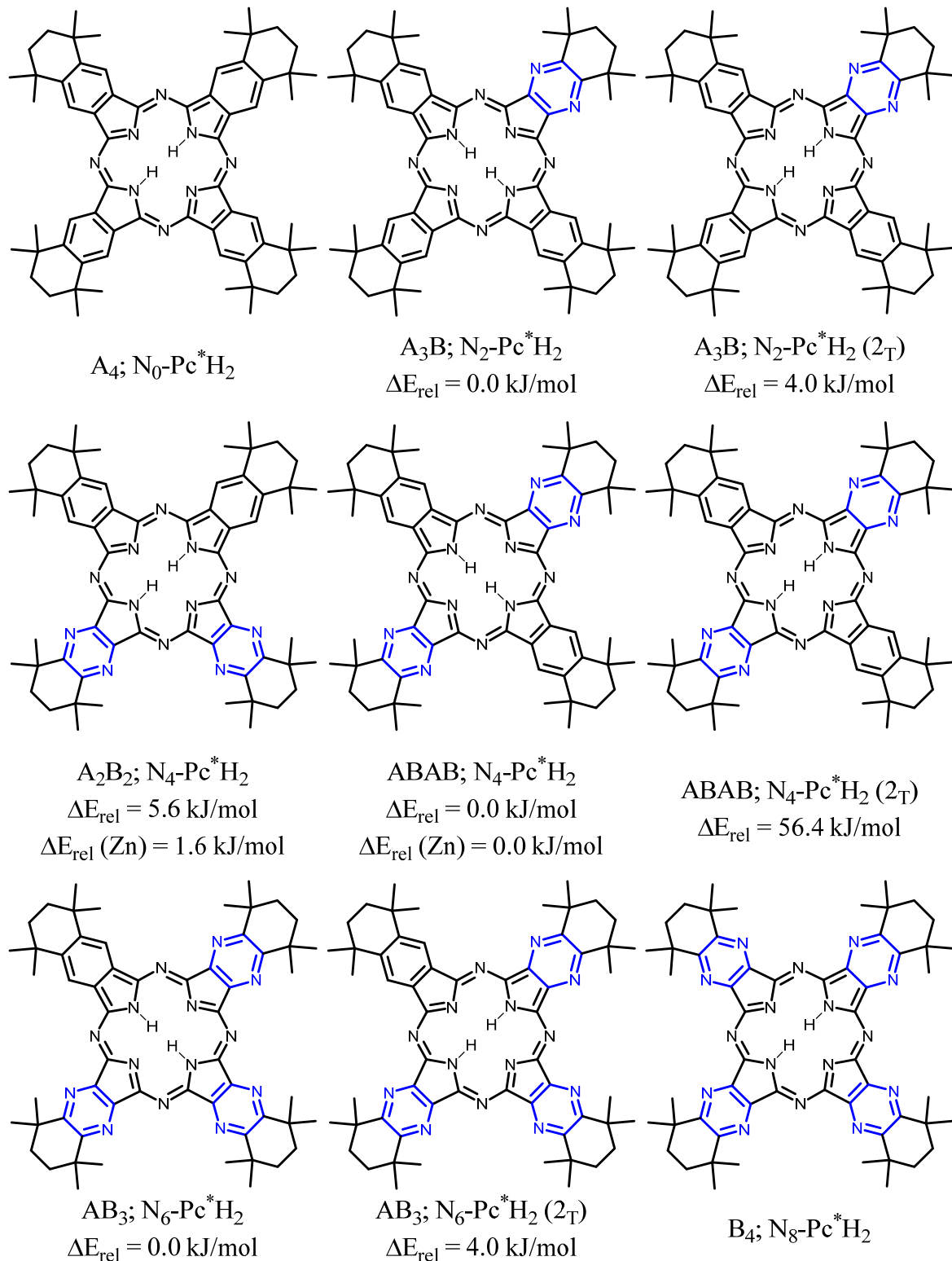


Figure SI-5. The phthalocyanines $N_x\text{-Pc}^*\text{H}_2$ ($A_4\text{H}_2$, $A_3\text{B}_1$, $A_2\text{B}_2$, $A_1\text{B}_3$ and $B_4\text{H}_2$) computationally investigated. Regioisomers are numbered and tautomers marked (subscript T). Energies are given relative to the most stable isomer (ΔE_{rel}). Zn-substituted phthalocyanines [Pc^*Zn] are derived by substituting the two central H atoms by Zn. Relative isomer energies are given as $\Delta E_{\text{rel}}(\text{Zn})$, no tautomers are found for [Pc^*Zn].

Table SI-1: Computed excitation energies (λ in nm), oscillator strengths (f), frontier orbital gaps ($\Delta_{H-L/L+1}$ in nm) and molecular orbital character of the transitions for the Q-bands. Dipole moment (μ) and isotropic polarizability (α) in a.u.^a

Molecule	λ / nm	$\Delta\lambda$ / nm	f	Character	$\Delta_{H-L/L+1}$ [c]	μ [d]	$\Delta\alpha$ [e]
N ₈ -Pc*H ₂	541	0	0.42	H → L+1	781	0.00	0.0
	536	0	0.53	H → L	818		
N ₆ -Pc*H ₂	550	9	0.56	H → L	861	0.87	23.6
	549	13	0.49	H → L+1	797		
N ₆ -Pc*H ₂ (2T)	559	18	0.47	H → L+1	839	0.92	26.6
	552	16	0.60	H → L	848		
N ₄ -Pc*H ₂ (A ₂ B ₂)	563	22	0.55	H → L+1 (39%)	845	1.25	28.3
				H → L (27%)			
				H → L (41%)			
	559	23	0.63	H → L+1 (18%)			
N ₄ -Pc*H ₂ (ABAB)	561	20	0.62	H → L	910	0.00	47.8
	560	24	0.55	H → L+1	815		
N ₄ -Pc*H ₂ (ABAB, 2T)	583	42	0.56	H → L+1	892	0.06	61.8
	580	44	0.54	H → L	911		
N ₂ -Pc*H ₂	569	28	0.62	H → L+1	855	0.90	71.1
	564	28	0.72	H → L	915		
N ₂ -Pc*H ₂ (2T)	577	36	0.61	H → L+1	897	0.87	73.3
	571	35	0.69	H → L	900		
N ₀ -Pc*H ₂	580	39	0.69	H → L+1	903	0.00	94.9
	568	32	0.81	H → L	923		
N ₈ -[Pc*Zn]	532	0	0.51	H → L	788	0.00	0.0
	532	0	0.51	H → L+1	788		
N ₆ -[Pc*Zn]	549	17	0.55	H → L	840	0.89	24.6
	544	12	0.59	H → L+1	810		
N ₄ -[Pc*Zn] (A ₂ B ₂)	556	26	0.62	H → L	852	1.25	47.6
	554	22	0.63	H → L+1	848		
N ₄ -[Pc*Zn] (ABAB)	565	33	0.60	H → L	898	0.00	49.5
	557	26	0.63	H → L+1	831		
N ₂ -[Pc*Zn]	566	34	0.69	H → L	897	0.88	71.1
	564	32	0.69	H → L+1	863		
N ₀ -[Pc*Zn]	570	38	0.77	H → L	902	0.00	93.7
	570	38	0.77	H → L+1	901		

[a] Shift relative to Q1/Q2 band of B₄M. [b] dominant MO transitions for the Q-bands (H: HOMO, H-2: HOMO-2, L: LUMO, L+1: LUMO+1). For A₂B₂H₂₋₁, relative contributions are given in percent. [c] Frontier MO gap of the orbitals given in the “character” column HOMO/LUMO and HOMO/LUMO+1) in nm. [d] All compounds exhibit an in-plane dipole moment only pointing toward the nitrogen-rich parts of the molecule. [e] Polarizabilities are given relative to B₄H₂ ($\alpha = 1091.3$ a.u.) and B₄Zn ($\alpha = 1097.1$ a.u.), respectively.

1.5 ^1H NMR Spectra

1.5.1 Subphthalocyanines

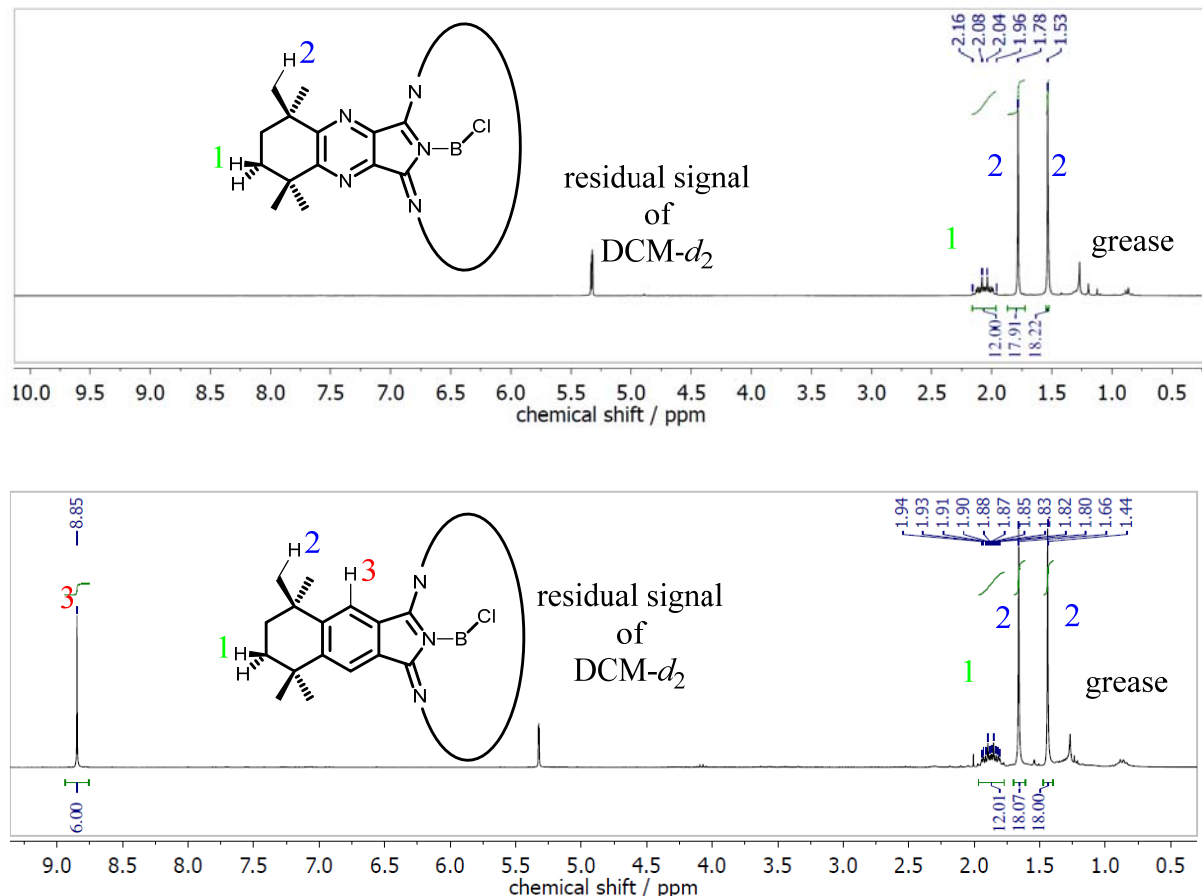


Figure SI-6. ^1H NMR spectrum of [Sppz*BCl] (above) / [Spc*BCl] (below) in DCM-d_2 , 300 MHz.

1.5.2 Azaphthalocyanines

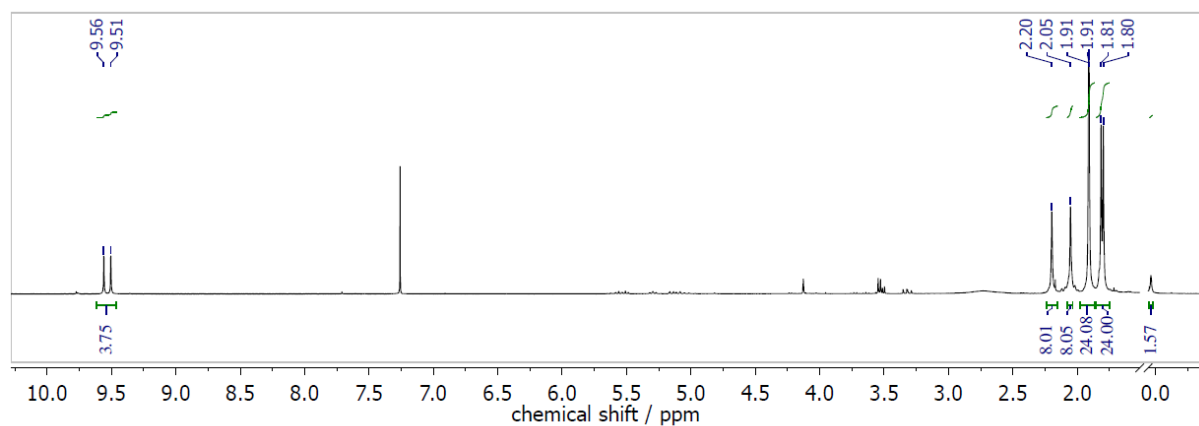
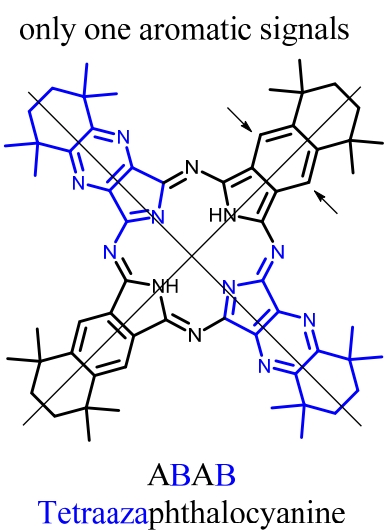
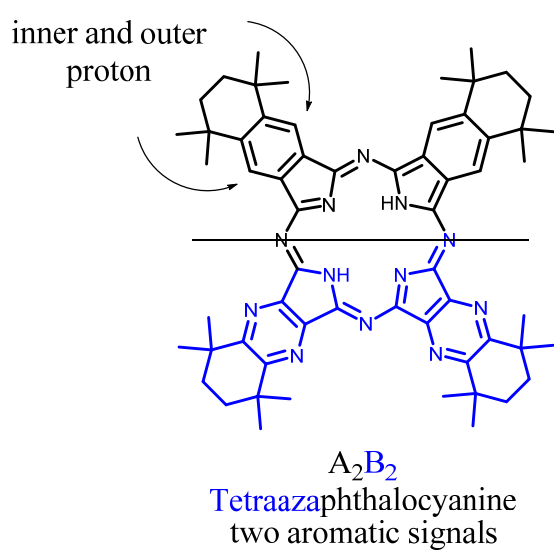
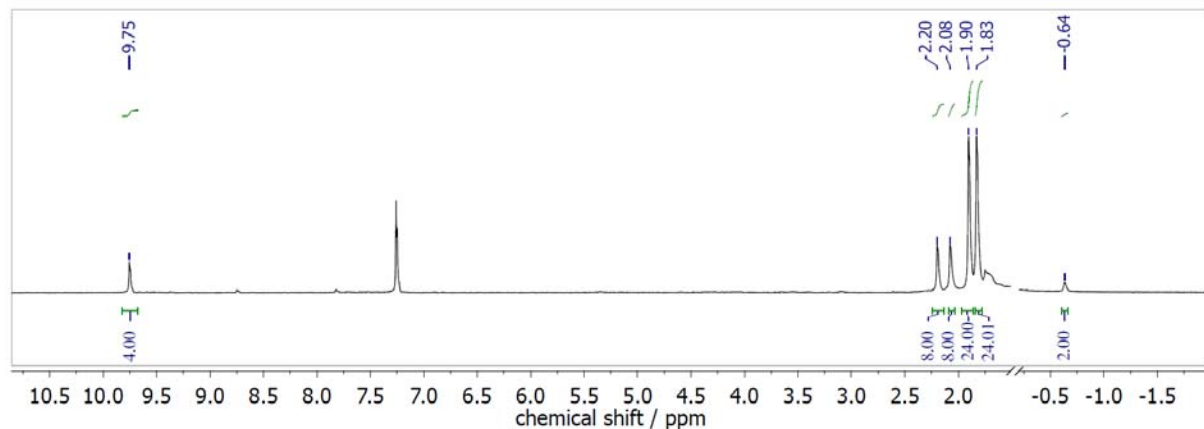


Figure SI-7. ^1H NMR spectrum of ABAB (above) / A_2B_2 (below) $\text{N}_4\text{-H}_2\text{Pc}^\cdot$ in CDCl_3 , 300 MHz.

1.6 Cyclovoltammetric measurements

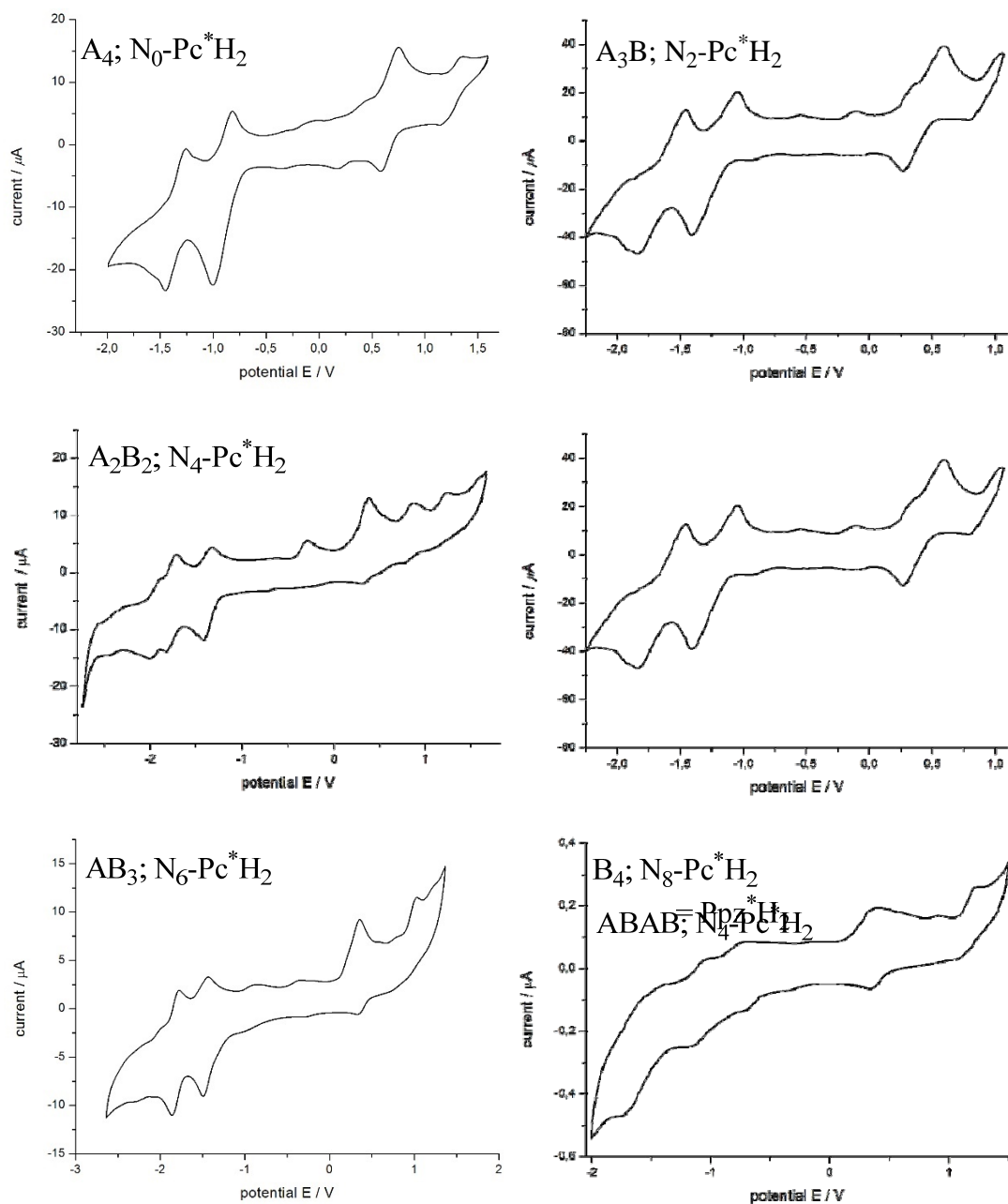


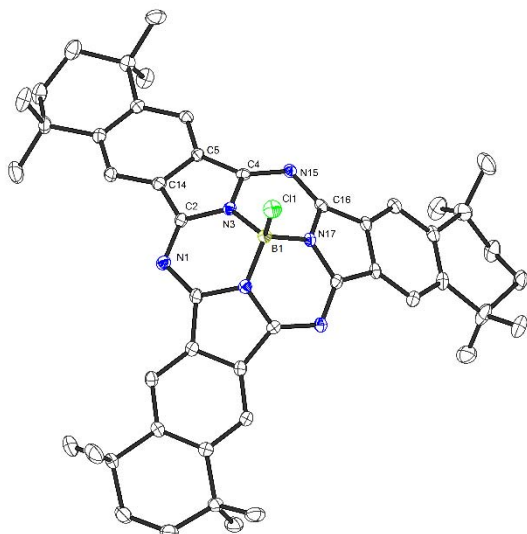
Figure SI-8. Cyclovoltammetric measurements of $\text{N}_x\text{-Pc}^*\text{H}_2$. All measurements were carried out in DCM, except of Ppz^*H_2 , which was measured in THF because of solubility. The red circles mark impurities caused by used DCM. In all cases, different scan rates were tested, here, 20 mV/s measurements are shown. The spectra are calibrated using Fc in the final scan, measured in $[\text{TBA}]PF_6$.

1.7 Crystal Structures

Crystal were measured with a Bruker D8 QUEST area detector. Crystal structures were resolved and refined by Dr. K. Harms of the service Department of Chemistry of the Philipps-Universität Marburg.

Diffractometer type	Bruker D8 QUEST area detector
Wavelength	0.71073 Å
Temperature	100(2) K
Index ranges	-14<=h<=14, -28<=k<=28, -15<=l<=15
Data collection software	BRUKER APEX2 2014.9-0 ^[6]
Cell refinement software	BRUKER SAINT ^[7]
Data reduction software	SAINT V8.34A (Bruker AXS Inc., 2013) ^[7]
Programs used	XT V2014/1 (Bruker AXS Inc., 2014) ^[8,9] SHELXL-2014/7 (Sheldrick, 2014) ^[8,10] DIAMOND (Crystal Impact) ^[11]

1.7.1 Crystal Structure of [Spc^{*}BCl]



Habitus, colour	prism, colourless
Crystal size	0.22 x 0.22 x 0.09 mm ³
Crystal system	Orthorhombic
Space group	Cmc ₂ ₁ Z = 4
Unit cell dimensions	a = 24.8236(10) Å α= 90°. b = 16.3090(6) Å β= 90°. c = 10.9728(4) Å γ = 90°.
Volume	4442.3(3) Å ³
Cell determination	9874 peaks with Theta 2.4 to 25.4°.
Empirical formula	C ₄₉ H ₅₆ B Cl ₃ N ₆
Moiety formula	C ₄₈ H ₅₄ B Cl N ₆ , CH ₂ Cl ₂
Formula weight	846.15
Density (calculated)	1.265 Mg/m ³
Absorption coefficient	0.248 mm ⁻¹
F(000)	1792
Solution and refinement:	
Reflections collected	28577
Independent reflections	4177 [R(int) = 0.0342]
Completeness to theta = 25.242°	99.9 %
Observed reflections	4031[I>2sigma(I)]
Reflections used for refinement	4177
Absorption correction	Semi-empirical from equivalents ^[12]
Max. and min. transmission	0.98 and 0.86
Flack parameter (absolute struct.)	0.001(14)
Largest diff. peak and hole	0.283 and -0.192 e.Å ⁻³
Solution	Direct methods ^[8]
Refinement	Full-matrix least-squares on F ² ^[8]
Treatment of hydrogen atoms	Calculated positions, constr. ref.
Data / restraints / parameters	4177 / 44 / 311
Goodness-of-fit on F ²	1.049
R index (all data)	wR2 = 0.0754
R index conventional [I>2sigma(I)]	R1 = 0.0293

Table SI-2. Atomic coordinates and equivalent isotropic displacement parameters (\AA^2) for ML153F_0m. U(eq) is defined as one third of the trace of the orthogonalized U^{ij} tensor.

	x	y	z	U(eq)	Occupancy
N1	0.5000	0.08718(16)	0.7070(3)	0.0163(6)	1
N3	0.54732(7)	0.15242(11)	0.54643(17)	0.0130(4)	1
N15	0.59330(7)	0.26327(11)	0.45407(16)	0.0136(4)	1
N17	0.5000	0.24139(16)	0.4157(2)	0.0127(5)	1
C2	0.54616(9)	0.11154(13)	0.6547(2)	0.0149(4)	1
C4	0.59270(8)	0.19816(13)	0.5299(2)	0.0128(4)	1
C5	0.62944(9)	0.17210(13)	0.6260(2)	0.0138(4)	1
C6	0.68271(9)	0.19023(13)	0.6541(2)	0.0141(4)	1
C7	0.70788(9)	0.15358(13)	0.7545(2)	0.0144(4)	1
C8	0.76727(10)	0.17460(14)	0.7780(2)	0.0186(5)	1
C9	0.79202(10)	0.11748(16)	0.8738(2)	0.0253(6)	1
C10	0.75505(11)	0.10051(17)	0.9799(2)	0.0257(6)	1
C11	0.70338(10)	0.05628(15)	0.9411(2)	0.0197(5)	1
C12	0.67783(9)	0.10049(13)	0.8318(2)	0.0150(4)	1
C13	0.62411(9)	0.08414(14)	0.8058(2)	0.0162(5)	1
C14	0.60011(9)	0.11829(13)	0.7033(2)	0.0148(5)	1
C16	0.54605(9)	0.28670(13)	0.40512(19)	0.0137(4)	1
C18	0.52856(9)	0.36689(14)	0.3620(2)	0.0145(4)	1
C19	0.55637(9)	0.43836(13)	0.3359(2)	0.0174(5)	1
C20	0.52846(9)	0.51054(14)	0.3088(2)	0.0180(5)	1
C21	0.56208(11)	0.58749(16)	0.2815(3)	0.0287(6)	1
C22	0.5284(2)	0.6650(3)	0.2921(7)	0.0259(11)	0.5
C23	0.4778(2)	0.6530(3)	0.2168(6)	0.0242(11)	0.5
C24	0.66584(12)	0.05663(19)	1.0520(2)	0.0328(6)	1
C25	0.71454(12)	-0.03249(16)	0.9045(3)	0.0306(6)	1
C26	0.80131(9)	0.16592(17)	0.6619(2)	0.0267(6)	1
C27	0.77020(10)	0.26457(15)	0.8206(2)	0.0242(5)	1
C28	0.59861(12)	0.57227(19)	0.1717(3)	0.0376(7)	1
C29	0.5886(4)	0.6179(6)	0.3816(10)	0.033(2)	0.5
C29A	0.6058(3)	0.6001(6)	0.3970(9)	0.0251(17)	0.5
B1	0.5000	0.1569(2)	0.4646(3)	0.0130(7)	1
Cl1	0.5000	0.07386(5)	0.34930(7)	0.02119(19)	1
C1S	0.5136(3)	0.1520(5)	1.0477(6)	0.054(3)	0.5
Cl1S	0.56140(14)	0.22218(19)	1.1014(2)	0.0507(6)	0.5
Cl2S	0.44951(15)	0.1926(3)	1.0606(5)	0.1026(15)	0.5

Table SI-3. Bond lengths [Å] and angles [°] for ML153F_0m.

N1-C2	1.342(3)	C20-C21	1.537(3)
N1-C2#1	1.342(3)	C21-C29	1.374(10)
N3-C2	1.363(3)	C21-C22	1.521(6)
N3-C4	1.363(3)	C21-C28	1.528(4)
N3-B1	1.480(3)	C21-C29A	1.682(8)
N15-C16	1.345(3)	C22-C23	1.514(7)
N15-C4	1.349(3)	C22-C29	1.947(10)
N17-C16	1.366(3)	C22-H22A	0.9700
N17-C16#1	1.366(3)	C22-H22B	0.9700
N17-B1	1.479(4)	C23-H23A	0.9700
C2-C14	1.446(3)	C23-H23B	0.9701
C4-C5	1.457(3)	C24-H24A	0.9800
C5-C6	1.390(3)	C24-H24B	0.9800
C5-C14	1.421(3)	C24-H24C	0.9800
C6-C7	1.401(3)	C25-H25A	0.9800
C6-H6	0.9500	C25-H25B	0.9800
C7-C12	1.423(3)	C25-H25C	0.9800
C7-C8	1.536(3)	C26-H26A	0.9800
C8-C9	1.533(3)	C26-H26B	0.9800
C8-C26	1.535(3)	C26-H26C	0.9800
C8-C27	1.542(3)	C27-H27A	0.9800
C9-C10	1.508(4)	C27-H27B	0.9800
C9-H9A	0.9900	C27-H27C	0.9800
C9-H9B	0.9900	C28-H28A	0.9800
C10-C11	1.532(3)	C28-H28B	0.9800
C10-H10A	0.9900	C28-H28C	0.9800
C10-H10B	0.9900	C29-H29A	0.9800
C11-C25	1.528(4)	C29-H29B	0.9800
C11-C24	1.533(4)	C29-H29C	0.9800
C11-C12	1.537(3)	C29A-H29D	0.9800
C12-C13	1.389(3)	C29A-H29E	0.9800
C13-C14	1.390(3)	C29A-H29F	0.9800
C13-H13	0.9500	B1-N3#1	1.480(3)
C16-C18	1.457(3)	B1-C11	1.853(4)
C18-C19	1.385(3)	C1S-C12S	1.730(9)
C18-C18#1	1.418(4)	C1S-C11S	1.750(7)
C19-C20	1.398(3)	C1S-H1S1	0.9900
C19-H19	0.9500	C1S-H1S2	0.9900
C20-C20#1	1.413(5)		
C2-N1-C2#1	117.3(3)	C7-C6-H6	119.7
C2-N3-C4	113.63(19)	C6-C7-C12	119.6(2)
C2-N3-B1	122.4(2)	C6-C7-C8	117.7(2)
C4-N3-B1	123.3(2)	C12-C7-C8	122.6(2)
C16-N15-C4	117.41(18)	C9-C8-C26	107.0(2)
C16-N17-C16#1	113.6(3)	C9-C8-C7	111.37(19)
C16-N17-B1	122.34(13)	C26-C8-C7	111.61(19)
C16#1-N17-B1	122.34(13)	C9-C8-C27	110.59(19)
N1-C2-N3	122.4(2)	C26-C8-C27	108.3(2)
N1-C2-C14	131.0(2)	C7-C8-C27	107.97(19)
N3-C2-C14	105.34(19)	C10-C9-C8	113.4(2)
N15-C4-N3	121.43(19)	C10-C9-H9A	108.9
N15-C4-C5	131.98(19)	C8-C9-H9A	108.9
N3-C4-C5	105.18(18)	C10-C9-H9B	108.9
C6-C5-C14	119.1(2)	C8-C9-H9B	108.9
C6-C5-C4	133.9(2)	H9A-C9-H9B	107.7
C14-C5-C4	106.92(19)	C9-C10-C11	112.4(2)
C5-C6-C7	120.5(2)	C9-C10-H10A	109.1
C5-C6-H6	119.7	C11-C10-H10A	109.1

C9-C10-H10B	109.1	H24A-C24-H24C	109.5
C11-C10-H10B	109.1	H24B-C24-H24C	109.5
H10A-C10-H10B	107.9	C11-C25-H25A	109.5
C25-C11-C10	111.6(2)	C11-C25-H25B	109.5
C25-C11-C24	108.8(2)	H25A-C25-H25B	109.5
C10-C11-C24	106.7(2)	C11-C25-H25C	109.5
C25-C11-C12	108.3(2)	H25A-C25-H25C	109.5
C10-C11-C12	110.0(2)	H25B-C25-H25C	109.5
C24-C11-C12	111.6(2)	C8-C26-H26A	109.5
C13-C12-C7	119.9(2)	C8-C26-H26B	109.5
C13-C12-C11	117.8(2)	H26A-C26-H26B	109.5
C7-C12-C11	122.30(19)	C8-C26-H26C	109.5
C12-C13-C14	120.0(2)	H26A-C26-H26C	109.5
C12-C13-H13	120.0	H26B-C26-H26C	109.5
C14-C13-H13	120.0	C8-C27-H27A	109.5
C13-C14-C5	120.7(2)	C8-C27-H27B	109.5
C13-C14-C2	131.7(2)	H27A-C27-H27B	109.5
C5-C14-C2	107.56(19)	C8-C27-H27C	109.5
N15-C16-N17	122.8(2)	H27A-C27-H27C	109.5
N15-C16-C18	130.1(2)	H27B-C27-H27C	109.5
N17-C16-C18	105.30(19)	C21-C28-H28A	109.5
C19-C18-C18#1	119.90(13)	C21-C28-H28B	109.5
C19-C18-C16	132.4(2)	H28A-C28-H28B	109.5
C18#1-C18-C16	107.34(12)	C21-C28-H28C	109.5
C18-C19-C20	120.4(2)	H28A-C28-H28C	109.5
C18-C19-H19	119.8	H28B-C28-H28C	109.5
C20-C19-H19	119.8	C21-C29-C22	51.0(3)
C19-C20-C20#1	119.71(13)	C21-C29-H29A	109.5
C19-C20-C21	117.4(2)	C22-C29-H29A	159.2
C20#1-C20-C21	122.90(13)	C21-C29-H29B	109.5
C29-C21-C22	84.4(5)	C22-C29-H29B	75.8
C29-C21-C28	113.9(5)	H29A-C29-H29B	109.5
C22-C21-C28	121.5(3)	C21-C29-H29C	109.5
C29-C21-C20	113.5(5)	C22-C29-H29C	86.5
C22-C21-C20	111.4(3)	H29A-C29-H29C	109.5
C28-C21-C20	110.1(2)	H29B-C29-H29C	109.5
C28-C21-C29A	103.4(4)	C21-C29A-H29D	109.5
C20-C21-C29A	107.6(4)	C21-C29A-H29E	109.5
C23-C22-C21	107.8(4)	H29D-C29A-H29E	109.5
C23-C22-C29	149.3(5)	C21-C29A-H29F	109.5
C21-C22-C29	44.6(4)	H29D-C29A-H29F	109.5
C23-C22-H22A	110.5	H29E-C29A-H29F	109.5
C21-C22-H22A	110.3	N17-B1-N3#1	105.42(18)
C29-C22-H22A	94.7	N17-B1-N3	105.42(18)
C23-C22-H22B	109.7	N3#1-B1-N3	105.0(3)
C21-C22-H22B	109.9	N17-B1-Cl1	115.7(2)
C29-C22-H22B	76.7	N3#1-B1-Cl1	112.22(16)
H22A-C22-H22B	108.6	N3-B1-Cl1	112.22(16)
C22-C23-H23A	109.0	Cl2S-C1S-Cl1S	110.2(4)
C22-C23-H23B	109.8	Cl2S-C1S-H1S1	109.6
H23A-C23-H23B	108.2	Cl1S-C1S-H1S1	109.6
C11-C24-H24A	109.5	Cl2S-C1S-H1S2	109.6
C11-C24-H24B	109.5	Cl1S-C1S-H1S2	109.6
H24A-C24-H24B	109.5	H1S1-C1S-H1S2	108.1
C11-C24-H24C	109.5		

Symmetry transformations used to generate equivalent atoms:

#1 -x+1,y,z

Table SI-4. Anisotropic displacement parameters (\AA^2) for ML153F_0m.The anisotropic displacement factor exponent takes the form: $-2\pi^2 [h^2 a^{*2} U^{11} + \dots + 2 h k a^{*} b^{*} U^{12}]$

	U ¹¹	U ²²	U ³³	U ²³	U ¹³	U ¹²
N1	0.0136(13)	0.0147(13)	0.0207(14)	0.0030(11)	0.000	0.000
N3	0.0135(9)	0.0100(9)	0.0155(9)	0.0009(7)	0.0006(7)	0.0013(7)
N15	0.0156(9)	0.0129(9)	0.0123(9)	-0.0002(7)	0.0014(7)	0.0011(7)
N17	0.0153(13)	0.0113(12)	0.0114(12)	0.0010(10)	0.000	0.000
C2	0.0173(11)	0.0102(10)	0.0173(11)	0.0029(9)	0.0010(9)	0.0025(9)
C4	0.0122(10)	0.0117(10)	0.0147(10)	-0.0022(9)	0.0022(9)	0.0010(8)
C5	0.0167(11)	0.0100(10)	0.0148(10)	0.0005(8)	0.0019(8)	0.0025(9)
C6	0.0153(10)	0.0122(10)	0.0148(10)	-0.0007(9)	0.0028(9)	0.0001(9)
C7	0.0164(11)	0.0109(10)	0.0161(10)	-0.0032(9)	0.0000(9)	0.0017(8)
C8	0.0185(11)	0.0173(11)	0.0199(12)	0.0001(9)	-0.0031(9)	-0.0025(9)
C9	0.0220(12)	0.0222(12)	0.0318(15)	0.0045(11)	-0.0094(11)	-0.0037(10)
C10	0.0293(13)	0.0249(13)	0.0228(13)	0.0037(10)	-0.0088(11)	-0.0007(11)
C11	0.0214(12)	0.0212(12)	0.0165(12)	0.0062(9)	-0.0038(9)	-0.0004(10)
C12	0.0191(10)	0.0128(10)	0.0132(11)	-0.0013(8)	-0.0010(9)	0.0024(8)
C13	0.0188(11)	0.0141(10)	0.0159(10)	0.0025(9)	0.0013(9)	0.0019(9)
C14	0.0157(11)	0.0118(10)	0.0168(11)	0.0001(8)	0.0017(9)	0.0014(8)
C16	0.0168(11)	0.0143(11)	0.0100(10)	-0.0016(9)	0.0027(9)	-0.0014(9)
C18	0.0201(11)	0.0139(10)	0.0094(9)	0.0008(8)	0.0016(9)	0.0012(9)
C19	0.0190(10)	0.0170(10)	0.0163(11)	0.0021(9)	0.0024(10)	-0.0019(9)
C20	0.0263(12)	0.0137(11)	0.0139(10)	0.0023(9)	0.0025(9)	-0.0004(10)
C21	0.0269(14)	0.0163(12)	0.0429(16)	0.0090(11)	0.0101(12)	-0.0015(11)
C22	0.032(3)	0.013(2)	0.033(3)	0.004(2)	-0.007(2)	-0.004(2)
C23	0.028(2)	0.015(2)	0.030(3)	0.010(2)	-0.003(2)	-0.0007(18)
C24	0.0364(15)	0.0440(17)	0.0179(13)	0.0104(12)	-0.0024(11)	-0.0013(13)
C25	0.0389(15)	0.0209(13)	0.0318(13)	0.0056(11)	-0.0133(13)	0.0037(11)
C26	0.0145(11)	0.0363(14)	0.0293(14)	-0.0023(12)	-0.0007(11)	-0.0002(10)
C27	0.0251(12)	0.0206(12)	0.0268(13)	-0.0015(10)	-0.0076(10)	-0.0041(10)
C28	0.0354(16)	0.0410(16)	0.0362(17)	0.0160(14)	0.0075(13)	-0.0115(13)
C29	0.030(5)	0.024(4)	0.046(5)	0.008(3)	-0.010(4)	-0.006(3)
C29A	0.022(4)	0.018(4)	0.035(4)	0.002(3)	-0.016(3)	-0.005(3)
B1	0.0137(17)	0.0111(16)	0.0141(17)	-0.0016(14)	0.000	0.000
C11	0.0270(4)	0.0151(4)	0.0215(4)	-0.0066(3)	0.000	0.000
C1S	0.081(8)	0.047(3)	0.035(3)	0.002(3)	-0.009(3)	-0.023(4)
C11S	0.0548(13)	0.0534(15)	0.0440(11)	0.0083(9)	-0.0010(9)	-0.0125(11)
C12S	0.062(2)	0.095(3)	0.151(4)	0.058(3)	-0.045(2)	-0.032(2)

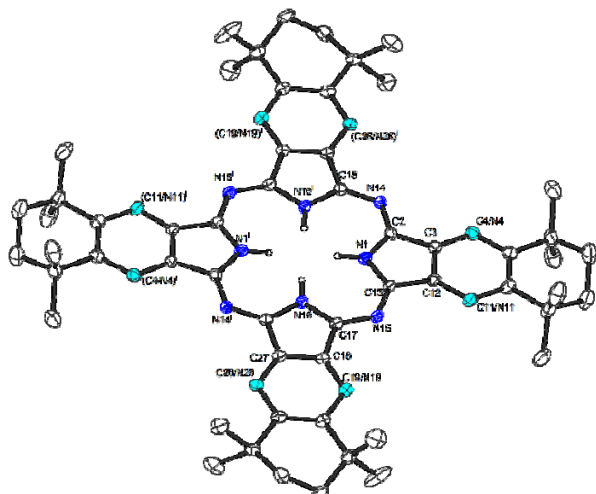
Table SI-5. Hydrogen coordinates and isotropic displacement parameters (\AA^2) for ML153F_0m.

	x	y	z	U(eq)	Occupancy
H6	0.7022	0.2278	0.6048	0.017	1
H9A	0.8016	0.0648	0.8344	0.030	1
H9B	0.8257	0.1425	0.9048	0.030	1
H10A	0.7454	0.1530	1.0196	0.031	1
H10B	0.7743	0.0665	1.0405	0.031	1
H13	0.6038	0.0496	0.8582	0.019	1
H19	0.5946	0.4383	0.3364	0.021	1
H22A	0.5486	0.7120	0.2629	0.031	0.5
H22B	0.5187	0.6744	0.3766	0.031	0.5
H23A	0.4878	0.6332	0.1366	0.029	0.5
H23B	0.4593	0.7050	0.2071	0.029	0.5
H24A	0.6331	0.0256	1.0330	0.049	1
H24B	0.6562	0.1133	1.0725	0.049	1
H24C	0.6842	0.0313	1.1215	0.049	1
H25A	0.6806	-0.0596	0.8834	0.046	1
H25B	0.7315	-0.0614	0.9727	0.046	1
H25C	0.7387	-0.0334	0.8339	0.046	1
H26A	0.8392	0.1772	0.6810	0.040	1
H26B	0.7886	0.2050	0.6005	0.040	1
H26C	0.7979	0.1100	0.6302	0.040	1
H27A	0.8079	0.2797	0.8350	0.036	1
H27B	0.7497	0.2709	0.8963	0.036	1
H27C	0.7549	0.3003	0.7577	0.036	1
H28A	0.6183	0.6227	0.1519	0.056	1
H28B	0.5767	0.5558	0.1016	0.056	1
H28C	0.6243	0.5286	0.1911	0.056	1
H29A	0.6135	0.5764	0.4130	0.050	0.5
H29B	0.5623	0.6320	0.4449	0.050	0.5
H29C	0.6088	0.6671	0.3584	0.050	0.5
H29D	0.6335	0.5572	0.3933	0.038	0.5
H29E	0.5866	0.5963	0.4748	0.038	0.5
H29F	0.6230	0.6540	0.3904	0.038	0.5
H1S1	0.5212	0.1388	0.9613	0.065	0.5
H1S2	0.5160	0.1006	1.0955	0.065	0.5

Table SI-6. Torsion angles [°] for ML153F_0m.

C2#1-N1-C2-N3	-6.4(4)	C16#1-N17-C16-C18	-10.8(3)
C2#1-N1-C2-C14	158.84(17)	B1-N17-C16-C18	-176.2(2)
C4-N3-C2-N1	156.6(2)	N15-C16-C18-C19	14.2(4)
B1-N3-C2-N1	-14.2(3)	N17-C16-C18-C19	179.0(3)
C4-N3-C2-C14	-11.9(2)	N15-C16-C18-C18#1	-158.6(2)
B1-N3-C2-C14	177.3(2)	N17-C16-C18-C18#1	6.19(19)
C16-N15-C4-N3	6.9(3)	C18#1-C18-C19-C20	-0.4(3)
C16-N15-C4-C5	-157.4(2)	C16-C18-C19-C20	-172.5(2)
C2-N3-C4-N15	-156.0(2)	C18-C19-C20-C20#1	0.4(3)
B1-N3-C4-N15	14.7(3)	C18-C19-C20-C21	179.7(2)
C2-N3-C4-C5	12.0(2)	C19-C20-C21-C29	-69.4(5)
B1-N3-C4-C5	-177.4(2)	C20#1-C20-C21-C29	109.9(4)
N15-C4-C5-C6	-19.3(4)	C19-C20-C21-C22	-162.6(4)
N3-C4-C5-C6	174.6(2)	C20#1-C20-C21-C22	16.7(4)
N15-C4-C5-C14	159.3(2)	C19-C20-C21-C28	59.7(3)
N3-C4-C5-C14	-6.9(2)	C20#1-C20-C21-C28	-121.05(18)
C14-C5-C6-C7	2.4(3)	C19-C20-C21-C29A	-52.3(4)
C4-C5-C6-C7	-179.2(2)	C20#1-C20-C21-C29A	127.0(4)
C5-C6-C7-C12	-3.1(3)	C29-C21-C22-C23	-163.8(6)
C5-C6-C7-C8	178.3(2)	C28-C21-C22-C23	81.5(5)
C6-C7-C8-C9	-168.6(2)	C20-C21-C22-C23	-50.7(5)
C12-C7-C8-C9	12.9(3)	C28-C21-C22-C29	-114.6(6)
C6-C7-C8-C26	-49.0(3)	C20-C21-C22-C29	113.1(5)
C12-C7-C8-C26	132.4(2)	C28-C21-C29-C22	122.0(4)
C6-C7-C8-C27	69.8(3)	C20-C21-C29-C22	-110.9(4)
C12-C7-C8-C27	-108.7(2)	C16-N17-B1-N3#1	137.5(2)
C26-C8-C9-C10	-163.7(2)	C16#1-N17-B1-N3#1	-26.6(3)
C7-C8-C9-C10	-41.5(3)	C16-N17-B1-N3	26.6(3)
C27-C8-C9-C10	78.6(3)	C16#1-N17-B1-N3	-137.5(2)
C8-C9-C10-C11	62.5(3)	C16-N17-B1-Cl1	-98.0(2)
C9-C10-C11-C25	71.0(3)	C16#1-N17-B1-Cl1	98.0(2)
C9-C10-C11-C24	-170.3(2)	C2-N3-B1-N17	140.7(2)
C9-C10-C11-C12	-49.2(3)	C4-N3-B1-N17	-29.2(3)
C6-C7-C12-C13	1.2(3)	C2-N3-B1-N3#1	29.6(3)
C8-C7-C12-C13	179.7(2)	C4-N3-B1-N3#1	-140.25(18)
C6-C7-C12-C11	178.1(2)	C2-N3-B1-Cl1	-92.6(2)
C8-C7-C12-C11	-3.4(3)	C4-N3-B1-Cl1	97.6(2)
C25-C11-C12-C13	75.7(3)		
C10-C11-C12-C13	-162.2(2)		
C24-C11-C12-C13	-44.1(3)		
C25-C11-C12-C7	-101.3(3)		
C10-C11-C12-C7	20.8(3)		
C24-C11-C12-C7	139.0(2)		
C7-C12-C13-C14	1.3(3)		
C11-C12-C13-C14	-175.7(2)		
C12-C13-C14-C5	-2.0(3)		
C12-C13-C14-C2	179.6(2)		
C6-C5-C14-C13	0.1(3)		
C4-C5-C14-C13	-178.7(2)		
C6-C5-C14-C2	178.88(19)		
C4-C5-C14-C2	0.1(2)		
N1-C2-C14-C13	18.2(4)		
N3-C2-C14-C13	-174.7(2)		
N1-C2-C14-C5	-160.4(3)		
N3-C2-C14-C5	6.7(2)		
C4-N15-C16-N17	-9.1(3)		
C4-N15-C16-C18	153.4(2)		
C16#1-N17-C16-N15	155.38(15)		
B1-N17-C16-N15	-10.0(4)		

1.7.2 Crystal Structure of N₂-Pc*H₂



Habitus, colour	plate, dark
Crystal size	0.29 x 0.22 x 0.05 mm ³
Crystal system	Monoclinic
Space group	P2 ₁ /c
Unit cell dimensions	Z = 2 a = 11.7078(4) Å b = 23.2759(7) Å c = 12.9884(5) Å 3539.3(2) Å ³
Volume	α= 90°. β= 90.620(3)°. γ = 90°.
Cell determination	9908 peaks with Theta 2.3 to 25.2°.
Empirical formula	C ₆₆ H ₇₆ Cl ₁₂ N ₁₀
Moiety formula	C ₆₂ H ₇₂ N ₁₀ , 4(CHCl ₃)
Formula weight	1434.76
Density (calculated)	1.346 Mg/m ³
Absorption coefficient	0.516 mm ⁻¹
F(000)	1492

Solution and refinement:	
Reflections collected	35003
Independent reflections	6438 [R(int) = 0.0640]
Completeness to theta = 25.242°	99.9 %
Observed reflections	4815[I>2sigma(I)]
Reflections used for refinement	6438
Absorption correction	Semi-empirical from equivalents ^[12]
Max. and min. transmission	0.97 and 0.84
Largest diff. peak and hole	0.491 and -0.364 e.Å ⁻³
Solution	Direct methods ^[8]
Refinement	Full-matrix least-squares on F ² ^[8]
Treatment of hydrogen atoms	Mixture of constr. and indep. refinement
Data / restraints / parameters	6438 / 203 / 602
Goodness-of-fit on F ²	1.023
R index (all data)	wR2 = 0.1178
R index conventional [I>2sigma(I)]	R1 = 0.0489

Table SI-7. Atomic coordinates and equivalent isotropic displacement parameters (\AA^2) for ML026F1_0m. U(eq) is defined as one third of the trace of the orthogonalized U^{ij} tensor.

	x	y	z	U(eq)	Occupancy
N1	0.46545(16)	0.57666(8)	0.44525(14)	0.0153(4)	1
C2	0.3647(2)	0.60621(10)	0.45428(17)	0.0157(5)	1
C3	0.3755(2)	0.66129(10)	0.40227(17)	0.0156(5)	1
C4	0.30198(19)	0.70643(10)	0.38898(17)	0.0184(5)	0.75
N4	0.30198(19)	0.70643(10)	0.38898(17)	0.0184(5)	0.25
C5	0.3388(2)	0.75406(11)	0.33488(19)	0.0204(5)	1
C6	0.2532(2)	0.80284(11)	0.3170(2)	0.0268(6)	1
C7	0.3150(2)	0.85787(12)	0.2849(2)	0.0333(7)	1
C8	0.4002(2)	0.84750(12)	0.2011(2)	0.0338(7)	1
C9	0.4967(2)	0.80731(11)	0.2343(2)	0.0268(6)	1
C10	0.4506(2)	0.75531(11)	0.29354(18)	0.0202(5)	1
C11	0.5243(2)	0.70961(10)	0.30888(17)	0.0193(5)	0.75
N11	0.5243(2)	0.70961(10)	0.30888(17)	0.0193(5)	0.25
C12	0.4863(2)	0.66329(10)	0.36324(17)	0.0160(5)	1
C13	0.54049(19)	0.60941(10)	0.39127(17)	0.0154(5)	1
N14	0.27091(16)	0.59019(8)	0.50347(14)	0.0148(4)	1
N15	0.64678(16)	0.59652(8)	0.36288(15)	0.0171(4)	1
C15	0.26385(19)	0.54088(10)	0.55360(17)	0.0151(5)	1
N16	0.65576(16)	0.50203(8)	0.44055(14)	0.0152(4)	1
C17	0.6968(2)	0.54665(10)	0.38416(17)	0.0161(5)	1
C18	0.81001(19)	0.53126(10)	0.34750(17)	0.0154(5)	1
C19	0.88411(19)	0.55965(10)	0.28424(17)	0.0177(5)	0.75
N19	0.88411(19)	0.55965(10)	0.28424(17)	0.0177(5)	0.25
C20	0.9858(2)	0.53270(10)	0.25919(18)	0.0178(5)	1
C21	1.0653(2)	0.56474(11)	0.18526(19)	0.0230(6)	1
C22	1.1584(4)	0.5251(2)	0.1448(4)	0.0275(11)	0.8
C23	1.2118(3)	0.48884(18)	0.2312(3)	0.0250(9)	0.8
C22A	1.1861(17)	0.5330(11)	0.1886(15)	0.039(6)	0.2
C23A	1.1811(17)	0.4745(8)	0.1838(17)	0.040(4)	0.2
C24	1.1240(2)	0.44669(11)	0.27591(18)	0.0190(5)	1
C25	1.0129(2)	0.47795(10)	0.30069(17)	0.0170(5)	1
C26	0.93612(18)	0.45022(10)	0.36436(17)	0.0162(5)	0.75
N26	0.93612(18)	0.45022(10)	0.36436(17)	0.0162(5)	0.25
C27	0.83524(19)	0.47700(10)	0.38659(17)	0.0158(5)	1
C28	0.9988(3)	0.58457(17)	0.0908(2)	0.0527(10)	1
C29	1.1156(3)	0.61711(13)	0.2400(3)	0.0416(8)	1
C30	1.1785(5)	0.4210(2)	0.3759(4)	0.0294(12)	0.8
C31	1.1000(5)	0.3983(2)	0.2006(4)	0.0241(11)	0.8
C30A	1.193(2)	0.4464(8)	0.3646(18)	0.035(6)	0.2
C31A	1.0955(19)	0.3834(11)	0.2407(18)	0.031(5)	0.2
C33	0.1689(2)	0.78408(13)	0.2317(2)	0.0380(7)	1
C34	0.1873(3)	0.81629(13)	0.4147(3)	0.0427(8)	1
C35	0.5593(3)	0.78816(14)	0.1376(2)	0.0475(9)	1
C36	0.5807(3)	0.83935(13)	0.3052(3)	0.0411(8)	1
C1S	0.4189(4)	1.07467(18)	0.3759(3)	0.0589(10)	1
Cl1	0.3082(13)	0.9987(7)	0.4049(13)	0.087(4)	0.089(3)
Cl2	0.384(2)	0.9986(8)	0.3634(16)	0.080(4)	0.079(3)
Cl3	0.4567(5)	1.00427(14)	0.3302(4)	0.0668(13)	0.635(3)
Cl4	0.4849(10)	1.0172(5)	0.3321(10)	0.069(3)	0.234(3)
Cl5	0.5264(15)	1.0658(9)	0.3633(14)	0.080(4)	0.070(2)
Cl6	0.54339(12)	1.11200(7)	0.41534(12)	0.0615(4)	0.843(3)
Cl7	0.488(3)	1.1245(12)	0.411(2)	0.077(6)	0.054(3)
Cl8	0.345(2)	1.1101(9)	0.4684(17)	0.137(8)	0.103(3)
Cl9	0.31974(12)	1.07437(15)	0.47132(11)	0.0788(8)	0.794(3)
C110	0.3195(16)	1.0394(10)	0.4564(17)	0.098(5)	0.099(3)
C2S	0.8490(3)	0.70760(18)	0.4147(3)	0.0404(10)	0.9

C2SA	0.962(4)	0.733(2)	0.560(4)	0.078(6)	0.1
Cl11	0.844(2)	0.7483(13)	0.650(2)	0.092(6)	0.049(2)
Cl12	0.788(2)	0.8059(13)	0.5125(17)	0.090(5)	0.058(3)
Cl13	0.80543(14)	0.76779(9)	0.49037(10)	0.0609(5)	0.785(3)
Cl14	0.7662(10)	0.7308(7)	0.4884(9)	0.088(3)	0.123(3)
Cl15	0.887(2)	0.7915(12)	0.4584(19)	0.097(5)	0.058(2)
Cl16	0.7871(13)	0.6961(7)	0.4299(14)	0.090(5)	0.095(3)
Cl17	0.85946(7)	0.72932(4)	0.28604(6)	0.0343(3)	0.884(2)
Cl18	0.9371(18)	0.6712(10)	0.4653(18)	0.068(5)	0.079(3)
Cl19	0.98215(13)	0.68209(7)	0.46156(13)	0.0437(4)	0.809(3)
Cl20	0.9905(18)	0.7094(11)	0.524(2)	0.081(5)	0.061(3)

Table SI-8. Bond lengths [Å] and angles [°] for ML026F1_0m.

N1-C13	1.363(3)	C22A-H22C	0.9900
N1-C2	1.371(3)	C22A-H22D	0.9900
N1-H1	0.8800	C23A-C24	1.521(19)
C2-N14	1.330(3)	C23A-H23C	0.9900
C2-C3	1.455(3)	C23A-H23D	0.9900
C3-N4	1.368(3)	C24-C30A	1.40(3)
C3-C4	1.368(3)	C24-C31	1.516(7)
C3-C12	1.398(3)	C24-C25	1.528(3)
C4-C5	1.384(3)	C24-C30	1.561(6)
C4-H4	0.9500	C24-C31A	1.58(3)
N4-C5	1.384(3)	C25-N26	1.387(3)
C5-C10	1.421(3)	C25-C26	1.387(3)
C5-C6	1.531(3)	C26-C27	1.369(3)
C6-C34	1.524(4)	C26-H26	0.9500
C6-C7	1.532(4)	N26-C27	1.369(3)
C6-C33	1.539(4)	C27-C15#1	1.464(3)
C7-C8	1.503(4)	C28-H28A	0.9800
C7-H7A	0.9900	C28-H28B	0.9800
C7-H7B	0.9900	C28-H28C	0.9800
C8-C9	1.525(4)	C29-H29A	0.9800
C8-H8A	0.9900	C29-H29B	0.9800
C8-H8B	0.9900	C29-H29C	0.9800
C9-C35	1.527(4)	C30-H30A	0.9800
C9-C36	1.534(4)	C30-H30B	0.9800
C9-C10	1.535(3)	C30-H30C	0.9800
C10-N11	1.382(3)	C31-H31A	0.9800
C10-C11	1.382(3)	C31-H31B	0.9800
C11-C12	1.366(3)	C31-H31C	0.9800
C11-H11	0.9500	C30A-H30D	0.9800
N11-C12	1.366(3)	C30A-H30E	0.9800
C12-C13	1.450(3)	C30A-H30F	0.9800
C13-N15	1.336(3)	C31A-H31D	0.9800
N14-C15	1.323(3)	C31A-H31E	0.9800
N15-C17	1.328(3)	C31A-H31F	0.9800
C15-N16#1	1.374(3)	C33-H33A	0.9800
C15-C27#1	1.464(3)	C33-H33B	0.9800
N16-C17	1.362(3)	C33-H33C	0.9800
N16-C15#1	1.374(3)	C34-H34A	0.9800
N16-H16	0.8800	C34-H34B	0.9800
C17-C18	1.458(3)	C34-H34C	0.9800
C18-N19	1.371(3)	C35-H35A	0.9800
C18-C19	1.371(3)	C35-H35B	0.9800
C18-C27	1.392(3)	C35-H35C	0.9800
C19-C20	1.388(3)	C36-H36A	0.9800
C19-H19	0.9500	C36-H36B	0.9800
N19-C20	1.388(3)	C36-H36C	0.9800
C20-C25	1.418(3)	C1S-Cl5	1.287(17)
C20-C21	1.537(3)	C1S-Cl7	1.48(3)
C21-C28	1.518(4)	C1S-Cl4	1.648(12)
C21-C29	1.527(4)	C1S-Cl8	1.701(18)
C21-C22	1.527(6)	C1S-Cl9	1.708(4)
C21-C22A	1.60(2)	C1S-Cl6	1.768(5)
C22-C23	1.531(6)	C1S-Cl10	1.774(18)
C22-H22A	0.9900	C1S-Cl3	1.799(6)
C22-H22B	0.9900	C1S-Cl2	1.82(2)
C23-C24	1.539(5)	C1S-Cl1	2.227(18)
C23-H23A	0.9900	C1S-H1S	1.09(5)
C23-H23B	0.9900	Cl1-Cl2	1.04(3)
C22A-C23A	1.36(3)	Cl1-Cl10	1.17(3)

Cl1-Cl4	2.32(2)	C2SA-Cl18	1.92(6)
Cl2-Cl4	1.33(3)	C2SA-Cl15	2.08(6)
Cl2-Cl10	1.72(3)	C2SA-H2SA	1.0000
Cl2-Cl5	2.29(3)	Cl11-Cl14	2.32(3)
Cl4-Cl5	1.29(2)	Cl11-Cl12	2.32(4)
Cl5-Cl7	1.57(4)	Cl12-Cl15	1.40(3)
Cl7-Cl8	1.87(4)	Cl12-Cl14	1.79(3)
Cl8-Cl10	1.68(3)	Cl14-Cl16	1.138(18)
C2S-Cl17	1.751(4)	Cl14-Cl15	2.04(3)
C2S-Cl19	1.770(4)	Cl14-Cl18	2.46(2)
C2S-Cl13	1.789(5)	Cl15-Cl20	2.41(3)
C2S-H2S	1.0000	Cl16-Cl18	1.90(2)
C2SA-Cl11	1.85(6)	Cl18-Cl20	1.32(3)
C13-N1-C2	108.86(19)	C11-C10-C9	117.2(2)
C13-N1-H1	125.6	C5-C10-C9	122.4(2)
C2-N1-H1	125.6	C12-C11-C10	118.4(2)
N14-C2-N1	128.0(2)	C12-C11-H11	120.8
N14-C2-C3	123.1(2)	C10-C11-H11	120.8
N1-C2-C3	108.85(19)	C12-N11-C10	118.4(2)
N4-C3-C12	120.9(2)	N11-C12-C3	121.5(2)
C4-C3-C12	120.9(2)	C11-C12-C3	121.5(2)
N4-C3-C2	132.7(2)	N11-C12-C13	131.9(2)
C4-C3-C2	132.7(2)	C11-C12-C13	131.9(2)
C12-C3-C2	106.4(2)	C3-C12-C13	106.58(19)
C3-C4-C5	118.7(2)	N15-C13-N1	128.6(2)
C3-C4-H4	120.6	N15-C13-C12	122.1(2)
C5-C4-H4	120.6	N1-C13-C12	109.27(19)
C3-N4-C5	118.7(2)	C15-N14-C2	122.4(2)
N4-C5-C10	120.1(2)	C17-N15-C13	123.3(2)
C4-C5-C10	120.1(2)	N14-C15-N16#1	127.7(2)
N4-C5-C6	117.7(2)	N14-C15-C27#1	124.2(2)
C4-C5-C6	117.7(2)	N16#1-C15-C27#1	108.09(19)
C10-C5-C6	122.2(2)	C17-N16-C15#1	109.80(19)
C34-C6-C5	111.3(2)	C17-N16-H16	125.1
C34-C6-C7	107.4(2)	C15#1-N16-H16	125.1
C5-C6-C7	110.5(2)	N15-C17-N16	128.4(2)
C34-C6-C33	109.4(2)	N15-C17-C18	123.2(2)
C5-C6-C33	108.2(2)	N16-C17-C18	108.4(2)
C7-C6-C33	110.1(2)	N19-C18-C27	121.5(2)
C8-C7-C6	112.5(2)	C19-C18-C27	121.5(2)
C8-C7-H7A	109.1	N19-C18-C17	131.3(2)
C6-C7-H7A	109.1	C19-C18-C17	131.3(2)
C8-C7-H7B	109.1	C27-C18-C17	107.1(2)
C6-C7-H7B	109.1	C18-C19-C20	118.2(2)
H7A-C7-H7B	107.8	C18-C19-H19	120.9
C7-C8-C9	112.9(2)	C20-C19-H19	120.9
C7-C8-H8A	109.0	C18-N19-C20	118.2(2)
C9-C8-H8A	109.0	N19-C20-C25	120.4(2)
C7-C8-H8B	109.0	C19-C20-C25	120.4(2)
C9-C8-H8B	109.0	N19-C20-C21	117.0(2)
H8A-C8-H8B	107.8	C19-C20-C21	117.0(2)
C8-C9-C35	107.9(2)	C25-C20-C21	122.6(2)
C8-C9-C36	109.8(2)	C28-C21-C29	109.0(3)
C35-C9-C36	109.0(3)	C28-C21-C22	105.5(3)
C8-C9-C10	111.2(2)	C29-C21-C22	111.7(3)
C35-C9-C10	110.9(2)	C28-C21-C20	110.1(2)
C36-C9-C10	108.0(2)	C29-C21-C20	109.2(2)
N11-C10-C5	120.4(2)	C22-C21-C20	111.1(3)
C11-C10-C5	120.4(2)	C28-C21-C22A	127.5(7)
N11-C10-C9	117.2(2)	C29-C21-C22A	91.1(10)

C20-C21-C22A	107.5(8)	H29A-C29-H29C	109.5
C21-C22-C23	111.6(3)	H29B-C29-H29C	109.5
C21-C22-H22A	109.3	C24-C30-H30A	109.5
C23-C22-H22A	109.3	C24-C30-H30B	109.5
C21-C22-H22B	109.3	H30A-C30-H30B	109.5
C23-C22-H22B	109.3	C24-C30-H30C	109.5
H22A-C22-H22B	108.0	H30A-C30-H30C	109.5
C22-C23-C24	111.0(3)	H30B-C30-H30C	109.5
C22-C23-H23A	109.4	C24-C31-H31A	109.5
C24-C23-H23A	109.4	C24-C31-H31B	109.5
C22-C23-H23B	109.4	H31A-C31-H31B	109.5
C24-C23-H23B	109.4	C24-C31-H31C	109.5
H23A-C23-H23B	108.0	H31A-C31-H31C	109.5
C23A-C22A-C21	115.0(18)	H31B-C31-H31C	109.5
C23A-C22A-H22C	108.5	C24-C30A-H30D	109.5
C21-C22A-H22C	108.5	C24-C30A-H30E	109.5
C23A-C22A-H22D	108.5	H30D-C30A-H30E	109.5
C21-C22A-H22D	108.5	C24-C30A-H30F	109.5
H22C-C22A-H22D	107.5	H30D-C30A-H30F	109.5
C22A-C23A-C24	114.1(16)	H30E-C30A-H30F	109.5
C22A-C23A-H23C	108.7	C24-C31A-H31D	109.5
C24-C23A-H23C	108.7	C24-C31A-H31E	109.5
C22A-C23A-H23D	108.7	H31D-C31A-H31E	109.5
C24-C23A-H23D	108.7	C24-C31A-H31F	109.5
H23C-C23A-H23D	107.6	H31D-C31A-H31F	109.5
C30A-C24-C23A	113.4(13)	H31E-C31A-H31F	109.5
C30A-C24-C25	108.2(9)	C6-C33-H33A	109.5
C31-C24-C25	109.7(3)	C6-C33-H33B	109.5
C23A-C24-C25	110.2(8)	H33A-C33-H33B	109.5
C31-C24-C23	110.5(3)	C6-C33-H33C	109.5
C25-C24-C23	110.5(2)	H33A-C33-H33C	109.5
C31-C24-C30	108.9(3)	H33B-C33-H33C	109.5
C25-C24-C30	110.4(3)	C6-C34-H34A	109.5
C23-C24-C30	106.9(3)	C6-C34-H34B	109.5
C30A-C24-C31A	110.6(12)	H34A-C34-H34B	109.5
C23A-C24-C31A	105.2(11)	C6-C34-H34C	109.5
C25-C24-C31A	109.1(8)	H34A-C34-H34C	109.5
N26-C25-C20	120.1(2)	H34B-C34-H34C	109.5
C26-C25-C20	120.1(2)	C9-C35-H35A	109.5
N26-C25-C24	117.6(2)	C9-C35-H35B	109.5
C26-C25-C24	117.6(2)	H35A-C35-H35B	109.5
C20-C25-C24	122.4(2)	C9-C35-H35C	109.5
C27-C26-C25	118.7(2)	H35A-C35-H35C	109.5
C27-C26-H26	120.7	H35B-C35-H35C	109.5
C25-C26-H26	120.7	C9-C36-H36A	109.5
C27-N26-C25	118.7(2)	C9-C36-H36B	109.5
N26-C27-C18	121.1(2)	H36A-C36-H36B	109.5
C26-C27-C18	121.1(2)	C9-C36-H36C	109.5
N26-C27-C15#1	132.3(2)	H36A-C36-H36C	109.5
C26-C27-C15#1	132.3(2)	H36B-C36-H36C	109.5
C18-C27-C15#1	106.6(2)	Cl5-C1S-Cl7	68.5(16)
C21-C28-H28A	109.5	Cl5-C1S-Cl4	50.5(11)
C21-C28-H28B	109.5	Cl7-C1S-Cl4	118.9(14)
H28A-C28-H28B	109.5	Cl5-C1S-Cl8	132.2(13)
C21-C28-H28C	109.5	Cl7-C1S-Cl8	71.5(15)
H28A-C28-H28C	109.5	Cl4-C1S-Cl8	151.7(9)
H28B-C28-H28C	109.5	Cl9-C1S-Cl6	110.9(2)
C21-C29-H29A	109.5	Cl5-C1S-Cl10	130.5(11)
C21-C29-H29B	109.5	Cl7-C1S-Cl10	122.5(14)
H29A-C29-H29B	109.5	Cl4-C1S-Cl10	98.1(9)
C21-C29-H29C	109.5	Cl8-C1S-Cl10	57.7(9)

Cl9-C1S-Cl3	114.0(3)	Cl5-CI7-Cl8	105.2(19)
Cl6-C1S-Cl3	109.8(3)	Cl10-CI8-C1S	63.3(10)
Cl5-C1S-Cl2	92.9(13)	Cl10-CI8-Cl7	107.3(15)
Cl7-C1S-Cl2	155.0(14)	C1S-Cl8-Cl7	48.8(10)
Cl4-C1S-Cl2	44.5(9)	Cl1-Cl10-Cl8	150(2)
Cl8-C1S-Cl2	114.7(11)	Cl1-Cl10-Cl2	36.5(12)
Cl10-C1S-Cl2	57.1(11)	Cl8-Cl10-Cl2	121.9(15)
Cl5-C1S-Cl1	117.8(11)	Cl1-Cl10-C1S	96.2(15)
Cl7-C1S-Cl1	152.2(11)	Cl8-Cl10-C1S	59.0(9)
Cl4-C1S-Cl1	72.0(6)	Cl2-Cl10-C1S	62.9(10)
Cl8-C1S-Cl1	87.9(9)	Cl17-C2S-Cl19	110.8(2)
Cl10-C1S-Cl1	31.4(8)	Cl17-C2S-Cl13	108.8(2)
Cl2-C1S-Cl1	27.7(8)	Cl19-C2S-Cl13	109.2(2)
Cl5-C1S-H1S	116(3)	Cl17-C2S-H2S	109.4
Cl7-C1S-H1S	99(3)	Cl19-C2S-H2S	109.4
Cl4-C1S-H1S	109(2)	Cl13-C2S-H2S	109.4
Cl8-C1S-H1S	94(3)	Cl11-C2SA-Cl18	116(3)
Cl9-C1S-H1S	103(2)	Cl11-C2SA-Cl15	88(3)
Cl6-C1S-H1S	114(2)	Cl18-C2SA-Cl15	91(2)
Cl10-C1S-H1S	109(3)	Cl11-C2SA-H2SA	118.1
Cl3-C1S-H1S	106(2)	Cl18-C2SA-H2SA	118.1
Cl2-C1S-H1S	105(2)	Cl15-C2SA-H2SA	118.1
Cl1-C1S-H1S	101(2)	C2SA-Cl11-Cl14	71.6(19)
Cl2-Cl1-Cl10	102(2)	C2SA-Cl11-Cl12	80(2)
Cl2-Cl1-C1S	54.2(13)	Cl14-Cl11-Cl12	45.5(9)
Cl10-Cl1-C1S	52.4(11)	Cl15-Cl12-Cl14	78.4(18)
Cl2-Cl1-Cl4	12.7(13)	Cl15-Cl12-Cl11	91.2(18)
Cl10-Cl1-Cl4	89.2(13)	Cl14-Cl12-Cl11	67.0(12)
C1S-Cl1-Cl4	42.4(4)	Cl16-Cl14-Cl12	140.9(17)
Cl1-Cl2-Cl4	157(2)	Cl16-Cl14-Cl15	102.1(14)
Cl1-Cl2-Cl10	41.6(14)	Cl12-Cl14-Cl15	42.2(11)
Cl4-Cl2-Cl10	115.7(15)	Cl16-Cl14-Cl11	130.2(13)
Cl1-Cl2-C1S	98.2(16)	Cl12-Cl14-Cl11	67.4(12)
Cl4-Cl2-C1S	60.7(9)	Cl15-Cl14-Cl11	77.6(11)
Cl10-Cl2-C1S	60.0(9)	Cl16-Cl14-Cl18	48.4(10)
Cl1-Cl2-Cl5	128.5(18)	Cl12-Cl14-Cl18	117.0(11)
Cl4-Cl2-Cl5	28.8(8)	Cl15-Cl14-Cl18	78.4(9)
Cl10-Cl2-Cl5	87.0(12)	Cl11-Cl14-Cl18	84.1(10)
C1S-Cl2-Cl5	34.2(6)	Cl12-Cl15-Cl14	59.4(17)
Cl5-Cl4-Cl2	121.5(13)	Cl12-Cl15-C2SA	101(2)
Cl5-Cl4-C1S	50.1(8)	Cl14-Cl15-C2SA	73.6(18)
Cl2-Cl4-C1S	74.8(9)	Cl12-Cl15-Cl20	115(2)
Cl5-Cl4-Cl1	111.6(11)	Cl14-Cl15-Cl20	74.4(11)
Cl2-Cl4-Cl1	10.0(10)	C2SA-Cl15-Cl20	18.9(14)
C1S-Cl4-Cl1	65.6(6)	Cl14-Cl16-Cl18	105.0(13)
C1S-Cl5-Cl4	79.4(13)	Cl20-Cl18-Cl16	111.4(17)
C1S-Cl5-Cl7	61.7(14)	Cl20-Cl18-C2SA	19.4(18)
Cl4-Cl5-Cl7	141.0(19)	Cl16-Cl18-C2SA	93.5(19)
C1S-Cl5-Cl2	52.8(9)	Cl20-Cl18-Cl14	86.0(15)
Cl4-Cl5-Cl2	29.6(9)	Cl16-Cl18-Cl14	26.6(6)
Cl7-Cl5-Cl2	112.6(16)	C2SA-Cl18-Cl14	67.4(17)
C1S-Cl7-Cl5	49.8(11)	Cl18-Cl20-Cl15	95.7(17)
C1S-Cl7-Cl8	59.6(13)		

Symmetry transformations used to generate equivalent atoms:

#1 -x+1,-y+1,-z+1

Table SI-9. Anisotropic displacement parameters (\AA^2) for ML026F1_0m.The anisotropic displacement factor exponent takes the form: $-2\pi^2 [h^2 a^{*2} U^{11} + \dots + 2 h k a^* b^* U^{12}]$

	U^{11}	U^{22}	U^{33}	U^{23}	U^{13}	U^{12}
N1	0.0131(10)	0.0183(10)	0.0147(10)	0.0016(8)	0.0015(8)	0.0013(8)
C2	0.0179(12)	0.0154(12)	0.0139(12)	-0.0022(9)	-0.0003(9)	0.0006(10)
C3	0.0167(12)	0.0150(12)	0.0149(12)	-0.0002(9)	0.0002(9)	0.0008(10)
C4	0.0167(12)	0.0184(12)	0.0202(12)	-0.0007(10)	0.0023(9)	0.0010(10)
N4	0.0167(12)	0.0184(12)	0.0202(12)	-0.0007(10)	0.0023(9)	0.0010(10)
C5	0.0208(13)	0.0205(13)	0.0199(13)	-0.0022(10)	0.0001(10)	-0.0006(11)
C6	0.0256(14)	0.0201(14)	0.0348(15)	0.0019(12)	0.0036(12)	0.0048(11)
C7	0.0317(16)	0.0253(15)	0.0430(17)	0.0067(13)	-0.0007(13)	0.0037(12)
C8	0.0312(16)	0.0294(16)	0.0407(17)	0.0159(13)	0.0001(13)	0.0002(13)
C9	0.0256(14)	0.0273(15)	0.0277(14)	0.0121(12)	0.0007(11)	0.0007(12)
C10	0.0206(13)	0.0229(13)	0.0170(12)	0.0025(10)	-0.0023(10)	-0.0023(11)
C11	0.0176(12)	0.0224(13)	0.0181(12)	0.0059(10)	0.0013(9)	0.0007(10)
N11	0.0176(12)	0.0224(13)	0.0181(12)	0.0059(10)	0.0013(9)	0.0007(10)
C12	0.0161(12)	0.0179(12)	0.0140(12)	0.0021(9)	-0.0001(9)	0.0012(10)
C13	0.0151(12)	0.0184(12)	0.0128(11)	0.0030(9)	0.0009(9)	-0.0005(10)
N14	0.0148(10)	0.0149(10)	0.0146(10)	0.0012(8)	0.0010(8)	0.0003(8)
N15	0.0151(10)	0.0193(11)	0.0171(10)	0.0047(8)	0.0033(8)	0.0016(8)
C15	0.0126(12)	0.0183(12)	0.0145(12)	-0.0012(10)	0.0004(9)	-0.0008(10)
N16	0.0138(10)	0.0161(10)	0.0156(10)	0.0023(8)	0.0006(8)	0.0005(8)
C17	0.0156(12)	0.0182(13)	0.0145(12)	0.0014(9)	0.0011(9)	-0.0004(10)
C18	0.0141(12)	0.0197(13)	0.0124(11)	-0.0010(9)	0.0011(9)	-0.0004(10)
C19	0.0185(12)	0.0186(12)	0.0160(12)	0.0022(9)	-0.0004(9)	-0.0016(10)
N19	0.0185(12)	0.0186(12)	0.0160(12)	0.0022(9)	-0.0004(9)	-0.0016(10)
C20	0.0158(12)	0.0227(13)	0.0147(12)	-0.0005(10)	-0.0006(10)	-0.0052(10)
C21	0.0219(13)	0.0247(14)	0.0225(13)	0.0026(11)	0.0043(11)	-0.0045(11)
C22	0.030(3)	0.031(2)	0.022(3)	0.005(2)	0.012(2)	-0.0058(18)
C23	0.013(2)	0.024(2)	0.038(3)	-0.0029(19)	0.0085(17)	-0.0014(16)
C22A	0.017(10)	0.084(18)	0.018(11)	0.024(11)	0.009(8)	0.016(10)
C23A	0.029(11)	0.038(12)	0.053(13)	0.002(10)	0.007(9)	-0.002(8)
C24	0.0164(12)	0.0230(13)	0.0178(13)	-0.0017(10)	0.0024(10)	0.0000(10)
C25	0.0148(12)	0.0231(13)	0.0130(11)	-0.0027(10)	-0.0014(9)	-0.0030(10)
C26	0.0145(11)	0.0177(12)	0.0164(11)	-0.0011(9)	0.0010(9)	-0.0007(9)
N26	0.0145(11)	0.0177(12)	0.0164(11)	-0.0011(9)	0.0010(9)	-0.0007(9)
C27	0.0151(12)	0.0192(12)	0.0130(11)	-0.0003(9)	0.0005(9)	-0.0003(10)
C28	0.0424(19)	0.086(3)	0.0302(17)	0.0246(17)	0.0032(14)	-0.0227(19)
C29	0.0400(18)	0.0344(17)	0.051(2)	-0.0028(15)	0.0123(15)	-0.0174(14)
C30	0.020(2)	0.043(3)	0.026(2)	0.007(3)	-0.0024(17)	0.009(3)
C31	0.022(2)	0.023(3)	0.027(3)	-0.004(2)	0.004(2)	-0.0021(19)
C30A	0.051(13)	0.031(12)	0.023(9)	0.015(10)	0.017(8)	0.032(12)
C31A	0.009(8)	0.038(14)	0.047(16)	-0.009(10)	0.007(10)	0.002(8)
C33	0.0272(16)	0.0336(17)	0.053(2)	0.0007(14)	-0.0085(14)	0.0079(13)
C34	0.0494(19)	0.0290(16)	0.050(2)	0.0006(14)	0.0182(16)	0.0109(15)
C35	0.056(2)	0.047(2)	0.0390(19)	0.0223(15)	0.0205(16)	0.0119(17)
C36	0.0308(16)	0.0363(17)	0.056(2)	0.0178(15)	-0.0056(15)	-0.0115(14)
C1S	0.064(2)	0.076(3)	0.0364(19)	-0.0010(17)	-0.0009(17)	0.0133(19)
Cl1	0.076(6)	0.081(7)	0.103(9)	0.023(5)	-0.001(5)	0.029(5)
Cl2	0.067(6)	0.080(6)	0.094(9)	0.007(5)	-0.005(6)	0.020(5)
Cl3	0.084(3)	0.0396(11)	0.0765(17)	0.0016(10)	-0.0378(18)	0.0096(13)
Cl4	0.049(4)	0.098(6)	0.058(4)	-0.012(4)	-0.008(3)	0.023(4)
Cl5	0.064(5)	0.101(7)	0.075(10)	-0.004(6)	-0.002(5)	0.015(5)
Cl6	0.0392(7)	0.0820(10)	0.0634(8)	0.0098(7)	0.0074(6)	-0.0053(7)
Cl7	0.086(10)	0.088(7)	0.057(11)	0.009(7)	0.005(9)	0.005(6)
Cl8	0.136(12)	0.112(8)	0.164(15)	-0.018(8)	0.074(11)	-0.011(7)
Cl9	0.0354(7)	0.154(2)	0.0474(8)	-0.0111(11)	0.0083(5)	-0.0282(11)
Cl10	0.084(8)	0.099(8)	0.112(9)	0.004(6)	0.031(7)	0.008(6)
C2S	0.027(2)	0.052(2)	0.043(2)	0.0160(17)	0.0086(17)	-0.0024(18)

C2SA	0.067(9)	0.091(12)	0.075(11)	-0.003(8)	0.003(7)	0.003(8)
Cl11	0.072(11)	0.119(14)	0.084(8)	-0.015(8)	0.004(7)	0.000(10)
Cl12	0.094(10)	0.103(9)	0.072(10)	-0.015(7)	0.009(8)	0.022(7)
Cl13	0.0700(10)	0.0714(11)	0.0415(7)	-0.0011(7)	0.0193(6)	0.0237(9)
Cl14	0.069(6)	0.107(8)	0.088(7)	-0.021(6)	0.004(5)	0.028(5)
Cl15	0.093(9)	0.112(9)	0.087(10)	-0.009(7)	0.010(7)	0.022(7)
Cl16	0.068(7)	0.091(8)	0.110(9)	-0.026(7)	-0.021(6)	0.030(6)
Cl17	0.0291(5)	0.0373(5)	0.0367(5)	0.0076(4)	0.0024(3)	0.0030(3)
Cl18	0.055(8)	0.083(9)	0.065(9)	0.003(7)	0.005(7)	0.006(7)
Cl19	0.0368(8)	0.0535(8)	0.0407(7)	0.0124(6)	-0.0020(7)	0.0067(7)
Cl20	0.064(8)	0.096(10)	0.084(11)	-0.005(8)	0.004(7)	0.000(7)

Table SI-10. Hydrogen coordinates and isotropic displacement parameters (\AA^2) for ML026F1_0m.

	x	y	z	U(eq)	Occupancy
H1	0.4794	0.5422	0.4702	0.018	0.5
H4	0.2271	0.7051	0.4164	0.022	0.75
H7A	0.2580	0.8864	0.2607	0.040	1
H7B	0.3550	0.8743	0.3457	0.040	1
H1S	0.373(4)	1.0953(19)	0.312(4)	0.102(15)	1
H8A	0.4332	0.8848	0.1799	0.041	1
H8B	0.3602	0.8308	0.1407	0.041	1
H11	0.5995	0.7104	0.2823	0.023	0.75
H16	0.5879	0.5008	0.4690	0.018	0.5
H19	0.8663	0.5968	0.2582	0.021	0.75
H22A	1.2186	0.5484	0.1120	0.033	0.8
H22B	1.1253	0.4993	0.0917	0.033	0.8
H23A	1.2405	0.5145	0.2865	0.030	0.8
H23B	1.2775	0.4670	0.2040	0.030	0.8
H22C	1.2323	0.5470	0.1303	0.047	0.2
H22D	1.2265	0.5440	0.2529	0.047	0.2
H23C	1.2597	0.4592	0.1783	0.048	0.2
H23D	1.1388	0.4633	0.1205	0.048	0.2
H26	0.9532	0.4134	0.3920	0.019	0.75
H28A	1.0514	0.6018	0.0414	0.079	1
H28B	0.9417	0.6131	0.1111	0.079	1
H28C	0.9603	0.5516	0.0589	0.079	1
H29A	1.1697	0.6364	0.1945	0.062	1
H29B	1.1553	0.6048	0.3031	0.062	1
H29C	1.0540	0.6438	0.2577	0.062	1
H30A	1.1319	0.3888	0.3999	0.044	0.8
H30B	1.1820	0.4506	0.4294	0.044	0.8
H30C	1.2559	0.4074	0.3613	0.044	0.8
H31A	1.0472	0.3708	0.2317	0.036	0.8
H31B	1.1716	0.3788	0.1839	0.036	0.8
H31C	1.0655	0.4141	0.1375	0.036	0.8
H30D	1.1548	0.4244	0.4188	0.052	0.2
H30E	1.2052	0.4859	0.3880	0.052	0.2
H30F	1.2664	0.4285	0.3491	0.052	0.2
H31D	1.0643	0.3619	0.2988	0.047	0.2
H31E	1.1654	0.3646	0.2169	0.047	0.2
H31F	1.0392	0.3844	0.1844	0.047	0.2
H33A	0.1170	0.8159	0.2154	0.057	1
H33B	0.1247	0.7510	0.2555	0.057	1
H33C	0.2114	0.7734	0.1700	0.057	1
H34A	0.1391	0.8502	0.4031	0.064	1
H34B	0.2413	0.8240	0.4712	0.064	1
H34C	0.1392	0.7834	0.4325	0.064	1
H35A	0.6271	0.7659	0.1574	0.071	1
H35B	0.5826	0.8220	0.0982	0.071	1
H35C	0.5084	0.7643	0.0952	0.071	1
H36A	0.6457	0.8143	0.3217	0.062	1
H36B	0.5421	0.8502	0.3689	0.062	1
H36C	0.6081	0.8740	0.2704	0.062	1
H2S	0.7907	0.6764	0.4201	0.048	0.9
H2SA	1.0422	0.7411	0.5841	0.093	0.1

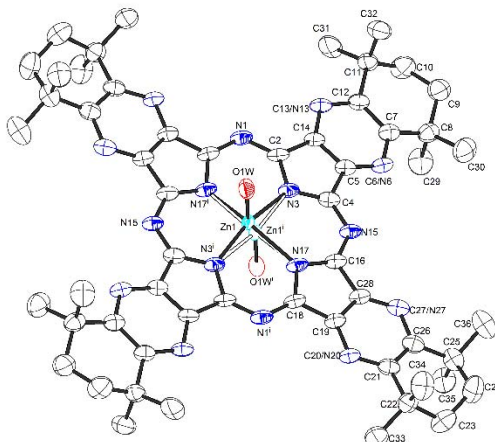
Table SI-11. Torsion angles [°] for ML026F1_0m.

C13-N1-C2-N14	-178.1(2)	C2-C3-C12-C11	179.5(2)
C13-N1-C2-C3	0.4(3)	N4-C3-C12-C13	179.6(2)
N14-C2-C3-N4	-1.0(4)	C4-C3-C12-C13	179.6(2)
N1-C2-C3-N4	-179.5(2)	C2-C3-C12-C13	0.5(2)
N14-C2-C3-C4	-1.0(4)	C2-N1-C13-N15	-178.1(2)
N1-C2-C3-C4	-179.5(2)	C2-N1-C13-C12	-0.1(3)
N14-C2-C3-C12	178.0(2)	N11-C12-C13-N15	-1.0(4)
N1-C2-C3-C12	-0.5(3)	C11-C12-C13-N15	-1.0(4)
C12-C3-C4-C5	0.8(3)	C3-C12-C13-N15	177.9(2)
C2-C3-C4-C5	179.7(2)	N11-C12-C13-N1	-179.2(2)
C12-C3-N4-C5	0.8(3)	C11-C12-C13-N1	-179.2(2)
C2-C3-N4-C5	179.7(2)	C3-C12-C13-N1	-0.3(3)
C3-N4-C5-C10	0.5(3)	N1-C2-N14-C15	0.8(4)
C3-N4-C5-C6	177.4(2)	C3-C2-N14-C15	-177.5(2)
C3-C4-C5-C10	0.5(3)	N1-C13-N15-C17	0.5(4)
C3-C4-C5-C6	177.4(2)	C12-C13-N15-C17	-177.4(2)
N4-C5-C6-C34	44.4(3)	C2-N14-C15-N16#1	-3.8(4)
C4-C5-C6-C34	44.4(3)	C2-N14-C15-C27#1	176.5(2)
C10-C5-C6-C34	-138.8(3)	C13-N15-C17-N16	-3.7(4)
N4-C5-C6-C7	163.7(2)	C13-N15-C17-C18	176.0(2)
C4-C5-C6-C7	163.7(2)	C15#1-N16-C17-N15	-178.2(2)
C10-C5-C6-C7	-19.5(3)	C15#1-N16-C17-C18	2.1(3)
N4-C5-C6-C33	-75.7(3)	N15-C17-C18-N19	-3.4(4)
C4-C5-C6-C33	-75.7(3)	N16-C17-C18-N19	176.3(2)
C10-C5-C6-C33	101.0(3)	N15-C17-C18-C19	-3.4(4)
C34-C6-C7-C8	169.3(3)	N16-C17-C18-C19	176.3(2)
C5-C6-C7-C8	47.8(3)	N15-C17-C18-C27	178.6(2)
C33-C6-C7-C8	-71.7(3)	N16-C17-C18-C27	-1.7(3)
C6-C7-C8-C9	-62.9(3)	C27-C18-C19-C20	0.3(3)
C7-C8-C9-C35	166.0(3)	C17-C18-C19-C20	-177.4(2)
C7-C8-C9-C36	-75.4(3)	C27-C18-N19-C20	0.3(3)
C7-C8-C9-C10	44.1(3)	C17-C18-N19-C20	-177.4(2)
N4-C5-C10-N11	-1.4(4)	C18-N19-C20-C25	-1.7(3)
C6-C5-C10-N11	-178.1(2)	C18-N19-C20-C21	178.0(2)
C4-C5-C10-C11	-1.4(4)	C18-C19-C20-C25	-1.7(3)
C6-C5-C10-C11	-178.1(2)	C18-C19-C20-C21	178.0(2)
N4-C5-C10-C9	-179.1(2)	N19-C20-C21-C28	-50.0(3)
C4-C5-C10-C9	-179.1(2)	C19-C20-C21-C28	-50.0(3)
C6-C5-C10-C9	4.2(4)	C25-C20-C21-C28	129.7(3)
C8-C9-C10-N11	166.5(2)	N19-C20-C21-C29	69.7(3)
C35-C9-C10-N11	46.4(3)	C19-C20-C21-C29	69.7(3)
C36-C9-C10-N11	-72.9(3)	C25-C20-C21-C29	-110.6(3)
C8-C9-C10-C11	166.5(2)	C19-C20-C21-C22	-166.6(3)
C35-C9-C10-C11	46.4(3)	C25-C20-C21-C22	13.1(4)
C36-C9-C10-C11	-72.9(3)	N19-C20-C21-C22A	167.3(9)
C8-C9-C10-C5	-15.7(3)	C25-C20-C21-C22A	-13.0(10)
C35-C9-C10-C5	-135.9(3)	C28-C21-C22-C23	-164.4(3)
C36-C9-C10-C5	104.8(3)	C29-C21-C22-C23	77.3(4)
C5-C10-C11-C12	0.9(4)	C20-C21-C22-C23	-45.0(4)
C9-C10-C11-C12	178.7(2)	C21-C22-C23-C24	65.6(4)
C5-C10-N11-C12	0.9(4)	C28-C21-C22A-C23A	-89.0(17)
C9-C10-N11-C12	178.7(2)	C29-C21-C22A-C23A	155.8(16)
C10-N11-C12-C3	0.5(4)	C20-C21-C22A-C23A	45.2(18)
C10-N11-C12-C13	179.3(2)	C21-C22A-C23A-C24	-65(2)
C10-C11-C12-C3	0.5(4)	C22A-C23A-C24-C30A	-75(2)
C10-C11-C12-C13	179.3(2)	C22A-C23A-C24-C25	46.6(19)
N4-C3-C12-N11	-1.4(4)	C22A-C23A-C24-C31A	164.1(18)
C2-C3-C12-N11	179.5(2)	C22-C23-C24-C31	72.6(4)
C4-C3-C12-C11	-1.4(4)	C22-C23-C24-C25	-48.9(4)

C22-C23-C24-C30	-169.0(4)	Cl8-C1S-Cl2-Cl5	-139.9(13)
N19-C20-C25-N26	1.9(3)	Cl10-C1S-Cl2-Cl5	-137.8(12)
C21-C20-C25-N26	-177.8(2)	Cl1-C1S-Cl2-Cl5	-155.2(16)
C19-C20-C25-C26	1.9(3)	Cl1-Cl2-Cl4-Cl5	-4(6)
C21-C20-C25-C26	-177.8(2)	Cl10-Cl2-Cl4-Cl5	-6(2)
N19-C20-C25-C24	-179.7(2)	C1S-Cl2-Cl4-Cl5	18.9(14)
C19-C20-C25-C24	-179.7(2)	Cl1-Cl2-Cl4-C1S	-23(5)
C21-C20-C25-C24	0.6(3)	Cl10-Cl2-Cl4-C1S	-24.9(13)
C30A-C24-C25-N26	-71.5(9)	Cl5-Cl2-Cl4-C1S	-18.9(14)
C23A-C24-C25-N26	164.0(9)	Cl10-Cl2-Cl4-Cl1	-2(4)
C31A-C24-C25-N26	49.0(9)	C1S-Cl2-Cl4-Cl1	23(5)
C31-C24-C25-C26	73.7(3)	Cl5-Cl2-Cl4-Cl1	4(6)
C23-C24-C25-C26	-164.2(3)	Cl7-C1S-Cl4-Cl5	-2.7(17)
C30-C24-C25-C26	-46.3(3)	Cl8-C1S-Cl4-Cl5	-108(2)
C30A-C24-C25-C20	110.0(9)	Cl10-C1S-Cl4-Cl5	-137.0(14)
C31-C24-C25-C20	-104.8(3)	Cl2-C1S-Cl4-Cl5	-158.9(16)
C23A-C24-C25-C20	-14.4(9)	Cl1-C1S-Cl4-Cl5	-154.6(12)
C23-C24-C25-C20	17.3(3)	Cl5-C1S-Cl4-Cl2	158.9(16)
C30-C24-C25-C20	135.2(3)	Cl7-C1S-Cl4-Cl2	156.2(15)
C31A-C24-C25-C20	-129.5(9)	Cl8-C1S-Cl4-Cl2	51(2)
C20-C25-C26-C27	-0.6(3)	Cl10-C1S-Cl4-Cl2	21.8(13)
C24-C25-C26-C27	-179.1(2)	Cl1-C1S-Cl4-Cl2	4.2(10)
C20-C25-N26-C27	-0.6(3)	Cl5-C1S-Cl4-Cl1	154.6(12)
C24-C25-N26-C27	-179.1(2)	Cl7-C1S-Cl4-Cl1	152.0(13)
C25-N26-C27-C18	-0.8(3)	Cl8-C1S-Cl4-Cl1	47(2)
C25-N26-C27-C15#1	177.3(2)	Cl10-C1S-Cl4-Cl1	17.6(9)
C25-C26-C27-C18	-0.8(3)	Cl2-C1S-Cl4-Cl1	-4.2(10)
C25-C26-C27-C15#1	177.3(2)	Cl7-C1S-Cl5-Cl4	177.5(16)
N19-C18-C27-N26	0.9(4)	Cl8-C1S-Cl5-Cl4	142.4(14)
C17-C18-C27-N26	179.1(2)	Cl10-C1S-Cl5-Cl4	62.4(18)
C19-C18-C27-C26	0.9(4)	Cl2-C1S-Cl5-Cl4	14.7(11)
C17-C18-C27-C26	179.1(2)	Cl1-C1S-Cl5-Cl4	27.4(13)
N19-C18-C27-C15#1	-177.6(2)	Cl4-C1S-Cl5-Cl7	-177.5(16)
C19-C18-C27-C15#1	-177.6(2)	Cl8-C1S-Cl5-Cl7	-35.0(18)
C17-C18-C27-C15#1	0.6(2)	Cl10-C1S-Cl5-Cl7	-115.0(18)
Cl10-Cl1-Cl2-Cl4	-3(6)	Cl2-C1S-Cl5-Cl7	-162.8(13)
C1S-Cl1-Cl2-Cl4	20(4)	Cl1-C1S-Cl5-Cl7	-150.1(12)
C1S-Cl1-Cl2-Cl10	22.8(17)	Cl7-C1S-Cl5-Cl2	162.8(13)
Cl4-Cl1-Cl2-Cl10	3(6)	Cl4-C1S-Cl5-Cl2	-14.7(11)
Cl10-Cl1-Cl2-C1S	-22.8(17)	Cl8-C1S-Cl5-Cl2	127.8(15)
Cl4-Cl1-Cl2-C1S	-20(4)	Cl10-C1S-Cl5-Cl2	47.8(15)
Cl10-Cl1-Cl2-Cl5	-5(2)	Cl1-C1S-Cl5-Cl2	12.7(9)
C1S-Cl1-Cl2-Cl5	17.6(10)	Cl2-Cl4-Cl5-C1S	-24.1(18)
Cl4-Cl1-Cl2-Cl5	-2(4)	Cl1-Cl4-Cl5-C1S	-24.8(11)
Cl5-C1S-Cl2-Cl1	155.2(16)	Cl2-Cl4-Cl5-Cl7	-21(4)
Cl7-C1S-Cl2-Cl1	115(3)	C1S-Cl4-Cl5-Cl7	4(2)
Cl4-C1S-Cl2-Cl1	171(2)	Cl1-Cl4-Cl5-Cl7	-21(3)
Cl8-C1S-Cl2-Cl1	15.3(19)	C1S-Cl4-Cl5-Cl2	24.1(18)
Cl10-C1S-Cl2-Cl1	17.3(14)	Cl1-Cl4-Cl5-Cl2	-0.7(11)
Cl5-C1S-Cl2-Cl4	-16.2(12)	Cl4-C1S-Cl7-Cl5	2.2(14)
Cl7-C1S-Cl2-Cl4	-57(3)	Cl8-C1S-Cl7-Cl5	153.4(14)
Cl8-C1S-Cl2-Cl4	-156.1(13)	Cl10-C1S-Cl7-Cl5	125.1(14)
Cl10-C1S-Cl2-Cl4	-154.0(15)	Cl2-C1S-Cl7-Cl5	44(3)
Cl11-C1S-Cl2-Cl4	-171(2)	Cl1-C1S-Cl7-Cl5	109(3)
Cl5-C1S-Cl2-Cl10	137.8(12)	Cl5-C1S-Cl7-Cl8	-153.4(14)
Cl7-C1S-Cl2-Cl10	97(3)	Cl4-C1S-Cl7-Cl8	-151.2(11)
Cl4-C1S-Cl2-Cl10	154.0(15)	Cl10-C1S-Cl7-Cl8	-28.2(17)
Cl8-C1S-Cl2-Cl10	-2.1(15)	Cl2-C1S-Cl7-Cl8	-109(3)
Cl11-C1S-Cl2-Cl10	-17.3(14)	Cl1-C1S-Cl7-Cl8	-44(3)
Cl7-C1S-Cl2-Cl5	-41(3)	Cl4-Cl5-Cl7-C1S	-4(2)
Cl4-C1S-Cl2-Cl5	16.2(12)	Cl2-Cl5-Cl7-C1S	-14.8(11)

C1S-CI5-CI7-CI8	23.6(13)	CI15-CI12-CI14-CI18	26.1(18)
CI4-CI5-CI7-CI8	20(3)	CI11-CI12-CI14-CI18	-70.3(12)
CI2-CI5-CI7-CI8	9(2)	CI11-CI12-CI15-CI14	66.3(11)
CI5-C1S-CI8-CI10	-117.6(17)	CI14-CI12-CI15-C2SA	-64(2)
CI7-C1S-CI8-CI10	-151.8(17)	CI11-CI12-CI15-C2SA	3(2)
CI4-C1S-CI8-CI10	-35(3)	CI14-CI12-CI15-CI20	-51.3(17)
CI2-C1S-CI8-CI10	2.1(15)	CI11-CI12-CI15-CI20	15(2)
CI1-C1S-CI8-CI10	9.1(11)	CI12-CI14-CI16-CI18	83(2)
CI5-C1S-CI8-CI7	34.3(19)	CI15-CI14-CI16-CI18	62.3(15)
CI4-C1S-CI8-CI7	117(2)	CI11-CI14-CI16-CI18	-22(3)
CI10-C1S-CI8-CI7	151.8(17)	CI16-CI18-CI20-CI15	-27.6(18)
CI2-C1S-CI8-CI7	153.9(14)	C2SA-CI18-CI20-CI15	-52(6)
CI1-C1S-CI8-CI7	160.9(13)	CI14-CI18-CI20-CI15	-35.9(11)
C1S-CI7-CI8-CI10	26.2(16)		
CI5-CI7-CI8-CI10	5(2)		
CI5-CI7-CI8-C1S	-20.8(11)		
CI2-CI1-CI10-CI8	55(4)		
C1S-C11-CI10-CI8	31(3)		
CI4-CI1-CI10-CI8	54(4)		
C1S-C11-CI10-CI2	-23.4(18)		
CI4-CI1-CI10-CI2	-0.6(13)		
CI2-CI1-CI10-C1S	23.4(17)		
CI4-CI1-CI10-C1S	22.8(9)		
C1S-CI8-CI10-CI1	-37(4)		
CI7-CI8-CI10-CI1	-59(5)		
C1S-CI8-CI10-CI2	-2.3(17)		
CI7-CI8-CI10-CI2	-24(3)		
CI7-CI8-CI10-C1S	-21.8(13)		
CI4-CI2-CI10-CI1	179(2)		
C1S-CI2-CI10-CI1	154(2)		
CI5-CI2-CI10-CI1	175.9(19)		
CI1-CI2-CI10-CI8	-151(3)		
CI4-CI2-CI10-CI8	27(3)		
C1S-CI2-CI10-CI8	2.2(17)		
CI5-CI2-CI10-CI8	24(2)		
CI1-CI2-CI10-C1S	-154(2)		
CI4-CI2-CI10-C1S	25.1(14)		
CI5-CI2-CI10-C1S	22.2(6)		
CI5-C1S-CI10-CI1	-77(2)		
CI7-C1S-CI10-CI1	-165.6(18)		
CI4-C1S-CI10-CI1	-33.5(15)		
CI8-C1S-CI10-CI1	162(2)		
CI2-C1S-CI10-CI1	-15.4(12)		
CI5-C1S-CI10-CI8	120.4(18)		
CI7-C1S-CI10-CI8	32(2)		
CI4-C1S-CI10-CI8	164.1(13)		
CI2-C1S-CI10-CI8	-177.8(16)		
CI1-C1S-CI10-CI8	-162(2)		
CI5-C1S-CI10-CI2	-61.8(18)		
CI7-C1S-CI10-CI2	-150.2(17)		
CI4-C1S-CI10-CI2	-18.1(10)		
CI8-C1S-CI10-CI2	177.8(16)		
CI1-C1S-CI10-CI2	15.4(12)		
CI18-C2SA-CI11-CI14	-42(3)		
CI15-C2SA-CI11-CI14	48.2(15)		
CI18-C2SA-CI11-CI12	-89(3)		
CI15-C2SA-CI11-CI12	1.9(17)		
CI15-CI12-CI14-CI16	-30(3)		
CI11-CI12-CI14-CI16	-127(2)		
CI11-CI12-CI14-CI15	-96.4(16)		
CI15-CI12-CI14-CI11	96.4(16)		

1.7.3 Crystal Structure of A₂B₂N₄-[Pc^{*}Zn·H₂O]



Habitus, colour
Crystal size
Crystal system
Space group
Unit cell dimensions

prism, dark
0.27 x 0.06 x 0.03 mm³
Monoclinic
P2₁/c
 $a = 6.0419(5)$ Å
 $b = 16.2175(13)$ Å
 $c = 31.008(2)$ Å

$Z = 2$
 $\alpha = 90^\circ$.
 $\beta = 95.305(3)^\circ$.
 $\gamma = 90^\circ$.

Volume
Cell determination
Empirical formula
Moiety formula
Formula weight
Density (calculated)
Absorption coefficient
F(000)

$3025.3(4)$ Å³
9556 peaks with Theta 2.3 to 25.2°.
 $C_{60} H_{70} N_{12} O Zn$
 $C_{60} H_{70} N_{12} O Zn$
1040.65
1.142 Mg/m³
0.454 mm⁻¹
1104

Solution and refinement:

Reflections collected
Independent reflections
Completeness to theta = 25.242°
Observed reflections
Reflections used for refinement
Absorption correction
Max. and min. transmission
Largest diff. peak and hole
Solution
Refinement
Treatment of hydrogen atoms
Programs used
Data / restraints / parameters
Goodness-of-fit on F²
R index (all data)
R index conventional [I>2sigma(I)]

32818
5598 [R(int) = 0.0711]
99.9 %
4276[I > 2(I)]
5598
Numerical Mu Calculated^[12]
0.99 and 0.89
0.288 and -0.347 e.Å⁻³
Direct methods
Full-matrix least-squares on F²
Calculated positions, constr. ref.
XT V2014/1 (Bruker AXS Inc., 2014)^[13]
SHELXL-2014/7 (Sheldrick, 2014)^[14]
DIAMOND (Crystal Impact)^[11]
ShelXle (Hübschle, Sheldrick, Dittrich, 2011)^[15]
5598 / 0 / 353
1.021
wR2 = 0.1467
R1 = 0.0580

Table SI-12. Atomic coordinates and equivalent isotropic displacement parameters (\AA^2) for mL105c2_0m_sq. U(eq) is defined as one third of the trace of the orthogonalized U^{ij} tensor.

	x	y	z	U(eq)	Occupancy
Zn1	1.49975(18)	0.51807(4)	0.50622(3)	0.0242(2)	0.5
N1	1.5282(5)	0.39227(14)	0.59501(8)	0.0354(6)	1
C2	1.3557(6)	0.37918(17)	0.56599(9)	0.0336(7)	1
N3	1.3123(5)	0.41696(14)	0.52645(8)	0.0330(6)	1
C4	1.1271(6)	0.38191(18)	0.50470(10)	0.0357(8)	1
C5	1.0459(5)	0.31799(17)	0.53226(9)	0.0324(7)	1
C6	0.8816(5)	0.26266(17)	0.52335(9)	0.0369(7)	0.5
N6	0.8816(5)	0.26266(17)	0.52335(9)	0.0369(7)	0.5
C7	0.8475(6)	0.20533(19)	0.55472(10)	0.0378(8)	1
C8	0.6829(6)	0.1355(2)	0.54251(11)	0.0459(9)	1
C9	0.6011(7)	0.0982(3)	0.58286(13)	0.0594(11)	1
C10	0.7865(8)	0.0790(2)	0.61729(13)	0.0609(11)	1
C11	0.9179(6)	0.1542(2)	0.63326(11)	0.0446(9)	1
C12	0.9761(6)	0.20836(19)	0.59537(10)	0.0362(8)	1
C13	1.1473(5)	0.26387(16)	0.60328(9)	0.0362(7)	0.5
N13	1.1473(5)	0.26387(16)	0.60328(9)	0.0362(7)	0.5
C14	1.1822(5)	0.31757(16)	0.57052(9)	0.0306(7)	1
N15	1.0358(5)	0.39883(15)	0.46520(8)	0.0350(6)	1
C16	1.1103(6)	0.45652(18)	0.43907(9)	0.0345(7)	1
N17	1.2882(5)	0.50688(15)	0.44710(8)	0.0348(6)	1
C18	1.3091(6)	0.55471(17)	0.41116(9)	0.0335(7)	1
C19	1.1260(6)	0.53481(17)	0.37847(9)	0.0339(7)	1
C20	1.0650(5)	0.56503(17)	0.33820(9)	0.0357(7)	0.5
N20	1.0650(5)	0.56503(17)	0.33820(9)	0.0357(7)	0.5
C21	0.8899(6)	0.52815(19)	0.31471(10)	0.0392(8)	1
C22	0.8002(6)	0.5685(2)	0.27201(11)	0.0448(8)	1
C23	0.6709(8)	0.5058(3)	0.24279(13)	0.0640(11)	1
C24	0.5072(8)	0.4553(3)	0.26589(15)	0.0672(12)	1
C25	0.6171(6)	0.4051(2)	0.30292(12)	0.0492(9)	1
C26	0.7813(6)	0.4578(2)	0.33098(11)	0.0417(8)	1
C27	0.8404(5)	0.43133(18)	0.37254(9)	0.0404(7)	0.5
N27	0.8404(5)	0.43133(18)	0.37254(9)	0.0404(7)	0.5
C28	1.0081(6)	0.47124(18)	0.39565(10)	0.0347(7)	1
C29	0.8078(7)	0.0725(2)	0.51705(15)	0.0657(12)	1
C30	0.4821(7)	0.1666(3)	0.51310(14)	0.0660(12)	1
C31	1.1256(7)	0.1267(3)	0.66111(13)	0.0644(12)	1
C32	0.7765(7)	0.2076(3)	0.66089(12)	0.0589(11)	1
C33	0.9850(7)	0.6044(3)	0.24761(13)	0.0650(12)	1
C34	0.6459(7)	0.6390(2)	0.28378(15)	0.0665(12)	1
C35	0.7495(7)	0.3332(2)	0.28583(14)	0.0601(11)	1
C36	0.4342(8)	0.3688(3)	0.32869(17)	0.0783(14)	1
O1W	1.3888(7)	0.6241(3)	0.53911(14)	0.0403(11)	0.5

Table SI-13. Bond lengths [Å] and angles [°] for mL105c2_0m_sq.

Zn1-Zn1#1	0.7019(11)	C20-H20	0.9400
Zn1-N17#1	1.886(3)	C21-C26	1.431(5)
Zn1-N3#1	1.908(3)	C21-C22	1.531(5)
Zn1-N3	2.121(3)	C22-C33	1.521(5)
Zn1-O1W	2.138(4)	C22-C23	1.528(5)
Zn1-N17	2.143(3)	C22-C34	1.540(5)
N1-C2	1.330(4)	C23-C24	1.514(6)
N1-C18#1	1.333(4)	C23-H23A	0.9800
C2-N3	1.374(4)	C23-H23B	0.9800
C2-C14	1.464(4)	C24-C25	1.510(6)
N3-C4	1.375(4)	C24-H24A	0.9800
N3-Zn1#1	1.908(3)	C24-H24B	0.9800
C4-N15	1.325(4)	C25-C26	1.521(5)
C4-C5	1.457(4)	C25-C35	1.537(5)
C5-C6	1.348(4)	C25-C36	1.540(6)
C5-C14	1.380(4)	C26-C27	1.373(5)
C6-C7	1.375(4)	C27-C28	1.351(4)
C6-H6	0.9400	C27-H27	0.9400
C7-C12	1.419(5)	C29-H29A	0.9700
C7-C8	1.531(5)	C29-H29B	0.9700
C8-C9	1.513(5)	C29-H29C	0.9700
C8-C29	1.531(5)	C30-H30A	0.9700
C8-C30	1.534(5)	C30-H30B	0.9700
C9-C10	1.507(6)	C30-H30C	0.9700
C9-H9A	0.9800	C31-H31A	0.9700
C9-H9B	0.9800	C31-H31B	0.9700
C10-C11	1.514(5)	C31-H31C	0.9700
C10-H10A	0.9800	C32-H32A	0.9700
C10-H10B	0.9800	C32-H32B	0.9700
C11-C31	1.523(5)	C32-H32C	0.9700
C11-C32	1.533(5)	C33-H33A	0.9700
C11-C12	1.533(4)	C33-H33B	0.9700
C12-C13	1.376(4)	C33-H33C	0.9700
C13-C14	1.369(4)	C34-H34A	0.9700
C13-H13	0.9400	C34-H34B	0.9700
N15-C16	1.343(4)	C34-H34C	0.9700
C16-N17	1.355(4)	C35-H35A	0.9700
C16-C28	1.448(4)	C35-H35B	0.9700
N17-C18	1.373(4)	C35-H35C	0.9700
N17-Zn1#1	1.886(3)	C36-H36A	0.9700
C18-N1#1	1.333(4)	C36-H36B	0.9700
C18-C19	1.465(5)	C36-H36C	0.9700
C19-C20	1.360(4)	O1W-H1WA	0.8643
C19-C28	1.387(4)	O1W-H1WB	0.8644
C20-C21	1.366(5)		
Zn1#1-Zn1-N17#1	101.9(2)	N3-Zn1-N17	83.97(10)
Zn1#1-Zn1-N3#1	97.8(2)	O1W-Zn1-N17	106.71(14)
N17#1-Zn1-N3#1	97.51(12)	C2-N1-C18#1	123.2(2)
Zn1#1-Zn1-N3	63.01(17)	N1-C2-N3	127.3(3)
N17#1-Zn1-N3	87.16(11)	N1-C2-C14	124.6(3)
N3#1-Zn1-N3	160.86(4)	N3-C2-C14	108.1(3)
Zn1#1-Zn1-O1W	162.0(2)	C2-N3-C4	109.4(3)
N17#1-Zn1-O1W	91.56(14)	C2-N3-Zn1#1	130.3(2)
N3#1-Zn1-O1W	92.15(14)	C4-N3-Zn1#1	117.73(19)
N3-Zn1-O1W	106.33(14)	C2-N3-Zn1	123.1(2)
Zn1#1-Zn1-N17	59.45(17)	C4-N3-Zn1	127.40(19)
N17#1-Zn1-N17	161.30(4)	Zn1#1-N3-Zn1	19.14(4)
N3#1-Zn1-N17	85.97(11)	N15-C4-N3	128.2(3)

N15-C4-C5	123.8(3)	C19-C20-H20	121.2
N3-C4-C5	108.0(3)	C21-C20-H20	121.2
C6-C5-C14	122.9(3)	C20-C21-C26	121.3(3)
C6-C5-C4	129.4(3)	C20-C21-C22	118.0(3)
C14-C5-C4	107.5(3)	C26-C21-C22	120.6(3)
C5-C6-C7	117.4(3)	C33-C22-C23	108.5(3)
C5-C6-H6	121.3	C33-C22-C21	112.1(3)
C7-C6-H6	121.3	C23-C22-C21	110.4(3)
C6-C7-C12	120.0(3)	C33-C22-C34	108.8(3)
C6-C7-C8	117.5(3)	C23-C22-C34	110.3(3)
C12-C7-C8	122.3(3)	C21-C22-C34	106.6(3)
C9-C8-C29	111.9(3)	C24-C23-C22	113.6(3)
C9-C8-C7	110.2(3)	C24-C23-H23A	108.9
C29-C8-C7	106.3(3)	C22-C23-H23A	108.9
C9-C8-C30	108.8(3)	C24-C23-H23B	108.9
C29-C8-C30	108.2(3)	C22-C23-H23B	108.9
C7-C8-C30	111.3(3)	H23A-C23-H23B	107.7
C10-C9-C8	112.9(3)	C25-C24-C23	113.0(4)
C10-C9-H9A	109.0	C25-C24-H24A	109.0
C8-C9-H9A	109.0	C23-C24-H24A	109.0
C10-C9-H9B	109.0	C25-C24-H24B	109.0
C8-C9-H9B	109.0	C23-C24-H24B	109.0
H9A-C9-H9B	107.8	H24A-C24-H24B	107.8
C9-C10-C11	113.5(3)	C24-C25-C26	110.5(3)
C9-C10-H10A	108.9	C24-C25-C35	110.7(3)
C11-C10-H10A	108.9	C26-C25-C35	106.9(3)
C9-C10-H10B	108.9	C24-C25-C36	108.4(4)
C11-C10-H10B	108.9	C26-C25-C36	112.3(3)
H10A-C10-H10B	107.7	C35-C25-C36	108.1(3)
C10-C11-C31	109.2(3)	C27-C26-C21	119.5(3)
C10-C11-C32	109.6(3)	C27-C26-C25	117.4(3)
C31-C11-C32	108.7(3)	C21-C26-C25	122.8(3)
C10-C11-C12	111.2(3)	C28-C27-C26	117.7(3)
C31-C11-C12	111.5(3)	C28-C27-H27	121.1
C32-C11-C12	106.5(3)	C26-C27-H27	121.1
C13-C12-C7	121.5(3)	C27-C28-C19	122.6(3)
C13-C12-C11	117.4(3)	C27-C28-C16	130.4(3)
C7-C12-C11	121.0(3)	C19-C28-C16	106.8(3)
C14-C13-C12	116.6(3)	C8-C29-H29A	109.5
C14-C13-H13	121.7	C8-C29-H29B	109.5
C12-C13-H13	121.7	H29A-C29-H29B	109.5
C13-C14-C5	121.4(3)	C8-C29-H29C	109.5
C13-C14-C2	131.8(3)	H29A-C29-H29C	109.5
C5-C14-C2	106.8(2)	H29B-C29-H29C	109.5
C4-N15-C16	124.6(3)	C8-C30-H30A	109.5
N15-C16-N17	127.9(3)	C8-C30-H30B	109.5
N15-C16-C28	122.6(3)	H30A-C30-H30B	109.5
N17-C16-C28	109.5(3)	C8-C30-H30C	109.5
C16-N17-C18	108.8(3)	H30A-C30-H30C	109.5
C16-N17-Zn1#1	118.9(2)	H30B-C30-H30C	109.5
C18-N17-Zn1#1	129.6(2)	C11-C31-H31A	109.5
C16-N17-Zn1	127.5(2)	C11-C31-H31B	109.5
C18-N17-Zn1	123.7(2)	H31A-C31-H31B	109.5
Zn1#1-N17-Zn1	18.69(4)	C11-C31-H31C	109.5
N1#1-C18-N17	127.2(3)	H31A-C31-H31C	109.5
N1#1-C18-C19	124.2(3)	H31B-C31-H31C	109.5
N17-C18-C19	108.5(3)	C11-C32-H32A	109.5
C20-C19-C28	121.0(3)	C11-C32-H32B	109.5
C20-C19-C18	132.7(3)	H32A-C32-H32B	109.5
C28-C19-C18	106.2(3)	C11-C32-H32C	109.5
C19-C20-C21	117.5(3)	H32A-C32-H32C	109.5

H32B-C32-H32C	109.5	C25-C35-H35B	109.5
C22-C33-H33A	109.5	H35A-C35-H35B	109.5
C22-C33-H33B	109.5	C25-C35-H35C	109.5
H33A-C33-H33B	109.5	H35A-C35-H35C	109.5
C22-C33-H33C	109.5	H35B-C35-H35C	109.5
H33A-C33-H33C	109.5	C25-C36-H36A	109.5
H33B-C33-H33C	109.5	C25-C36-H36B	109.5
C22-C34-H34A	109.5	H36A-C36-H36B	109.5
C22-C34-H34B	109.5	C25-C36-H36C	109.5
H34A-C34-H34B	109.5	H36A-C36-H36C	109.5
C22-C34-H34C	109.5	H36B-C36-H36C	109.5
H34A-C34-H34C	109.5	Zn1-O1W-H1WA	109.6
H34B-C34-H34C	109.5	Zn1-O1W-H1WB	109.6
C25-C35-H35A	109.5	H1WA-O1W-H1WB	109.2

Symmetry transformations used to generate equivalent atoms:

#1 -x+3,-y+1,-z+1

Table SI-14. Anisotropic displacement parameters (\AA^2) for mL105c2_0m_sq.The anisotropic displacement factor exponent takes the form: $-2\pi^2 [h^2 a^{*2} U^{11} + \dots + 2 h k a^{*} b^{*} U^{12}]$

	U^{11}	U^{22}	U^{33}	U^{23}	U^{13}	U^{12}
Zn1	0.0235(3)	0.0261(6)	0.0219(6)	0.0052(4)	-0.0039(4)	-0.0076(5)
N1	0.0602(19)	0.0240(13)	0.0228(14)	0.0029(10)	0.0085(13)	0.0018(13)
C2	0.058(2)	0.0241(15)	0.0201(16)	-0.0001(12)	0.0107(15)	0.0024(15)
N3	0.0509(17)	0.0247(12)	0.0239(13)	0.0044(10)	0.0071(12)	0.0008(12)
C4	0.053(2)	0.0245(15)	0.0316(18)	0.0031(13)	0.0125(15)	0.0041(15)
C5	0.048(2)	0.0214(15)	0.0295(17)	0.0023(12)	0.0100(14)	0.0044(14)
C6	0.0522(19)	0.0354(15)	0.0234(14)	0.0011(12)	0.0041(13)	0.0099(15)
N6	0.0522(19)	0.0354(15)	0.0234(14)	0.0011(12)	0.0041(13)	0.0099(15)
C7	0.046(2)	0.0348(17)	0.0340(18)	0.0005(14)	0.0079(15)	0.0119(15)
C8	0.049(2)	0.049(2)	0.0392(19)	-0.0031(16)	0.0024(16)	0.0106(17)
C9	0.065(3)	0.060(2)	0.053(2)	-0.0006(19)	0.007(2)	-0.012(2)
C10	0.079(3)	0.048(2)	0.054(2)	0.0135(18)	0.000(2)	-0.007(2)
C11	0.045(2)	0.052(2)	0.0362(19)	0.0154(16)	0.0047(16)	-0.0002(17)
C12	0.046(2)	0.0317(16)	0.0312(18)	0.0041(13)	0.0082(15)	0.0086(15)
C13	0.0548(19)	0.0303(15)	0.0248(15)	0.0056(12)	0.0104(13)	0.0044(14)
N13	0.0548(19)	0.0303(15)	0.0248(15)	0.0056(12)	0.0104(13)	0.0044(14)
C14	0.049(2)	0.0201(14)	0.0241(16)	0.0008(12)	0.0118(14)	0.0019(13)
N15	0.0520(18)	0.0293(13)	0.0243(14)	0.0046(11)	0.0072(12)	0.0039(12)
C16	0.055(2)	0.0250(15)	0.0249(16)	0.0013(12)	0.0090(15)	0.0038(15)
N17	0.0569(18)	0.0264(13)	0.0212(13)	0.0039(10)	0.0037(12)	0.0007(13)
C18	0.056(2)	0.0241(15)	0.0205(15)	0.0010(12)	0.0042(14)	0.0065(15)
C19	0.052(2)	0.0241(15)	0.0260(16)	-0.0009(12)	0.0054(14)	0.0025(14)
C20	0.0510(19)	0.0328(15)	0.0237(15)	0.0030(12)	0.0052(13)	0.0021(14)
N20	0.0510(19)	0.0328(15)	0.0237(15)	0.0030(12)	0.0052(13)	0.0021(14)
C21	0.048(2)	0.0360(18)	0.0354(18)	-0.0011(14)	0.0137(16)	0.0086(16)
C22	0.043(2)	0.048(2)	0.042(2)	0.0088(16)	-0.0002(16)	0.0076(17)
C23	0.080(3)	0.062(3)	0.047(2)	0.0016(19)	-0.009(2)	0.003(2)
C24	0.063(3)	0.058(2)	0.077(3)	0.000(2)	-0.014(2)	-0.010(2)
C25	0.047(2)	0.0400(19)	0.062(2)	-0.0024(17)	0.0103(18)	-0.0003(17)
C26	0.049(2)	0.0364(18)	0.042(2)	-0.0015(15)	0.0149(16)	0.0072(16)
C27	0.055(2)	0.0325(15)	0.0356(17)	0.0016(13)	0.0148(15)	0.0020(14)
N27	0.055(2)	0.0325(15)	0.0356(17)	0.0016(13)	0.0148(15)	0.0020(14)
C28	0.051(2)	0.0276(15)	0.0260(16)	0.0002(13)	0.0055(14)	0.0036(15)
C29	0.063(3)	0.052(2)	0.083(3)	-0.023(2)	0.011(2)	0.011(2)
C30	0.056(3)	0.078(3)	0.063(3)	-0.005(2)	-0.002(2)	0.015(2)
C31	0.057(3)	0.076(3)	0.061(3)	0.043(2)	0.007(2)	0.000(2)
C32	0.061(3)	0.071(3)	0.047(2)	0.002(2)	0.0188(19)	0.000(2)
C33	0.058(3)	0.092(3)	0.044(2)	0.029(2)	-0.0033(19)	0.003(2)
C34	0.058(3)	0.051(2)	0.089(3)	0.003(2)	-0.005(2)	0.016(2)
C35	0.064(3)	0.046(2)	0.070(3)	-0.0147(19)	0.008(2)	0.003(2)
C36	0.055(3)	0.081(3)	0.102(4)	0.003(3)	0.024(3)	-0.007(2)
O1W	0.027(2)	0.046(3)	0.047(3)	-0.007(2)	0.003(2)	-0.001(2)

Table SI-15. Hydrogen coordinates and isotropic displacement parameters (\AA^2) for mL105c2_0m_sq.

	x	y	z	U(eq)	Occupancy
H6	0.7937	0.2632	0.4967	0.044	0.5
H9A	0.4972	0.1366	0.5947	0.071	1
H9B	0.5197	0.0473	0.5750	0.071	1
H10A	0.8878	0.0393	0.6056	0.073	1
H10B	0.7234	0.0529	0.6419	0.073	1
H13	1.2358	0.2649	0.6298	0.043	0.5
H20	1.1406	0.6097	0.3269	0.043	0.5
H23A	0.5900	0.5351	0.2186	0.077	1
H23B	0.7766	0.4684	0.2307	0.077	1
H24A	0.3981	0.4925	0.2771	0.081	1
H24B	0.4270	0.4181	0.2450	0.081	1
H27	0.7666	0.3870	0.3845	0.049	0.5
H29A	0.7083	0.0278	0.5076	0.099	1
H29B	0.9329	0.0508	0.5355	0.099	1
H29C	0.8614	0.0991	0.4920	0.099	1
H30A	0.3726	0.1229	0.5088	0.099	1
H30B	0.5300	0.1829	0.4853	0.099	1
H30C	0.4169	0.2136	0.5265	0.099	1
H31A	1.2093	0.1748	0.6717	0.097	1
H31B	1.2170	0.0931	0.6439	0.097	1
H31C	1.0829	0.0947	0.6854	0.097	1
H32A	0.8638	0.2541	0.6725	0.088	1
H32B	0.7291	0.1749	0.6846	0.088	1
H32C	0.6470	0.2276	0.6431	0.088	1
H33A	0.9209	0.6314	0.2215	0.098	1
H33B	1.0830	0.5604	0.2399	0.098	1
H33C	1.0691	0.6441	0.2658	0.098	1
H34A	0.5716	0.6623	0.2575	0.100	1
H34B	0.7330	0.6814	0.2995	0.100	1
H34C	0.5359	0.6176	0.3018	0.100	1
H35A	0.8144	0.3006	0.3100	0.090	1
H35B	0.8668	0.3547	0.2697	0.090	1
H35C	0.6510	0.2988	0.2670	0.090	1
H36A	0.5014	0.3338	0.3517	0.118	1
H36B	0.3323	0.3364	0.3095	0.118	1
H36C	0.3536	0.4132	0.3412	0.118	1
H1WA	1.4889	0.6385	0.5594	0.060	0.5
H1WB	1.2668	0.6126	0.5504	0.060	0.5

Table SI-16. Torsion angles [°] for mL105c2_0m_sq.

C18#1-N1-C2-N3	-1.2(5)	C4-N15-C16-N17	0.7(5)
C18#1-N1-C2-C14	175.7(3)	C4-N15-C16-C28	178.3(3)
N1-C2-N3-C4	175.4(3)	N15-C16-N17-C18	178.1(3)
C14-C2-N3-C4	-2.0(3)	C28-C16-N17-C18	0.2(3)
N1-C2-N3-Zn1#1	14.4(5)	N15-C16-N17-Zn1#1	15.1(4)
C14-C2-N3-Zn1#1	-163.0(2)	C28-C16-N17-Zn1#1	-162.8(2)
N1-C2-N3-Zn1	-7.8(4)	N15-C16-N17-Zn1	-4.8(5)
C14-C2-N3-Zn1	174.78(18)	C28-C16-N17-Zn1	177.3(2)
C2-N3-C4-N15	-177.5(3)	C16-N17-C18-N1#1	-174.9(3)
Zn1#1-N3-C4-N15	-13.8(4)	Zn1#1-N17-C18-N1#1	-14.3(4)
Zn1-N3-C4-N15	5.9(5)	Zn1-N17-C18-N1#1	7.9(4)
C2-N3-C4-C5	0.4(3)	C16-N17-C18-C19	1.9(3)
Zn1#1-N3-C4-C5	164.15(19)	Zn1#1-N17-C18-C19	162.5(2)
Zn1-N3-C4-C5	-176.16(19)	Zn1-N17-C18-C19	-175.29(19)
N15-C4-C5-C6	4.4(5)	N1#1-C18-C19-C20	-5.1(5)
N3-C4-C5-C6	-173.6(3)	N17-C18-C19-C20	177.9(3)
N15-C4-C5-C14	179.4(3)	N1#1-C18-C19-C28	173.5(3)
N3-C4-C5-C14	1.4(3)	N17-C18-C19-C28	-3.4(3)
C14-C5-C6-C7	1.9(4)	C28-C19-C20-C21	-2.8(4)
C4-C5-C6-C7	176.1(3)	C18-C19-C20-C21	175.7(3)
C5-C6-C7-C12	2.9(4)	C19-C20-C21-C26	-3.0(5)
C5-C6-C7-C8	-171.9(3)	C19-C20-C21-C22	172.1(3)
C6-C7-C8-C9	-159.1(3)	C20-C21-C22-C33	37.8(4)
C12-C7-C8-C9	26.2(4)	C26-C21-C22-C33	-147.2(3)
C6-C7-C8-C29	79.4(4)	C20-C21-C22-C23	159.0(3)
C12-C7-C8-C29	-95.3(4)	C26-C21-C22-C23	-26.0(4)
C6-C7-C8-C30	-38.3(4)	C20-C21-C22-C34	-81.2(4)
C12-C7-C8-C30	147.0(3)	C26-C21-C22-C34	93.9(4)
C29-C8-C9-C10	70.3(4)	C33-C22-C23-C24	170.3(3)
C7-C8-C9-C10	-47.8(4)	C21-C22-C23-C24	47.0(4)
C30-C8-C9-C10	-170.1(3)	C34-C22-C23-C24	-70.6(4)
C8-C9-C10-C11	61.1(5)	C22-C23-C24-C25	-60.7(5)
C9-C10-C11-C31	-169.2(3)	C23-C24-C25-C26	46.8(5)
C9-C10-C11-C32	71.8(4)	C23-C24-C25-C35	-71.4(4)
C9-C10-C11-C12	-45.7(5)	C23-C24-C25-C36	170.3(4)
C6-C7-C12-C13	-5.0(5)	C20-C21-C26-C27	6.1(5)
C8-C7-C12-C13	169.6(3)	C22-C21-C26-C27	-168.8(3)
C6-C7-C12-C11	170.3(3)	C20-C21-C26-C25	-167.9(3)
C8-C7-C12-C11	-15.1(5)	C22-C21-C26-C25	17.2(5)
C10-C11-C12-C13	-160.9(3)	C24-C25-C26-C27	159.3(3)
C31-C11-C12-C13	-38.7(4)	C35-C25-C26-C27	-80.1(4)
C32-C11-C12-C13	79.8(4)	C36-C25-C26-C27	38.2(4)
C10-C11-C12-C7	23.6(4)	C24-C25-C26-C21	-26.5(5)
C31-C11-C12-C7	145.8(3)	C35-C25-C26-C21	94.0(4)
C32-C11-C12-C7	-95.7(4)	C36-C25-C26-C21	-147.7(3)
C7-C12-C13-C14	2.1(4)	C21-C26-C27-C28	-3.2(5)
C11-C12-C13-C14	-173.4(3)	C25-C26-C27-C28	171.1(3)
C12-C13-C14-C5	2.7(4)	C26-C27-C28-C19	-2.5(5)
C12-C13-C14-C2	-174.4(3)	C26-C27-C28-C16	-178.1(3)
C6-C5-C14-C13	-4.8(5)	C20-C19-C28-C27	5.8(5)
C4-C5-C14-C13	179.8(3)	C18-C19-C28-C27	-173.1(3)
C6-C5-C14-C2	172.9(3)	C20-C19-C28-C16	-177.7(3)
C4-C5-C14-C2	-2.5(3)	C18-C19-C28-C16	3.4(3)
N1-C2-C14-C13	2.8(5)	N15-C16-C28-C27	-4.3(5)
N3-C2-C14-C13	-179.8(3)	N17-C16-C28-C27	173.8(3)
N1-C2-C14-C5	-174.6(3)	N15-C16-C28-C19	179.6(3)
N3-C2-C14-C5	2.8(3)	N17-C16-C28-C19	-2.4(3)
N3-C4-N15-C16	-1.3(5)		
C5-C4-N15-C16	-178.9(3)		

Table SI-17. Hydrogen bonds for mL105c2_0m_sq [Å and °].

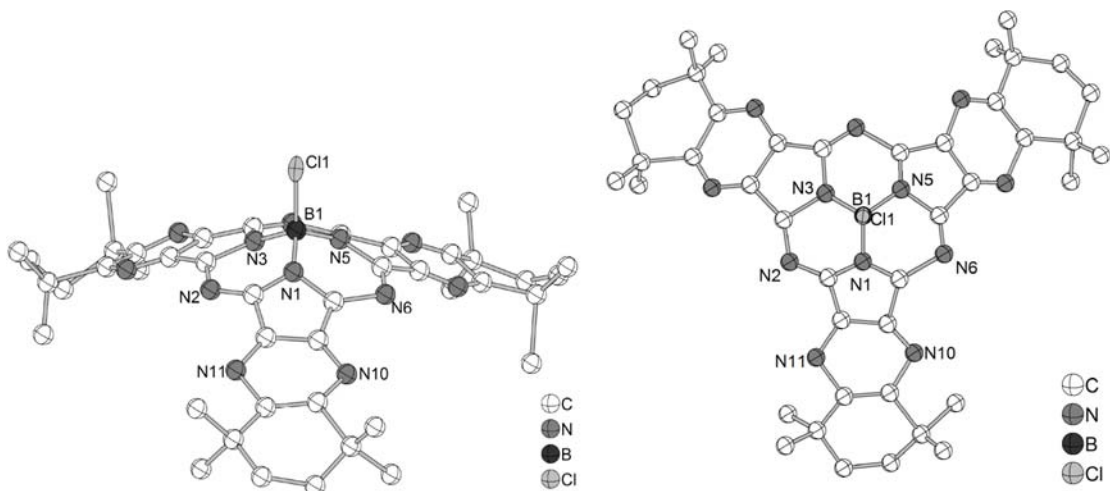
D-H...A	d(D-H)	d(H...A)	d(D...A)	∠(DHA)
O1W-H1WB...N15#2	0.86	1.86	2.583(5)	140.6
O1W-H1WB...N27#2	0.86	2.63	3.307(5)	135.7

Symmetry transformations used to generate equivalent atoms:

#1 -x+3,-y+1,-z+1 #2 -x+2,-y+1,-z+1

1.7.4 Crystal Structure of [Sppz^{*}BCl]

Crystallographer: Dr. Benjamin Oelkers



Empirical formula C49 H56 B Cl N12

Formula weight 859.32

Temperature 100(2) K

Wavelength 0.71073 Å

Crystal system Monoclinic

Space group P 21/c

Unit cell dimensions $a = 7.253(3)$ Å $\alpha = 90^\circ$.

$b = 25.008(5)$ Å $\beta = 98.83(3)^\circ$.

$c = 25.698(7)$ Å $\gamma = 90^\circ$.

Volume 4606(2) Å³

Z 4

Density (calculated) 1.239 Mg/m³

Absorption coefficient 0.132 mm⁻¹

F(000) 1824

Crystal size 0.3 x 0.06 x 0.03 mm³

Theta range for data collection 1.14 to 20.00°.

Index ranges -6<=h<=6, -24<=k<=24, -24<=l<=24

Reflections collected 13040

Independent reflections 4273 [R(int) = 0.2894]

Completeness to theta = 20.00° 99.8 %

Absorption correction None

Refinement method Full-matrix least-squares on F²

Data / restraints / parameters 4273 / 0 / 197

Goodness-of-fit on F² 0.841

Final R indices [I>2sigma(I)] R1 = 0.1654, wR2 = 0.3401

R indices (all data) R1 = 0.4135, wR2 = 0.4094

Largest diff. peak and hole 0.382 and -0.431 e.Å⁻³

Note: Because of the poor diffraction of the crystal, no satisfying refinement could be obtained. To gain a preliminary crystal structure of low resolution only reflexes up to theta = 20° were used. All deflection coefficients C, N, and B were held constant isotropic and refined with common parameters. The interpretation and orientation of the solvent molecules are, in contrast to the general figure of the complex molecule, not of sufficient quality for a discussion. Because of the poor data, no detailed discussion of bond lengths is possible however a documentation of the unit cell is possible.

1.8 References

- [1] S. A. Mikhalenko, L. I. Solov'eva, E. A. Luk'yanetz, *The Journal of General Chemistry of the USSR* **1991**, *61*, 996–1003.
- [2] P. Jones, G. B. Villeneuve, C. Fei, J. DeMarte, A. J. Haggarty, K. T. Nwe, D. A. Martin, A. M. Lebuis, J. M. Finkelstein, B. J. Gour-Salin et al., *J. Med. Chem.* **1998**, *41*, 3062–3077.
- [3] E. Seikel, B. Oelkers, O. Burghaus, J. Sundermeyer, *Inorg. Chem.* **2013**, *52*, 4451–4457.
- [4] E. Seikel, *Dissertation*, Philipps-Universität Marburg, Marburg, **2012**.
- [5] M. Liebold, *Masterarbeit*, Philipps-Universität Marburg, Marburg, **2012**.
- [6] APEX2, Bruker AXS Inc., Madison, Wisconsin, USA, **2014**.
- [7] SAINT, Bruker AXS Inc., Madison, Wisconsin, USA, **2013**.
- [8] G. M. Sheldrick, *Acta crystallographica. Section A, Foundations of crystallography* **2008**, *64*, 112–122.
- [9] G. M. Sheldrick, *SHELXT*, Universität Göttingen, Göttingen, Germany, **2014**.
- [10] G. M. Sheldrick, *SHELXL*, Universität Göttingen, Göttingen, Germany, **2014**.
- [11] K. Brandenburg, *Diamond - Crystal and Molecular Structure Visualization*, Crystal Impact - Dr. H. Putz & Dr. K. Brandenburg GbR, Bonn, Germany, **2014**.
- [12] SADABS, Bruker AXS Inc., Madison, Wisconsin, USA, **2014**.
- [13] G. M. Sheldrick, *Acta Crystallogr A Found Adv* **2015**, *71*, 3–8.
- [14] G. M. Sheldrick, *Acta crystallographica. Section C, Structural chemistry* **2015**, *71*, 3–8.
- [15] C. B. Hübschle, G. M. Sheldrick, B. Dittrich, *Journal of applied crystallography* **2011**, *44*, 1281–1284.